공학박사 학위논문

Shape-Controlled Metal-Semiconductor Heterostructured Nanocrystals for Photocatalytic Hydrogen Generation

형태가 조절된 금속-반도체 헤테로구조 나노입자의 광촉매 수소 제조

2016년 8월

서울대학교 대학원

공과대학 화학생물공학부

성 영 훈

Abstract

Shape-Controlled Metal-Semiconductor Heterostructured Nanocrystals for Photocatalytic Hydrogen Generation

Younghun Sung

School of Chemical and Biological Engineering

The Graduate School

Seoul National University

Colloidal heterostructured nanocrystals have recently gained keen attention due to the synergistic properties arising from different compositions within a single nanocrystal. Particularly, colloidal metal-semiconductor heterostructured nanocrystals have been extensively studied from the development of new synthetic chemistry, characterizations, carrier dynamics and various applications such as self-assembly, photocatalysis, bioimaging, electrical devices, and so forth. Furthermore, complex heterostructures consisting of multicomponents of two or more semiconductors and metals

were reported to precisely engineer the morphologies as well as electronic properties of each component to achieve high-performance heterostructured nanomaterials and devices.

Among many applications with the metal-semiconductor hybrid nanomaterials, the use of these heterostructured hybrid nanomaterials for photocatalysis has gained much attention due to increased interest in exploring new sources of renewable energy. Novel metals such as Au or Pt were typically employed as cocatalysts when combined with semiconductor nanomaterials with light-absorbing properties to generate excitons. Proper bandgap engineering of these multicomponent hybrid nanocrystals enabled the increase in photocatalytic hydrogen generation efficiencies by splitting water with electrons and holes generated.

More specifically, platinum-incorporated cadmium chalcogenide semiconductor nanocrystals have been studied to improve the efficiency of photocatalytic hydrogen generation reaction. Several research groups have already reported on the incorporation of Pt onto cadmium chalcogenide semiconductor nanocrystals with different synthetic mechanisms as well as with different morphologies. Tipping of Pt nanocrystals at the ends of CdSe or CdS nanorods and tetrapods has been introduced, followed by the decoration of Pt nanocrystals by the photodeposition of Pt precursors under irradiation with certain wavelength of light. These synthetic efforts enabled

to design new heterostructured nanocrystals and to study the carrier dynamics between Pt metal cocatalysts and CdSe or CdS semiconductor photocatalysts. Since metallic Pt nanocrystals act as reaction sites for the hydrogen evolution by combining with electrons generated from semiconductor nanocrystals, studies on the effect of Pt nanocrystals for the photocatalytic hydrogen generation reaction have also been reported by many research groups. Therefore, the surface properties of semiconductor nanocrystals combined with structural properties of metallic nanocrystals are important issues to be considered for the rational design of new metal-semiconductor heterostructured nanocrystal photocatalysts.

A key criterion in the design of efficient photocatalysts lies in the reliable synthesis of semiconductor nanocrystals with different shape. In general, controlling the surface energy of certain crystal facets by either using proper choices of strongly or weakly binding ligands, or controlling monomer concentration, is the commonly used approach. Alkylphosphonic acids were the typical ligands used to suppress the growth rate of specific crystal facets. Our group has previously reported on the synthesis of well-defined CdSe tetrapods by using alkyl halides and also by keeping the arm growth stage within the kinetic growth regime. As a result, each of these semiconductor nanocrystals prepared with different synthetic schemes has resulted in different surface chemistry and topography, which then need to be considered

for further rational design of metal-semiconductor heterostructured nanocrystals.

This thesis demonstrates the systematic study on the influence of each component in metal-semiconductor heterostructured nanocrystals for photocatalytic hydrogen generation application. Methodologies for the shape control of semiconductor nanocrystals followed by incorporation methods of metal nanocrystals onto semiconductor nanocrystals with different surface chemistry have been established. Morphological effects of individual metal and semiconductor nanocrystals on the final performance of photocatalytic hydrogen generation have been systematically studied. It is believed that this systematic study will guide to rational design of high-performance photocatalysts for photocatalytic water splitting applications.

Keywords: Nanocrystal, Metal-Semiconductor Heterostructure, Nanorod, Tetrapod, Photocatalyst, Hydrogen, Water Splitting

Student Number: 2010-22815

Contents

List of Figures

List of Schemes

List of Tables

Chapter 1. Introduction

1.1 Introduction to Colloidal Heterostructured Nanocrystals

Colloidal heterostructured nanocrystals are composed of two or more disparate materials within a single nanosystem, showing multifunctionalities within a single nanocrystal while maintaining intrinsic properties of each component.[1-4] Since the first discovery of colloidal semiconductor nanocrystals, so called quantum dots, tremendous efforts have been made to develop synthetic approaches to prepare colloidal semiconductor nanocrystals with high morphological uniformity and shape selectivity, followed by studies to understand fundamental principles for the nucleation and growth mechanisms as well as their intrinsic properties underlying complicated carrier dynamics arising from complex compositions and morphologies. Synthetic efforts to understand nucleation and growth mechanisms of colloidal semiconductor nanocrystals as well as surface chemistry also enabled shape control of colloidal semiconductor nanocrystals with various morphologies from zero-dimensional nanocrystals such as quantum dots, to one-dimensional nanorods, two-dimensional nanoplatelets and core/crown structures or three-dimensional multibranched structures such as tetrapods and octapods. Colloidal semiconductor nanocrystals exhibit

unique electronic properties as well as surface states depending on the morphologies and compositions, which further led for the development of complex colloidal heterostructured nanocrystals such as semiconductor-semiconductor or metal-semiconductor heterostructured nanocrystals with desired purpose. By efforts to understand fundamental synthetic mechanisms and carrier dynamics, rational design and synthesis of novel colloidal heterostructured nanocrystals with new properties are extensively in progress.

1.2 Colloidal semiconductor heterostructured nanocrystals

Colloidal semiconductor nanocrystals are nanometer-sized atomic clusters of 1,000 ~ 10,000 atoms confining excitons in three spatial dimensions, thus exhibiting broad absorption and narrow emission bandwidth and tunable bandgap in terms of size and composition due to quantum confinement effect. By their intrinsic compositions and morphologies, unique carrier dynamics are observed as well as photochemical stability depending on surface states with passivating organic ligands (Figure 1.2.1).[4-14]

As mentioned above, colloidal semiconductor nanocrystals show unique optoelectronic properties by quantum confinement effect, thus enormous efforts to develop synthetic approaches to precisely control the morphologies

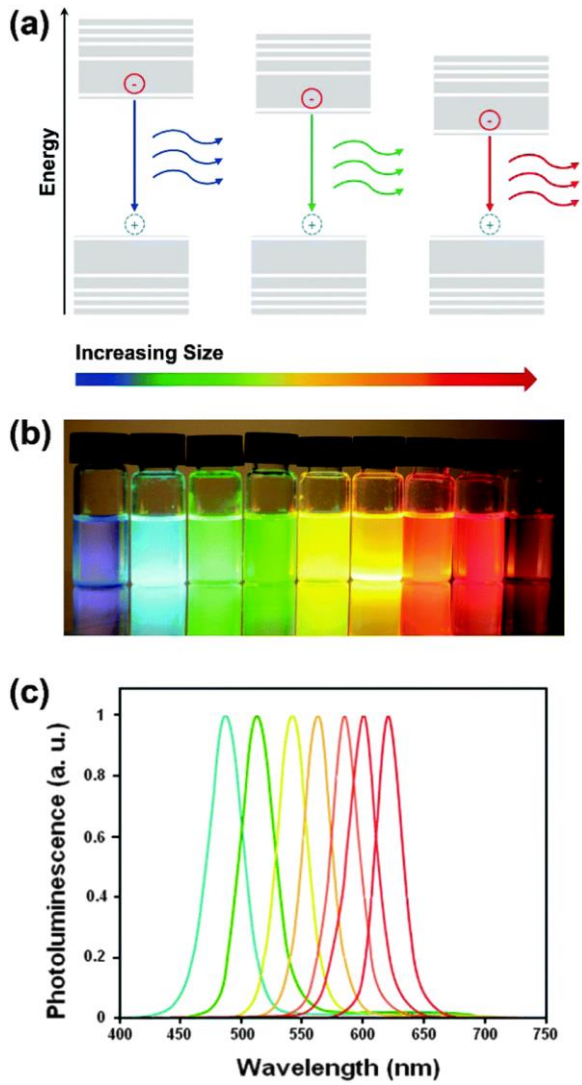

Figure 1.2.1 Schematic illustration on the relationship between the size of colloidal semiconductor nanocrystals and their electronic properties. © Royal Society of Chemistry.

and compositions of colloidal semiconductor nanocrystals have been made, which lead to design and control over the bandgap of colloidal semiconductor nanocrystals.[15-18] By precise engineering on the energy diagram of colloidal semiconductor nanocrystals with proper choice of compositions, morphologies and surface states, pathways for charged carriers could also be systematically designed, which are essential for proper use in various applications.[4, 19-23]

Introduction of two or more different semiconducting materials within a single colloidal semiconducting nanocrystals, which is called colloidal semiconductor heterostructured nanocrystals, show complicated energy diagram with controlled band offsets, thus leading to unique carrier dynamics for desired purposes (Figure 1.2.2). In general, bandgap configuration of colloidal semiconductor heterostructured nanocrystals could be categorized as such: type I and type II. In type I band alignment, core region of colloidal semiconductor heterostructured nanocrystals have higher valence band offset and lower conduction band offset than outer semiconducting region, thus electrons and holes wavefunctions are localized inside core region. Due to the alignment of band offsets of valence and conduction band, electrons and holes generated at outer region of colloidal semiconductor heterostructured nanocrystals also migrate to core region, which is suitable for exciton recombinations for luminescence properties.[24-28] By the proper choice of

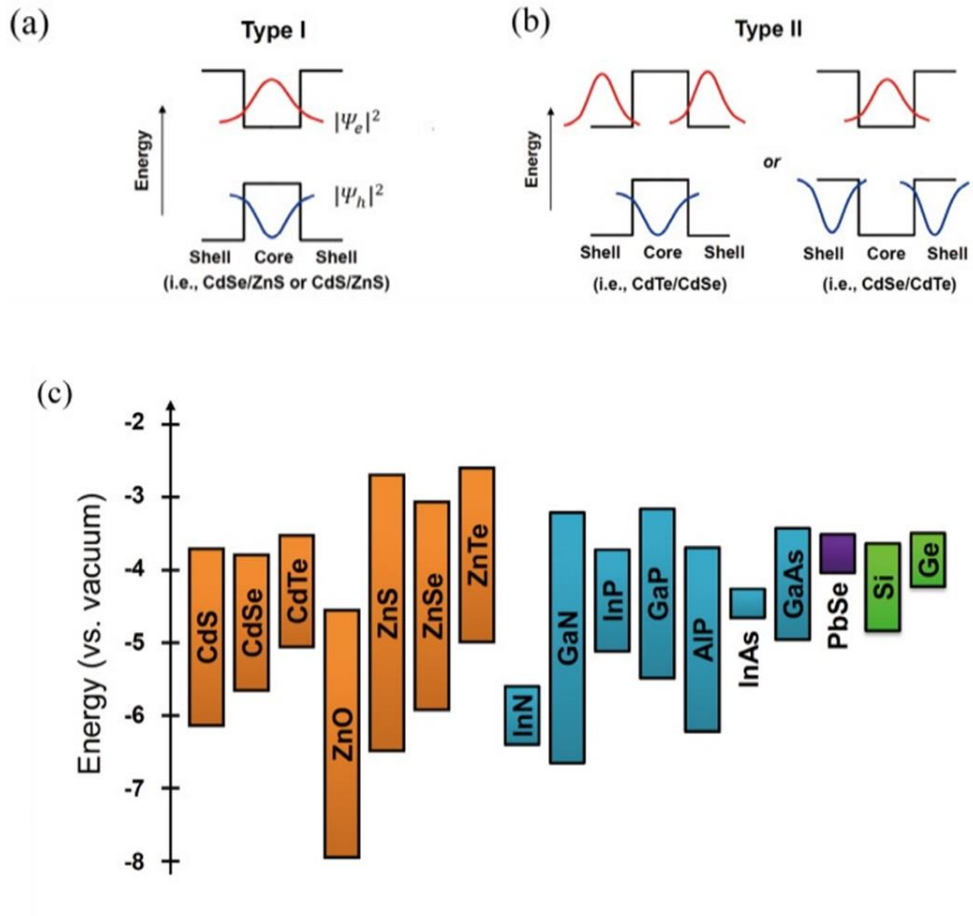

Figure 1.2.2 Schematic illustration of band configurations of (a) type I and (b) type II band alignment. (c) Bandgap positions of colloidal semiconductor nanocrystals in the literature. This illustration was redesigned from J. Lim et al. © The Optical Society.

semiconductor materials and control over compositions and morphologies, band offsets of different semiconducting regions could be precisely controlled for various applications.[29-33] In type II band alignment, stepwise position of band offsets of valence and conduction bands offers directed pathways for electrons and holes with different directions, which is suitable for the excitons to charge separate.[7, 34-39]

1.3 Colloidal metal-semiconductor heterostructured nanocrystals

In particular, colloidal metal-semiconductor heterostructured nanocrystals are of great interest due to the synergistic properties arising from different combinations of conducting and semiconducting structures within a single nanocrystal. These heterostructured nanocrystals show both metal and semiconductor properties with possible applications in various fields.[1, 40-45] With the intrinsic properties of each metal and semiconductor, the heterostructured nanocrystals with various combinations and morphologies of metals and semiconductors have extensively been studied from fundamental mechanistic studies, carrier dynamics to applications with a design for relevant use (Figure 1.3.1). Furthermore, complex heterostructures consisting of multicomponents of 2 or more semiconductors and metals were reported to precisely engineer morphologies as well as electronic properties of each component to achieve high-performance heterostructured nanomaterials and devices.[2, 46-52]

Hybridization mechanism for the nucleation and growth of metals and semiconductors as a single colloidal metal-semiconductor heterostructured nanocrystals still have many issues to be solved since chemical and

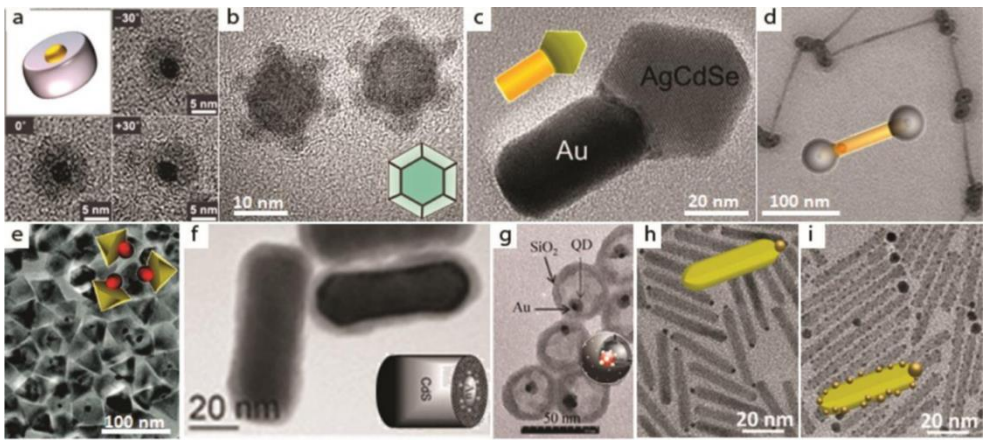

Figure 1.3.1 Colloidal metal-semiconductor heterostructured nanocrystals with various combinations of compositions and morphologies. (a) Cu_2S-Au, (b) Ru-CuS nanocage, (c) AgCdSe-Au nanorods, (d) Pt@Co_xO_y-CdSe@CdS self-assembled nanorods, (e) ZnO-Au hexagonal nanopyramids, (f) CdS-Au core@shell nanorods, (g) CdSe/CdS/ZnS-Au@hollow SiO_2 york/shell nanospheres, (h) Single Au-tipped CdS nanorods and (g) decoration of Au tips onto CdS nanorods. © American Chemical Society.

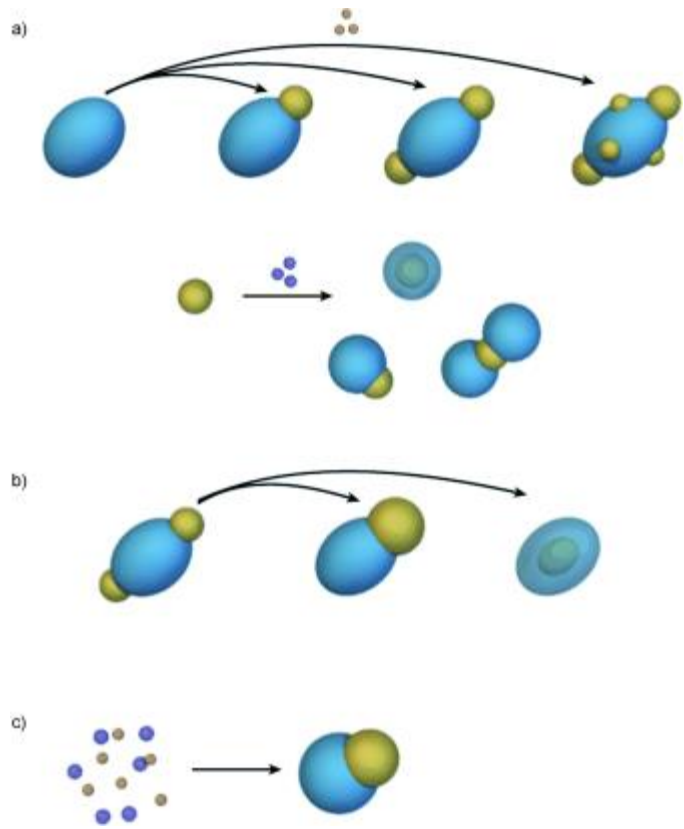

Figure 1.3.2 Schematic illustrations on the nucleation and growth mechanisms for colloidal metal-semiconductor heterostructured nanocrystals. (a) Surface nucleation and growth of a second phase on a seed nanoparticle, either metal and semiconductor, (b) surface nucleation followed by surface diffusion of the metal phase or an inward diffusion, (c) simultaneous nucleation and growth of both materials. © Wiley-VCH.

structural compatibility between different components is generally not expected. In terms of colloidal synthesis, different nucleation and growth mechanisms than typical colloidal semiconductor nanocrystals must be considered, which are shown in Figure 1.3.2.

First, surface nucleation and growth of either metal or semiconductor onto different nanocrystals. Here, energetics of the reaction is important, since the homogeneous nucleation and growth of individual nanocrystals are favored than the heterogeneous nucleation and growth of colloidal heterostructured nanocrystals. By controlling the overall reaction conditions such as temperature, organic ligands, nucleation and growth regime such as thermodynamic and kinetic, hybridization of metals and semiconductors could be induced than self-formation of free nanocrystals.

Second, surface nucleation and diffusion of metals to semiconductor nanocrystals of different regions. In this case, nanocrystals nucleated and grown at the surface of different nanocrystals could undergo diffusion process in which there is a transport process involving the coalescence of surface clusters at a single location, either on the surface or within the center of the heterostructured nanocrystals. For example, since cadmium chalcogenide nanocrystals with anisotropic shapes could be synthesized by the different growth rate of crystal facets, crystal facets at the surface of colloidal semiconductor nanocrystals will exhibit different energy for the nucleation

and growth of secondary metal nanocrystals. Therefore, control over symmetry of colloidal metal-semiconductor heterostructured nanocrystals in colloidal synthesis is extremely difficult since precise control over surface crystal facets as well as surface states along with surface energy is difficult. Moreover, different metal nanocrystals have different ripening process, for example Au nanocrystals have faster ripening process than Pt. By controlling the reaction conditions such as concentration of precursors and reaction time, ripening process of metal nanocrystals at the surface of colloidal semiconductor nanocrystals could be induced.

Finally, simultaneous nucleation and growth of both metals and semiconductors.

1.4 Applications of colloidal heterostructured nanocrystals

Due to complex optoelectronic properties from various combinations of morphologies and compositions or metals and semiconductors within a single nanocrystal system, colloidal heterostructured nanocrystals are widely applied to various applications.[53-59] In general, applications of colloidal heterostructured nanocrystals could be divided into two categories. First, electron-to-photon conversions mostly by colloidal semiconductor

heterostructured nanocrystals. Charged carriers generated within semiconductor region of colloidal heterostructured nanocrystals are emitted as controlled wavelengths of light, thus suitable for light-emitting diodes or imaging area. Here, colloidal metal-semiconductor heterostructured nanocrystals are not suitable for this application since metal nanocrystals with high electron density will quench as-generated charge carriers and suppress recombination process. But, metal nanocrystals with plasmonic properties such as Au could be incorporated in this type of application. Second, photon-to-electron conversion by colloidal metal-semiconductor heterostructured nanocrystals. Here, both colloidal semiconductor and metal-semiconductor heterostructured nanocrystals are good candidates since they both generate charge carriers within nanocrystal itself. By designing novel colloidal heterostructured nanocrystals with controlled energy alignment for proper uses, as-generated charged carriers by absorption of photon energy, which are electrons and holes, could be utilized in applications that requires generation of electric energy, such as photovoltaics and photocatalysts. Self-generation of electric energy without external conditions by colloidal heterostructured nanocrystals are most suitable for renewable energy applications that require nothing but nanocrystal itself. In contrast, colloidal heterostructured nanocrystals could be also used to promote generation of electric energy by their intrinsic optoelectronic properties. Therefore, colloidal heterostructured

nanocrystals play key role in the overall area of optoelectronic applications.

1.4.1 Electron-to-photon conversions

In general, colloidal semiconductor heterostructured nanocrystals are widely used in various applications in terms of electron-to-photon conversion such as light-emitting diodes, transistors and so forth. Excitons or charged carriers generated inside the colloidal heterostructured nanocrystals are converted to photon energy by recombination process. By tuning the morphologies and compositions of colloidal heterostructured nanocrystals, band alignment of components could be controlled, thus generating luminescence properties with controlled wavelength of light. For example, colloidal semiconductor nanocrystals show different emission properties depending on the size of nanocrystals due to quantum confinement effect. Therefore, simply by controlling the size of confined geometries, emission of different colors could be induced. By introducing colloidal semiconductor heterostructured nanocrystals with combinational compositions of II-VI and III-V semiconducting materials, luminescence of different wavelength of light with improved quantum efficiency could be achieved. In general, CdSe or CdS quantum dot cores, which are the model system well studied in the literature, are covered with shell region of ZnSe, ZnS or other semiconducting materials to promote recombination process by type I band configuration.[60-71]

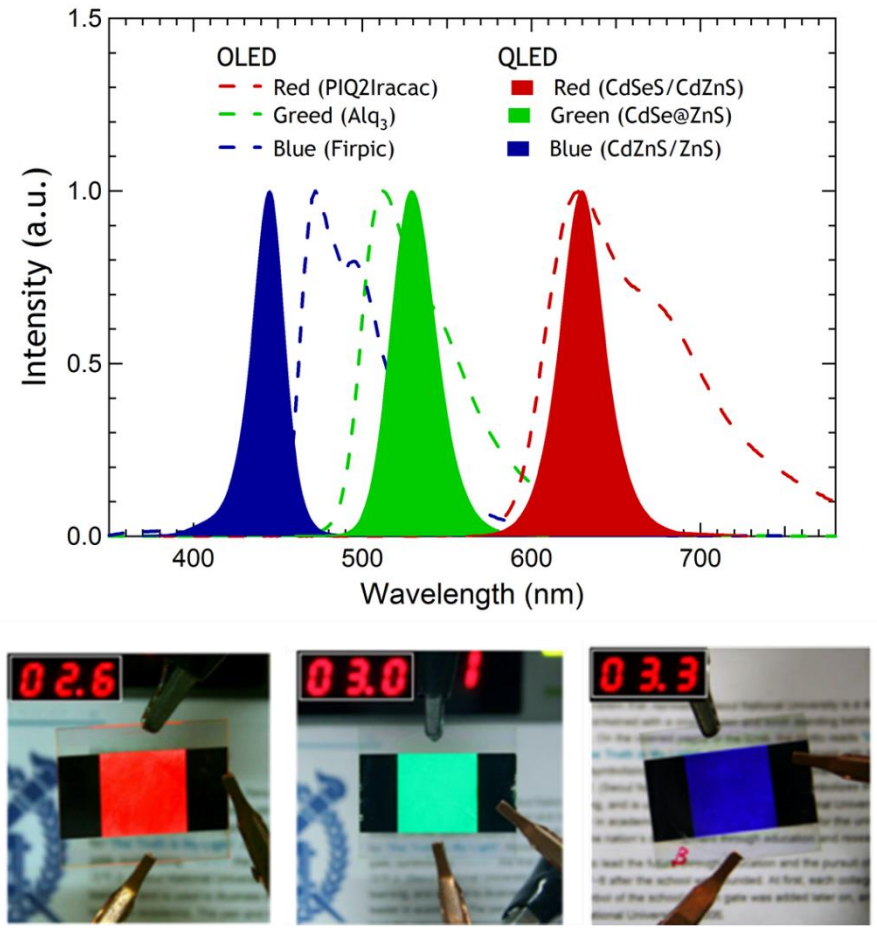

Figure 1.4.1 Colloidal semiconductor heterostructured nanocrystals for the application of quantum dot light-emitting diodes. © American Chemical Society.

By different synthetic methods to deposit and control morphologies of semiconducting shells, colloidal semiconductor heterostructured quantum dots with high photoemission properties could be achieved, such as choice of different semiconducting materials for shell region to either control the band alignment suitable for recombination process, or introduction of compositional gradient in shell region to both reduce lattice mismatches between core and shell as well as further promote photoluminescence properties of colloidal quantum dots (Figure 1.4.1). Further studies on the fabrication of light-emitting device structures help develop optoelectronic devices with better performance, such as inverted device structures or introduction of buffer layers. More recently, colloidal semiconductor heterostructured nanocrystals with giant shells or complex colloidal semiconductor heterostructured nanorods were reported to have higher photoluminescence properties for QLED applications. Moreover, due to regulation of toxic materials, Cd-free colloidal heterostructured quantum dots such as InP-based nanocrystals or perovskite nanocrystals have been well studied from the development of new synthetic chemistry as well as fundamental studies on carrier dynamics, and even commercialized to home electronics by large-scale production of companies as well.

Colloidal semiconductor heterostructured nanocrystals could also be used in transistor applications. In particular, transistors fabricated by colloidal

semiconductor nanocrystals with anisotropic shapes will contain more branching points with less surface sites with hopping transport of charge carriers. More recently, light-emitting diodes or transistors with flexible device structures have gained much attention due to increasing interest in wearable electronics, which shape-controlled colloidal semiconductor heterostructured nanocrystals will play an important role in materials point of view. Therefore, colloidal semiconductor heterostructured nanocrystals with various combinations of morphologies and compositions are promising functional nanomaterials in future optoelectronic devices.

1.4.2 Photon-to-electron conversions

Colloidal heterostructured nanocrystals are typically composed of semiconductors and metals within a single nanocrystal system. In general, semiconductor region act as light-absorbing materials and metal region act as quenching sites for charged carriers. Therefore, opposite to electron-to-photon conversion mentioned previously, photon energy by light-absorbing properties of semiconductor nanocrystals are converted to charge carriers, which are electric energy that could be utilized in many optoelectronic devices.[72-81]

Among many applications with colloidal metal-semiconductor heterostructured nanomaterials, the use of these heterostructured nanocrystals

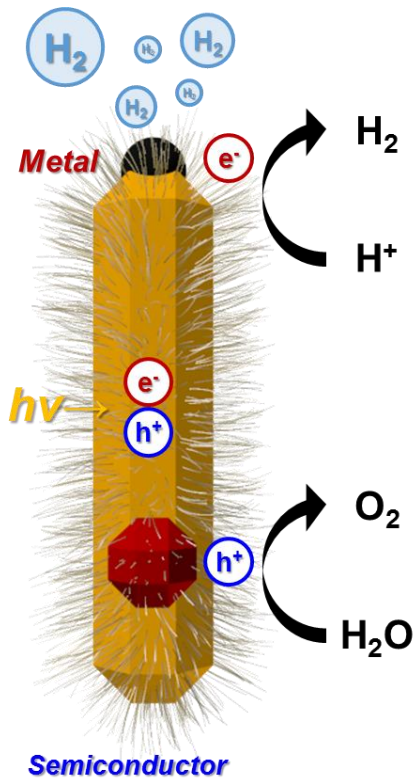

Scheme 1.4.1 Schematic illustration of colloidal metal-semiconductor heterostructured nanocrystals as photocatalysts for photocatalytic water splitting reaction.

for photocatalysis has gained much attention due to increased interest in exploring new sources of renewable energy, as shown in Scheme 1.4.1. By mimicking photosynthesis from nature leaves, which is called artificial photosynthesis, many research groups have demonstrated half- or overall photocatalytic water splitting reactions to generate hydrogen fuel. In principle, nanomaterials with minimum bandgap of 1.23 eV with proper energy level for oxidation and reduction potentials of water are good candidates for photocatalytic water splitting reaction. Photocatalysts first absorb sunlight to generate exciton, and these charged carriers migrate to cocatalysts incorporated at the surface of photocatalysts to either oxidize or reduce water to generate oxygen and hydrogen.[10, 46, 48, 82-88]

In terms of colloidal metal-semiconductor heterostructured nanocrystals as photocatalysts in photocatalytic water splitting reaction, novel metals such as Au or Pt were typically employed as cocatalysts when combined with various compositions of semiconductor nanomaterials with light-absorbing properties to generate excitons. Proper bandgap engineering of these multicomponent colloidal heterostructured nanocrystals enabled the increase in photocatalytic H_2 generation efficiencies by splitting water with electrons and holes generated. As mentioned above, various combinations of compositions and morphologies of colloidal metal-semiconductor heterostructured nanocrystals have been reported by many research groups. In general, platinum-

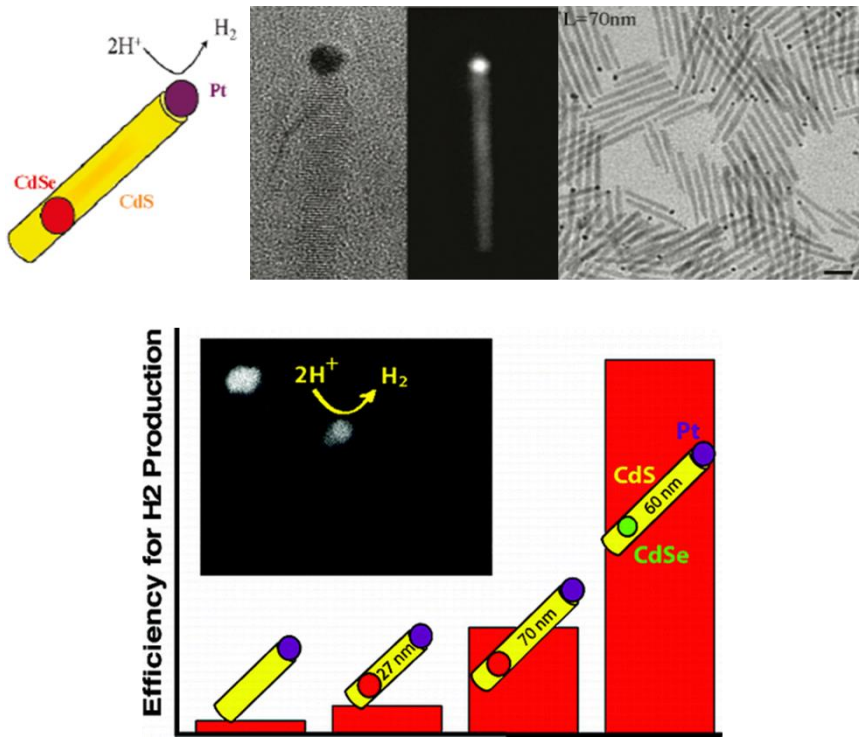

Figure 1.4.2 Pt-tipped cadmium chalcogenide heterostructured nanorods as photocatalysts in photocatalytic hydrogen generation reaction. © American Chemical Society.

incorporated cadmium chalcogenide heterostructured nanocrystals are extensively studied as model system for colloidal heterostructured photocatalysts in photocatalytic hydrogen generation reaction (Figure 1.4.2). Here, due to difficult synthetic methods to selectively deposit different types of metal cocatalysts within a single nanocrystal photocatalyst, half reaction of overall photocatalytic water splitting reaction, which is photocatalytic hydrogen generation reaction, was typically shown by adding hole scavengers to consume as-generated holes, while utilizing as-generated electrons only. Metal cocatalysts typically exhibit higher electron density with energy level, therefore as-generated electrons within semiconductor region migrate to metal cocatalysts with extremely fast quenching rate. Other metals such as Pd or Ni could also be used as different metal cocatalyst source. More recently, studies on the efficient management of holes by proper choice of hole scavengers such as sodium sulfide and alcohols as well as complicated morphologies and compositions to efficiently migrate holes to the surface states of colloidal heterostructured nanocrystals have been reported to significantly influence on the final performance of photocatalysts in photocatalytic hydrogen generation reaction. Moreover, colloidal semiconductor-only heterostructured nanocrystals could also be used as photocatalysts, since earth-rate and expensive novel metals.[50, 52, 89-97]

Colloidal semiconductor heterostructured nanocrystals, in terms of photon-

to-electron conversion, are used as sensitizers in photovoltaics. In both organic or inorganic solar cells, absorption of broad range of sunlight has been always important issue for high efficiency solar cells. Many research groups have extensively studied to synthetically develop new type of organic or inorganic materials with broad absorption spectra, but by adding colloidal heterostructured nanocrystals into the system as sensitizers and solar concentrators, absorption of devices was hugely enhanced, as well as colloidal metal-semiconductor heterostructured nanocrystals with Au of plasmonic effect.

Finally, metal nanocrystals in colloidal metal-semiconductor heterostructured nanocrystals also act as connection sites in self-assembly behavior. Due to selective functionalization of metal nanocrystals at specific surface sites, which in general termini of semiconductor nanocrystals, selective surface modification of metal nanocrystals enables self-assembly of colloidal heterostructured nanocrystals with either vertical alignment on the substrate or formation of network structures in solution of at the substrate.

Chapter 2. Shape Control of Semiconductor Nanocrystals

2.1 Introduction

Colloidal semiconductor nanocrystals show intrinsic optoelectronic properties depending on their morphologies and compositions.[15, 98-109] In particular, as the dimensions of colloidal semiconductor nanocrystals increase, light absorption properties such as absorption cross-section changes, which are shown in Figure 2.1. Computational simulations also show that colloidal semiconductor nanocrystals with different shapes have different spatial distribution of electrons and holes wavefunctions throughout the overall nanocrystal structures.[103, 110-116] As to fabricate optoelectronic devices, since electrons are transported by hopping mechanism, colloidal semiconductor nanocrystals with anisotropic shapes have less surface and interface for increased directivity to electrodes to minimize hopping transport. Therefore, the choice of specific shapes of colloidal semiconductor nanocrystals for proper applications is important.[37, 117-125]

Since the first discovery of colloidal semiconductor nanocrystals with spherical shape, which is well known as quantum dots, efforts to control the shape of colloidal semiconductor nanocrystals has been made to achieve

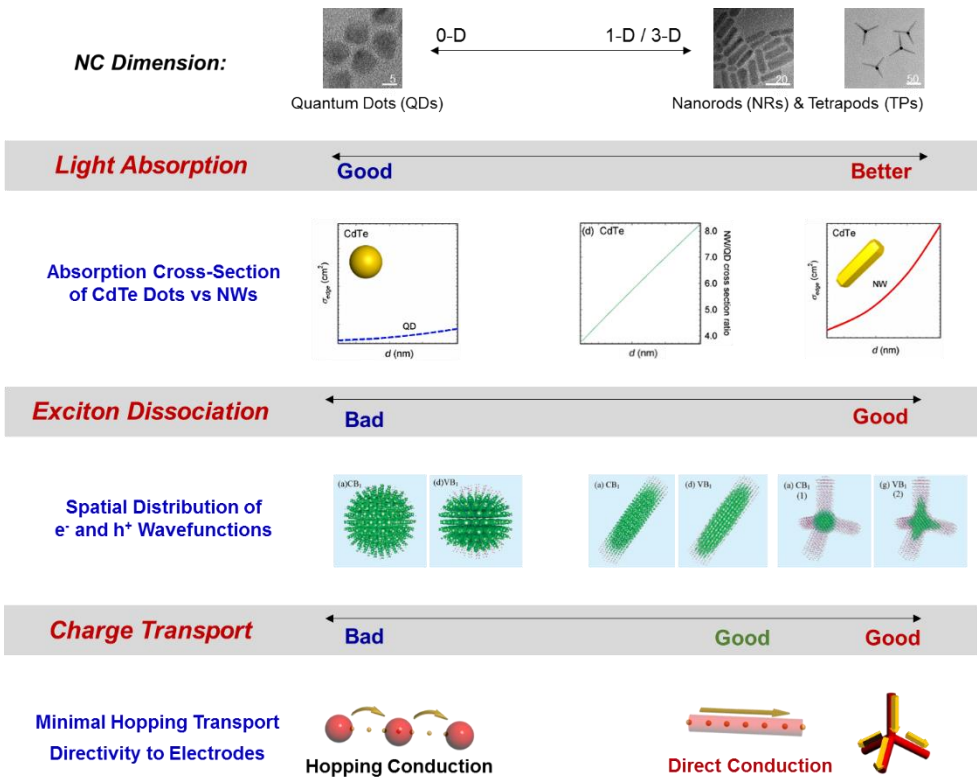

Figure 2.1 Intrinsic optoelectronic properties of colloidal semiconductor nanocrystals by dimensions. This figure was reconstructed from V. Protasenko et al., and J. Li et al. © American Chemical Society.

better optoelectronic properties. From the literature for the successive shape control of colloidal semiconductor nanocrystals, certain strategies are regarded as important factors to be considered, which is summarized in Figure 2.2. First, the choice of proper crystal structure of colloidal semiconductor quantum dots as seeds to further grow anisotropic shapes is important. In general, two main crystal structures of colloidal semiconductor nanocrystals have been extensively studied, which are wurtzite and zincblende crystal structures of CdSe colloidal semiconductor nanocrystals. Wurtzite CdSe quantum dots are typically used to synthesize colloidal semiconductor nanocrystals with rod-shape morphology due to faster growth rate of (0001) crystal facets. Zincblende CdSe quantum dots are generally used for nanocrystals with multibranched structured such as nanorods or octapods with faster growth rate of (111) crystal facets.[29, 33, 63, 126-142] Second, proper choice of organic ligands with different binding energy to crystal facets is important. In general, alkylphosphonic acids are typically used to supress certain crystal facets of colloidal semiconductor nanocrystals with wurtzite and zincblende crystal structures. Typical organic ligands such as oleic acids and oleylamines, which are used for the synthesis of sphereical colloidal nanocrystals, are relatively weakly-binding ligands compared with alkylphosphonic acids. Combinations of alkylphosphonic acids with different number of carbons in alkyl chains also affects the shape control of

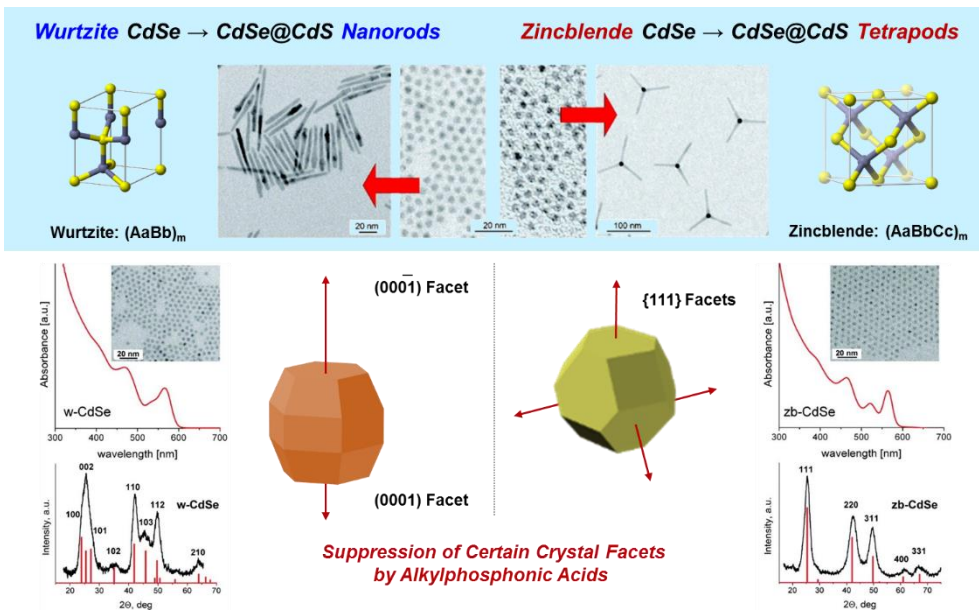

Figure 2.2 Seeded growth of CdSe@CdS nanorods and tetrapods by wurtzite and zincblende CdSe quantum dots as seeds. This illustration is redesigned from D. V. Talapin et al. © American Chemical Society.

nanocrystals. Incorporation of certain amount of alkyl halide ligands also enabled the shape control of colloidal semiconductor nanocrystals. With these considering factors that govern the overall synthetic chemistry of colloidal semiconductor nanocrystals, design of certain morphologies for proper applications was enabled with intrinsic optoelectronic properties.[22, 143-152]

2.2 Synthesis of CdSe@CdS Nanorods

This work was done under collaboration with M. M. Bull, L. J. Hill, and Prof. J. Pyun at the Department of Chemistry & Biochemistry, University of Arizona, United States.

2.2.1 Experimental Session

Materials Cadmium oxide (CdO, 99.95%) was purchased from Alfa Aesar. Selenium (Se, 99.99%), sulfur (S, 99.998%), n-trioctylphosphine (TOP, 90%), n-trioctylphosphine oxide (TOPO, 90%) were purchased from Sigma Aldrich. n-Octadecylphosphonic acid (ODPA, 97%) and n-hexytlphosphonic acid (HPA, 97%) were purchased from Strem Chemicals. Toluene and ethanol were purchased from Samchun Chemicals. All chemicals were used as purchased.

Preparation of SeTOP Stock Solution To a 20 mL glass vial with stir bar, was added 1.16 g (14.7 mmol) elemental Se. The vial was sealed, evacuated, and filled with Ar. TOP (8.66 mL) was then injected under argon and the mixture was stirred and sonicated until the stock solution became optically clear and colorless.

Wurtzite CdSe Quantum Dots The synthesis of CdSe quantum dots was adapted from the literature.[29] To a 100ml 3-neck round bottom flask equipped

with stirbar and condenser, were added CdO (0.06 g), ODPA (0.28 g) and TOPO (3.0 g). Under inert condition, the reaction mixture was then heated to 150 °C, followed by degassing for 30 min under vacuum to remove residual gas and H_2O. The reaction mixture was heated to 300 °C, followed by the injection of 1.8 mL TOP, and further heated to 380 °C until the reaction mixture becomes optically clear and colorless. Upon reaching at 380 °C, heating mantle was removed and the temperature was decreased to 370 °C, where 0.45 mL of as-prepared SeTOP stock solution was swiftly injected, followed by rinsing the flask with acetone for faster quenching. 5 mL of toluene was injected at 100 °C to prevent solidification. The crude mixture was transferred to centrifuge tube, and toluene and ethanol were added with same amount. The mixture was subjected to centrifugation at 8000 rpm for 5 min, and this purification step was repeated 3 times. Finally, the product was dissolved in organic solvents such as chloroform for further use.

Preparation of CdSeSTOP Stock Solution To a 20 mL glass vial with stir bar was added as-synthesized wurtzite CdSe quantum dots and elemental sulfur (0.6 g). The vial was sealed, evacuated, and filled with Ar. TOP (18 mL) was then injected under argon and the mixture was stirred and sonicated until the stock solution became translucent red and homogeneous.

CdSe@CdS Nanorods The synthesis of CdSe seeded CdS nanorods was adapted from literature.[29] TOPO (3.0 g), ODPA (0.29 g), CdO (0.075 g) and

HPA (0.08 g) were added to a 100 mL 3-neck round bottom flask equipped with a reflux condenser and stir bar. Under inert condition, the reaction mixture was heated to 150°C, followed by degassing for 30 minutes uder vacuum. The red, heterogeneous mixture was heated to 350°C under Ar where the formation of an optically clear and colorless solution was observed. TOP (1.5 g) was injected into the reaction vessel after which a transient drop in temperature was observed before recovery of the original reaction temperature of 350°C where it was held for 30 minutes prior to injection. The as-prepared CdSeSTOP stock solution (1.8 ml of stock) was swiftly injected into the flask and the nanocrystals were allowed to grow for 6 minutes. Toluene (5 mL) was injected after the internal reaction temperature had cooled to 100 °C to prevent solidification of low melting point solids (TOPO). The homogeneous yellow/orange dispersion was then purified as described below. Purification involved 3 centrifugation steps using 50 mL centrifuge tubes. The crude, room temperature product (ie: toluene solution) was transferred from the reaction vessel to one centrifuge tube with toluene. The total volume (ca. 20 mL) was then divided evenly over two centrifuge tubes, each was diluted to 20 mL with toluene and precipitated with the addition of 25 ml ethanol. Centrifugation at 7000 rpm for 7 minutes yielded yellow tinted supernatants and orange pellets. The supernatants were decanted and the pellets dispersed in 15 mL toluene before adding 30 mL EtOH to each

centrifuge tube. Centrifugation at 7000 rpm for 7 minutes yielded yellow tinted supernatants and orange pellets. The supernatants were decanted and the pellets dispersed in 7 mL toluene before adding 38 mL EtOH to each centrifuge tube. Centrifugation at 7000 rpm for 10 minutes yielded yellow tinted supernatants and orange pellets which were dried in vacuo at 55 °C overnight to achieve solid orange product.

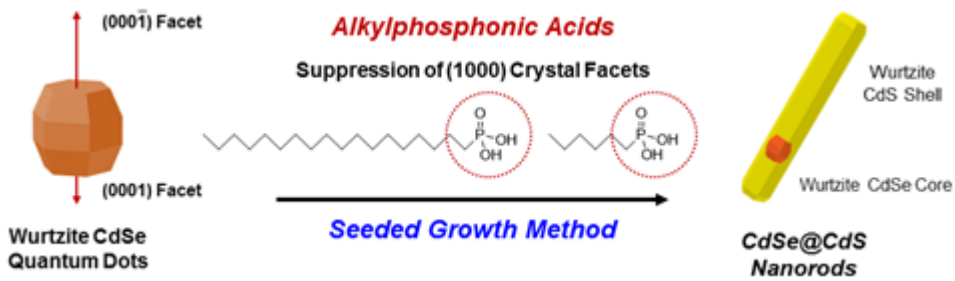

Scheme 2.2.1 Schematic illustration for the strategy of the synthesis of CdSe@CdS core@shell nanorods from wurtzite CdSe quantum dots and the use of alkylphosphonic acids by seeded growth method.

2.2.2 Results and Discussions

CdSe@CdS core@shell colloidal semiconductor nanocrystals with nanorod shapes were synthesized by the modified procedure from the literature.[29] For the synthesis, strategies described in previous paragraphs were used: using wurtzite CdSe quantum dot crystal structures and alkylphosphonic acids as organic ligands with seeded growth approach, as shown in Scheme 2.2.1.

First, wurtzite CdSe quantum dots, which will be further used as seeds to grow CdS nanorods, were synthesized by using CdO as cadmium precursor and n-octadecylphosphonic acids as ligands. Here, trioctylphosphine (TOP) and trioctyphopshpine oxide (TOPO) are used for the reaction media as coordinating solvents. The role of coordinating solvents is to control the overall reaction for the nucleation and growth of wurtzite CdSe quantum dots. Non-coordinating solvents such as 1-octadecene have no functional groups to participate in the reaction. Here, degassing step is very important to achieve monodisperse colloidal semiconductor nanocrystals with highly uniform morphology. When degassing step was not enough, before the injection of precursors, the color of reaction mixture is brown. In general, for the synthesis of colloidal semiconductor nanocrystals, nucleation and growth is typically done within a minute. Our strategy for the synthesis of wurtzite CdSe quantum dots with small size was to get minimum reaction time for the nucleation and growth of wurtzite CdSe quantum dots.

Therefore, heating mantle was removed at 380 °C and SeTOP was swiftly injected when the temperature reaches at 370 °C, followed by rinsing with acetone.

As-synthesized wurtzite CdSe quantum dots were dissolved in organic solvents with low boiling temperature such as chloroform or dichloromethane. For the synthesis of CdSe@CdS nanorods, wurtzite CdSe quantum dots and elemental sulfur with TOP were mixed as stock solution prior to the reaction. That is, for the seeded growth of CdSe@CdS nanorods, the amount of wurtzite CdSe quantum dots is the key factor to control the length of CdSe@CdS nanorods. Amount of precursors and ligands are the same, but only the amount of wurtzite CdSe quantum dots were controlled, which are the nucleation and growth sites for CdS nanorod region. Less amount of wurtzite CdSe quantum dots in stock solution of CdSeSTOP resulted in CdSe@CdS nanorods with longer length. Excess amount of wurtzite CdSe quantum dots resulted in shorter CdSe@CdS nanorods, as shown in Figure 2.2.1 and 2.2.2.

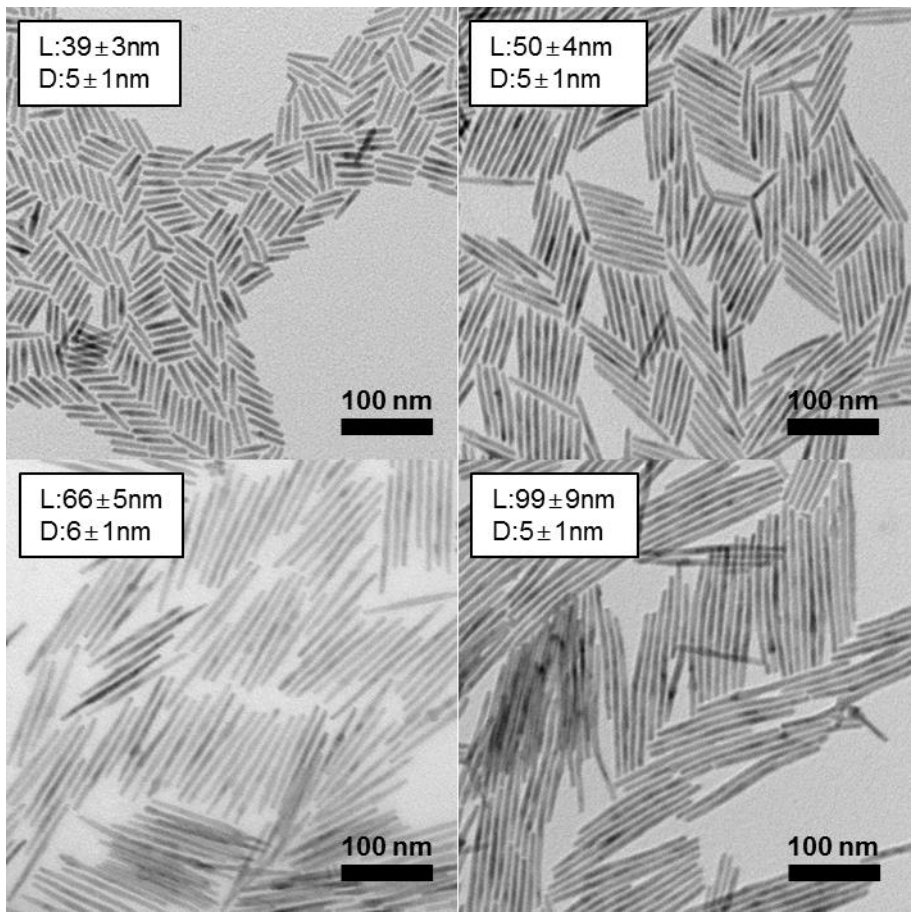

Figure 2.2.1 TEM images of CdSe@CdS nanorods with different lengths synthesized by seeded growth.

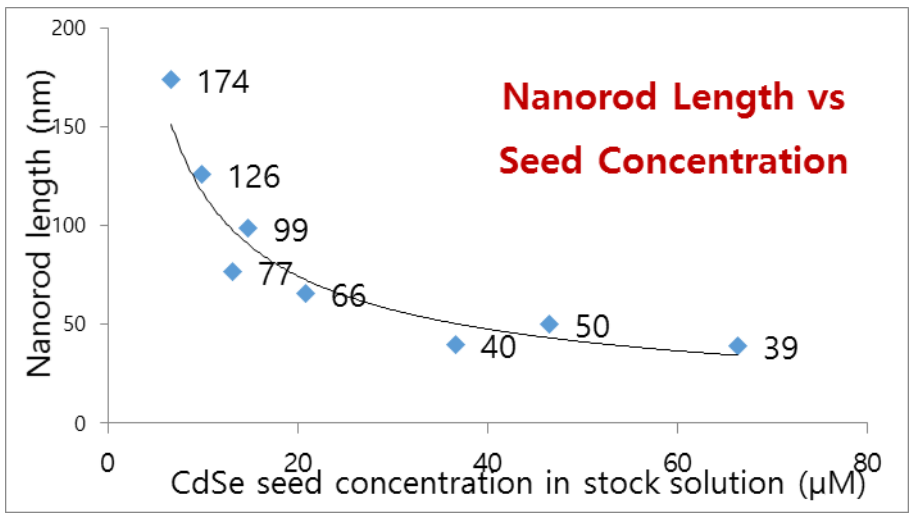

Figure 2.2.2 The length of CdSe@CdS nanorods with respect to the concentration of wurtzite CdSe quantum dots in CdSeSTOP stock solution.

2.2.3 Conclusions

CdSe@CdS core@shell nanorods were successfully synthesized by using wurtzite CdSe semiconductor quantum dots as seeds to grow wurtzite CdS shell region. Also, alkylphosphonic acids, which are well known to strongly bind to certain crystal facets, were used to suppress (100) and (110) crystal facets of wurtzite CdSe and CdS semiconductor nanocrystals. By controlling the concentration of wurtzite CdSe quantum dot seed stock solutions, the length of CdSe@CdS nanorods were successfully controlled.

2.3 Synthesis of CdSe Tetrapods by Continuous Precursor Injection Approach

This work was originally done by J. Lim et al[139]., followed by Y. Sung under supervision of Dr. Jaehoon Lim at Los Alamos National Laboratory, United States.

2.3.1 Experimental Session

Materials Cadmium Oxide (CdO, 99.95%) was purchased from Alfa Aesar. Selenium (Se, 99.99%), n-trioctylphosphine (TOP, 90%), 1-oleic acid (OA, 90%), 1-octadecene (ODE, 90%) and cetyltrimethylammonium bromide (CTAB, 99%) were purchased from Sigma Aldrich. Toluene and ethanol were purchased from Samchun Chemicals. All chemicals were used as purchased.

Preparation of Injection Solution For the preparation of cadmium oleate ($Cd(OA)_2$) solution, 12 mmol CdO, 10.8 mL OA and 6 mL ODE were placed in an 100mL 3-neck round flask equipped with a condenser. The reaction mixture was degassed under vacuum at 100 °C for degassing, followed by heating to 280 °C under Ar for 20 min to form an optically clear solution. The mixture was then cooled down to room temperature for further use. Separately, 12 mmol Se and 6 ml TOP were mixed in a 50 mL 3-neck round flask with a condenser and heated to 200 °C until powdered Se fully dissolved. After

SeTOP was cooled down to room temperature, 6 mL SeTOP solution was mixed with 14 mL $Cd(OA)_2$ solution for further injection.

Zincblende CdSe Quantum Dots Procedure for the synthesis of zincblende CdSe quantum dot seeds was adopted with a slight modification from the literature.[139] First, to a 100 mL 3-neck round flask equipped with a condenser, 1 mmol Se and 10 mL ODE were loaded and heated to 100 °C for degassing under vacuum. Under Ar, the reaction mixture was heated to 300°C for the injection of as-prepared $Cd(OA)_2$. At 300°C, 2.8 mL Cd(OA)2 and 7.2 mL ODE were injected to make the total volume of 20 mL and the reaction solution was reacted at 270 °C for 15 min. In common, spherical zincblende CdSe quantum dot seeds with ~5 nm diameter (1st exciton peak ~630 nm) were obtained, and this crude solution was used without further purification.

CdSe Tetrapods by Continuous Precursor Injection (CPI) Approach To a 100 mL 3-neck round flask equipped with a condenser, 5 mL zincblende CdSe seed solution, 2.25 mL OA, 1.5 mL TOP, 21.25 mL ODE and 0.21 mmol CTAB were loaded and heated to 100 °C under vacuum for degassing. Under Ar, the reaction mixture was heated to 270 °C for the injection of as-prepared $Cd(OA)_2$ and SeTOP injection solution, with the injection rate of 0.4 mL / min for 50 min by syringe pump. After the reaction, the crude mixture was loaded to centrifuge tube and equal amount of toluene and ethanol were added repeatedly for the precipitation of the products by centrifugation at 4000 rpm.

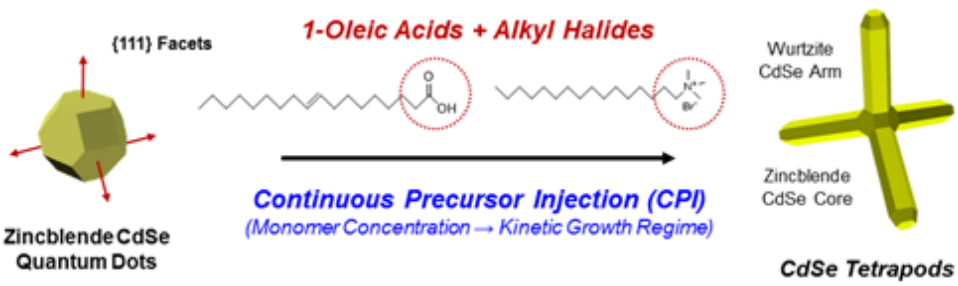

Scheme 2.3.1 Schematic illustration of the synthesis of CdSe tetrapods with using zincblende CdSe quantum dots as seeds, mixture of ligands of 1-oleic acids and CTAB, and continuous precursor injection approach within the kinetic growth regime.

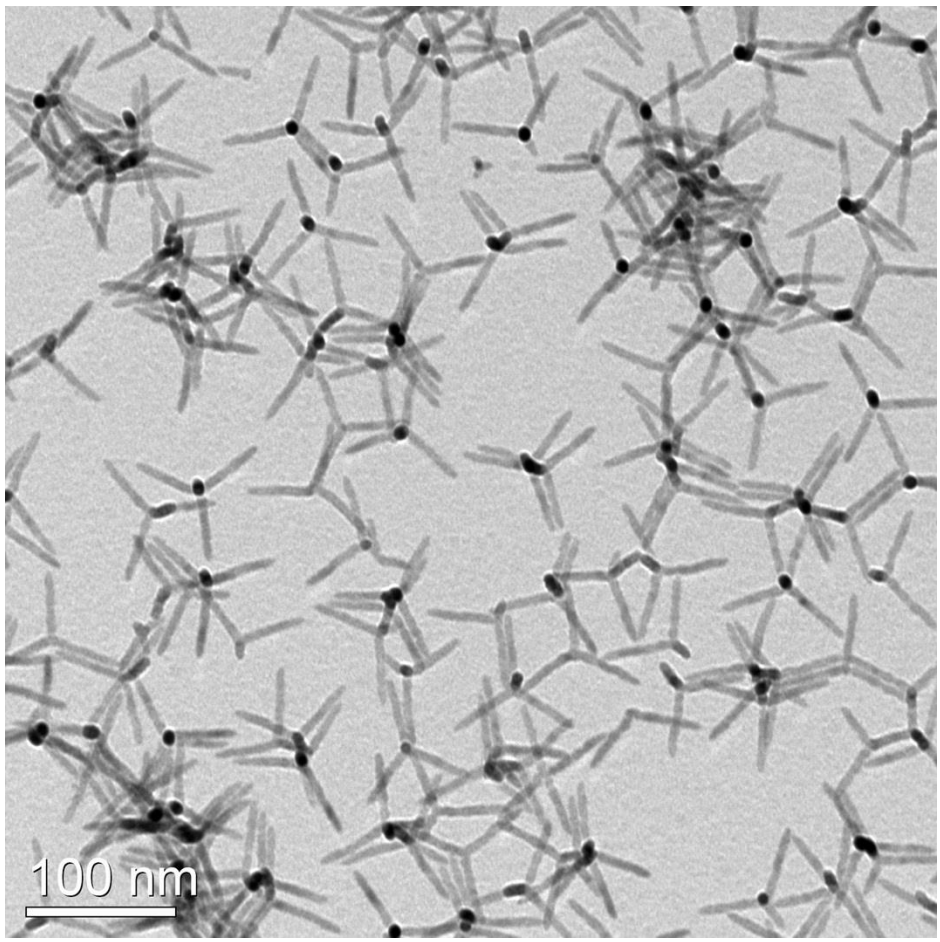

Figure 2.3.1 TEM image of CdSe tetrapods synthesized by continuous precursor injection approach.

2.3.2 Results and Discussions

Scheme 2.3.1 shows strategies for the synthesis of CdSe tetrapods. Figure 2.3.1 shows transmission electron microscopy image of CdSe tetrapods synthesized by continuous precursor approach previously reported by Lim et al.[139] Here, totally different strategy was used for the shape control of cadmium chalcogenide semiconductor nanocrystals: using zincblende CdSe quantum dots as seeds to grow wurtzite CdSe tetrapod arms, and the use of the ligand mixtures of alkylcarboxylic acids and alkyl halides, which in this case 1-oleic acid and cetyltrimethylammonium bromide (CTAB). Typical synthesis of colloidal semiconductor nanocrystals by hot injection approach consist of the nucleation and growth in thermodynamic growth regime, where burst nucleation and slow growth is important. There are reports on the synthesis of colloidal semiconductor nanocrystals within kinetic growth regime, where they used magic size of nuclei and the monomer concentration to control the morphologies of CdSe nanocrystals. Therefore, suppression of certain crystal facets by strongly binding ligands such as alkylphosphonic acids are necessary for the synthesis of colloidal semiconductor nanocrystals with anisotropic shapes. Disadvantages of using alkylphosphonic acids come with economic issues, such as extremely high price with limited suppliers. Therefore, scale-up of the reaction is not easy. But, continuous precursor injection (CPI) approach uses typical organic ligands such as oleic acids and

alkyl halides, which are relatively cheap and easy to access, even with high morphological uniformity and shape selectivity over 90 %. Unlike thermodynamic growth regime, since the suppression of certain crystal facet is limited, the nucleation and growth is done within the kinetic growth regime. Within kinetic growth regime, instead of the suppression of certain crystal facets to grow wurtzite CdSe tetrapod arms, precisely accelerate the growth rate of certain crystal facets with control over monomer concentration.

First, zincblende CdSe quantum dots were synthesized by the decomposition of CdO to prepare cadmium oleate with 1-oleic acid and 1-octadecene as non-coordinating solvents. Here, elemental selenium was used as precursor, instead of SeTOP complex which react faster than elemental Se. Therefore, the growth time for the synthesis of CdSe is relatively longer than other typical synthesis. After the synthesis, as-synthesized zincblende CdSe quantum dots were used without purification steps. Therefore, successive removal of unreacted Se is very important for further synthesis of CdSe tetrapods, otherwise self-nucleation of CdSe quantum dots instead of the selective nucleation and growth of wurtzite CdSe tetrapod arms from zincblende CdSe quantum dots. Certain amount of TOP is necessary for the stable control over nucleation and growth of wurtzite CdSe tetrapod arms. Here, certain amount ratio between oleic acids and CTAB is very important to both maintain zincblende CdSe quantum dot structures as well as the

growth of wurtzite CdSe tetrapod arm region. When CTAB is introduced for the growth of wurtzite CdSe tetrapod arms, main Cd precursor, which in this case if cadmium oleate ($Cd(OA)_2$), certain amount of surface ligands of oleic acids is ligand-exchanged with CTAB, generating ligand-free Cd-halide sites, which control the overall reaction rate for the growth of wurtzite CdSe tetrapod arms. Also, since the reaction is done within the kinetic growth regime with very slow growth rate, the growth of wurtzite CdSe tetrapod arms show two different stages. First, injected Cd and Se are nucleated and grown toward (0001) direction, which decide the length of CdSe tetrapods. Once the growth of (0001) direction is done within this monomer concentration, which in this case the injection rate of Cd and Se, arm diameter starts to grow. This is observed by taking kinetic samples during the growth of wurtzite CdSe tetrapod arms by CPI approach, which are shown in Figure 2.2.3. At early stage, CdSe tetrapods with thin arm diameter are mostly synthesized. As the amount of injection precursor increases, the arm diameter starts to increase, which was confirmed by the first exciton peak from absorbance spectrum in Figure 2.2.2. In general, first exciton peak determines the size of colloidal semiconductor nanocrystals with confined geometry, which in this case the arm diameter of CdSe tetrapods. Therefore, red shift of the first exciton peaks during the synthesis explains that the arm diameter of CdSe tetrapods increase. Since the reaction time is relatively slow than

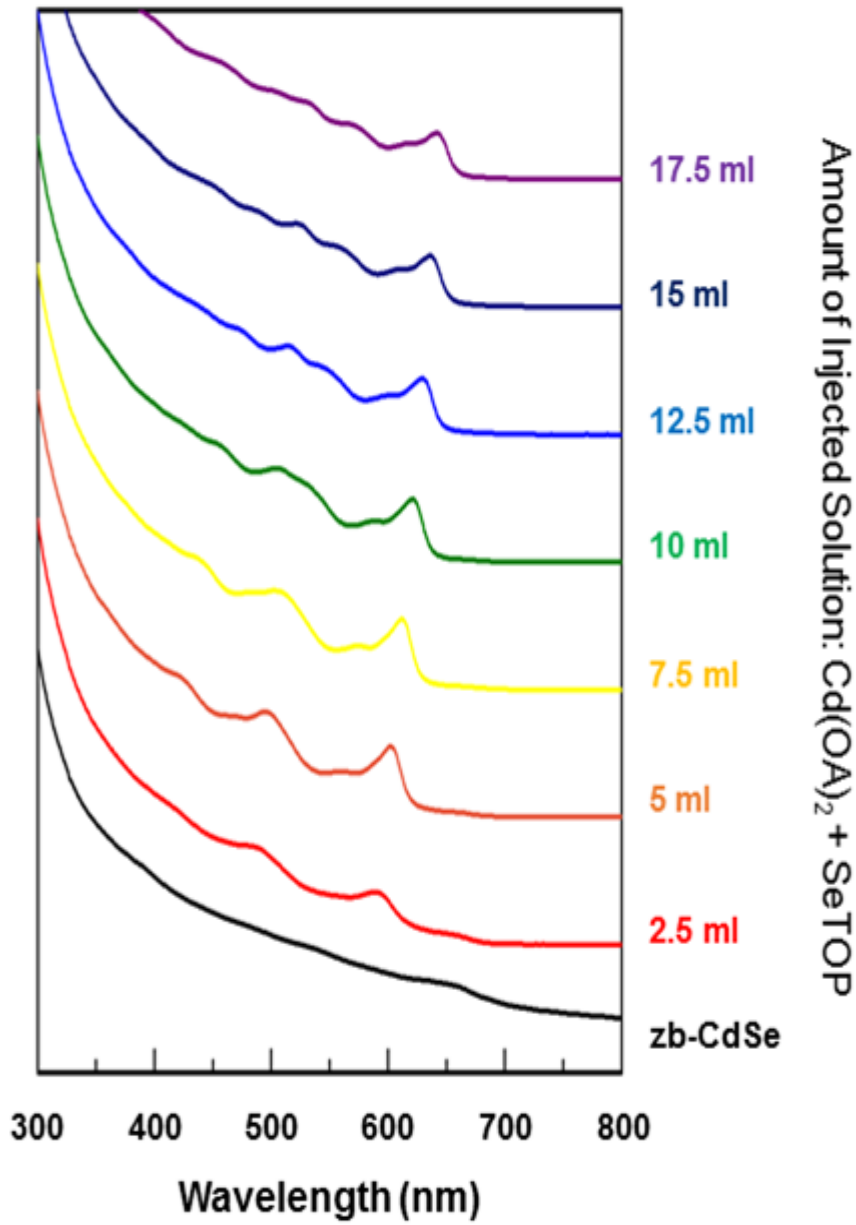

Figure 2.3.2 Real-time absorbance spectra during the synthesis of CdSe tetrapods by CPI approach.

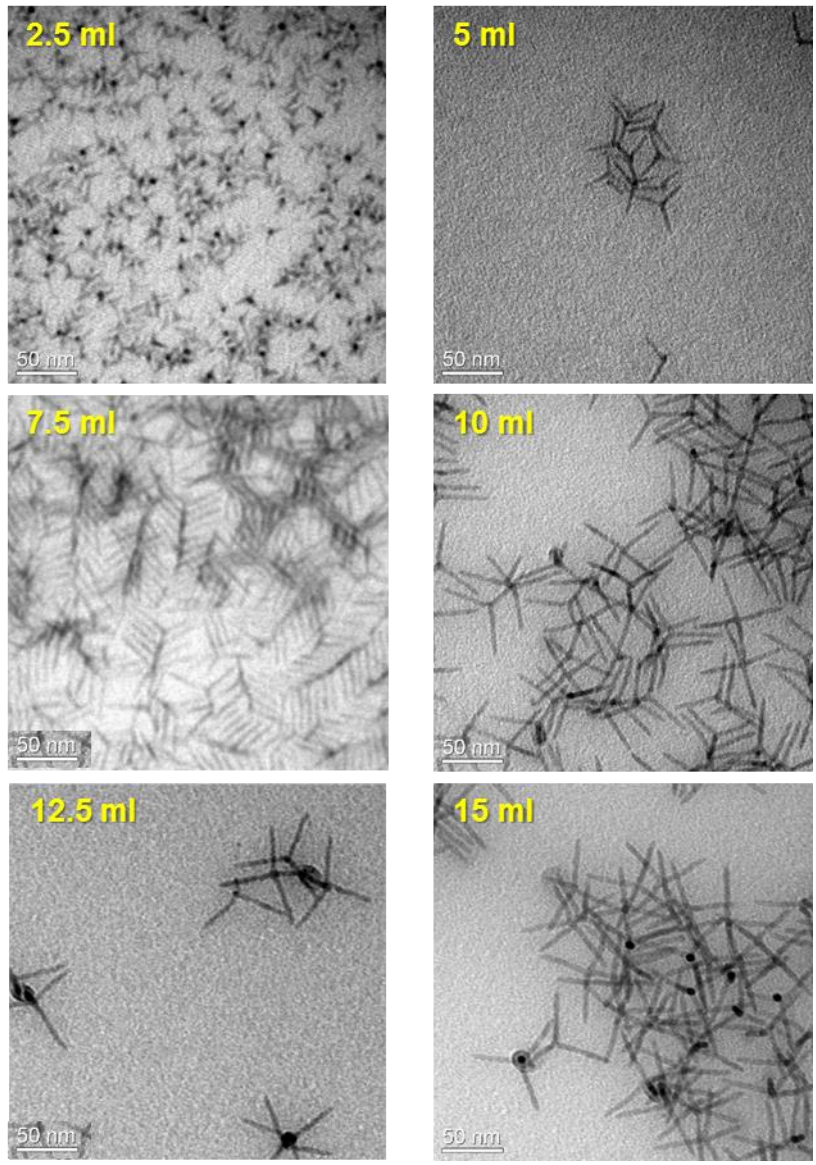

Figure 2.3.3 TEM images of kinetic samples during the growth of wurtzite CdSe tetrapod arms by CPI approach.

synthetic procedures by hot injection method or thermodynamic growth regime. Therefore, by monitoring the first exciton peak in real-time during the synthesis, we can precisely control the arm diameter of CdSe tetrapods by quenching the reaction at desired arm diameter. Also, the length of CdSe tetrapods are governed by the initial injection temperature and rate. It was studied that the typical temperature with respect to the injection rate determines the aspect ratio of CdSe tetrapods, and each injection temperature has limits for arm length of CdSe tetrapods. It is well known that the reaction temperature determines the diameter of colloidal semiconductor nanocrystals, that higher reaction temperature results in larger nanocrystals due to high energy for the nucleation and growth. Therefore, injection temperature determines the limit of arm diameter for CdSe tetrapods. Moreover, within the kinetic growth regime, the injection rate, which is related to the monomer concentration of the reaction mixture, corresponds to the growth rate of semiconductor nanocrystals. Therefore, high injection rate, which means the increased monomer concentration, resulted in longer wurtzite CdSe tetrapod arms. Here, the most important issue is the limit window for the nucleation and growth of CdSe tetrapods. Too much monomer concentration or excess monomers, which in this case is by faster injection rate and excess amount of precursors injected during the synthesis, resulted in self-nucleation and growth of CdSe quantum dots instead of wurtzite CdSe tetrapod arms.

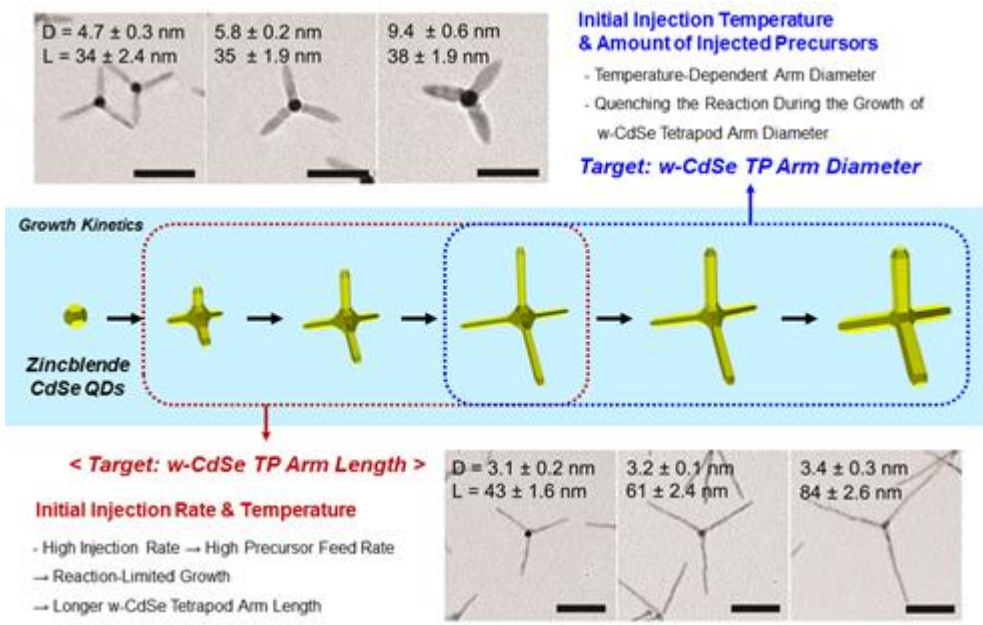

Figure 2.3.4 Strategies for the precise engineering of the morphology of CdSe tetrapods by CPI approach. This figure was redesigned from J. Lim et al. © American Chemical Society.

Therefore, by understanding the overall mechanism of CPI approach, it is possible to precisely engineer the morphologies of CdSe tetrapods with desired arm lengths or diameters.

2.3.3 Conclusions

CdSe tetrapods were successfully synthesized by using zincblende CdSe quantum dots as seeds to grow wurtzite CdSe tetrapod arms. Instead of alkylphosphonic acids for the typical use during the shape control of colloidal semiconductor nanocrystals, mixture of oleic acids and CTAB are introduced, with high shape selectivity and morphological uniformity. This also allowed for the scale-up synthesis of CdSe tetrapods. Continuous precursor injection (CPI) approach was used to synthesize highly-uniform and monodisperse CdSe tetrapods, which the morphology of CdSe tetrapods were controlled by monomer concentration within kinetic growth regime. Injection rate and temperature determine the arm length of CdSe tetrapods, and initial injection temperature and quenching the reaction with desired first exciton peak determine the arm diameter of CdSe tetrapods. Preventing the self-nucleation and growth of CdSe nanocrystals by understanding the overall synthetic mechanism of CPI approach is important. This allow to precisely engineer the morphologies of CdSe tetrapods, with possibilities to further extend into other anisotropic shapes with gram-scale capability.

Chapter 3. Metal-Semiconductor Heterostructured Nanocrystals

3.1 Introduction

For the preparation of colloidal metal-semiconductor heterostructured nanocrystals, it is expected that the nucleation and growth of metals at the surface of semiconductor nanocrystals mostly done at the certain surface sites with high energy at semiconductor nanocrystals.[42, 153-155] During the synthesis of colloidal semiconductor nanocrystals, ligands are used to passivate the overall surface of semiconductor nanocrystals. Chemical structures of ligands will hugely influence the surface chemistry or behavior of ligands, such as packing density. Colloidal semiconductor nanocrystals consist of the exposure of different crystal facets, which are the spherical morphologies or curvature structures at the termini of anisotropic shapes. These certain crystal facets could have less passivation of ligands. Also, due to the synthetic issues, lattice defects such as lattice mismatches are observed in colloidal semiconductor nanocrystals synthesized by wet chemistry. Therefore, it is hard to design and control the morphologies of colloidal metal-semiconductor heterostructured nanocrystals since the nucleation and growth mostly start from defect sites of semiconductor nanocrystals. Therefore, intentional

defects are sometimes introduced for the incorporation of metal nanocrystals at the surface of semiconductor nanocrystals.[1, 42, 154, 156-167]

Efforts to discover nucleation and growth mechanisms of colloidal metal-semiconductor heterostructured nanocrystals have been made by synthetic accessibilities with computational simulations. In the case of colloidal semiconductor nanocrystals with anisotropic shapes, it is observed that the nucleation and growth of metal nanocrystals start from the termini of semiconductor nanocrystals. Depending on the type of metal precursors, different morphologies of colloidal metal-semiconductor heterostructured nanocrystals are observed.

There are two main approaches for the incorporation of metal nanocrystals onto colloidal semiconductor nanocrystals. The most widely used method is by solution synthesis, and examples are shown in Figure 3.3.[40, 46, 50-51, 76, 157-158, 165, 167-173] During the synthesis of metal nanocrystals, simply by introducing colloidal semiconductor nanocrystals as nucleation and growth sites for metal nanocrystals, metal nanocrystals spontaneously nucleate and grow at the surface defect sites of colloidal semiconductor nanocrystals by the reduction of metal precursors by reducing agents with organic ligands. Self-nucleation and growth of metal nanocrystals are successfully eliminated by selective purification steps. Depending on the surface chemistry of colloidal semiconductor nanocrystals, which in this case types of ligands

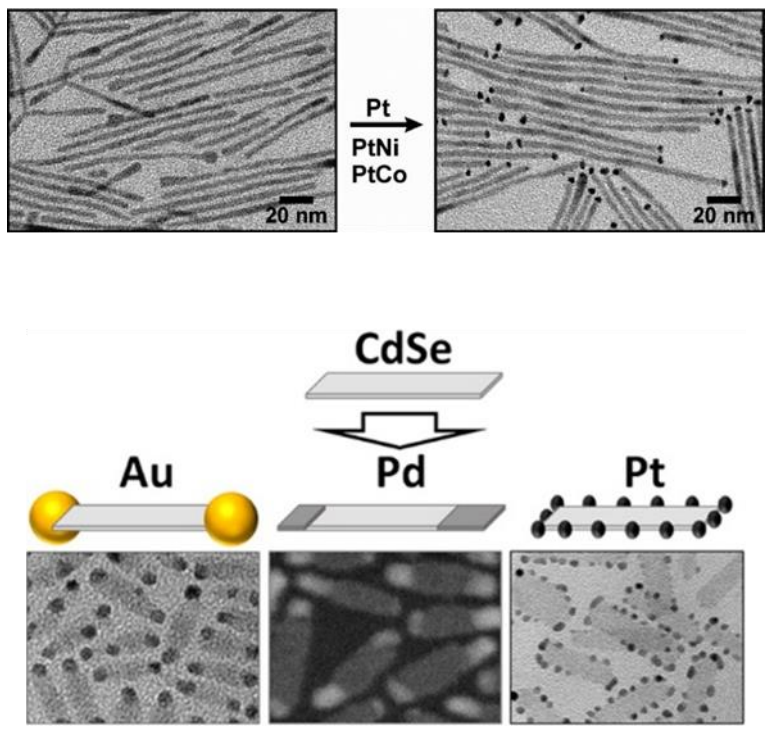

Figure 3.3 Incorporation of metal nanocrystals on colloidal semiconductor nanocrystals with anisotropic shapes such as nanorods and nanoplatelets. © American Chemical Society.

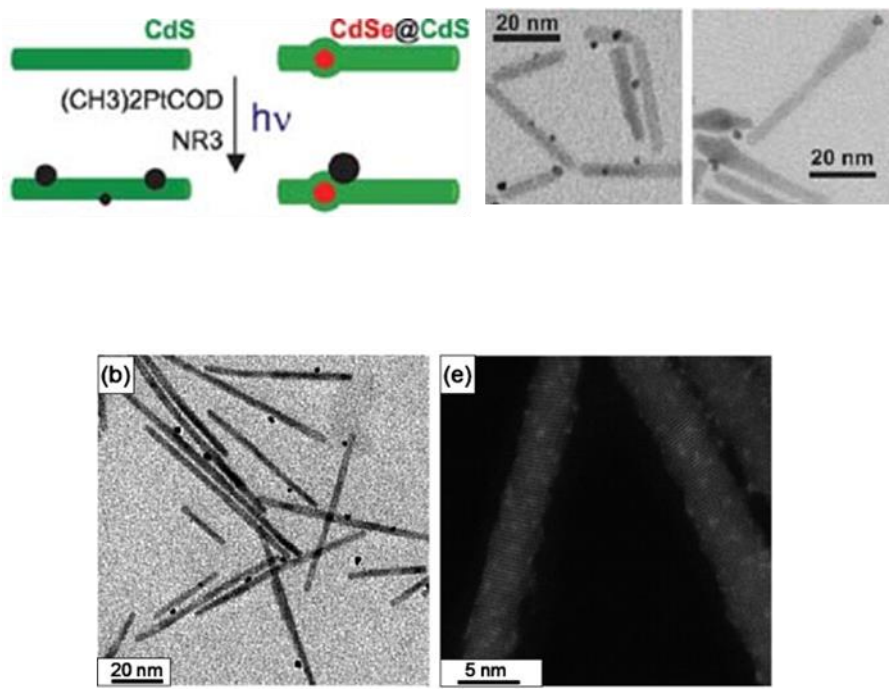

Figure 3.4 Metal-semiconductor heterostructured nanocrystals prepared by photoirradiation method. © Wiley-VCH © American Institute of Physics.

passivating at the surface of semiconductor nanocrystals or lattice defect sites, metal nanocrystals are incorporated with various morphologies of colloidal semiconductor nanocrystals such as nanorods, tetrapods, and nanoplatelets. Another method for the incorporation of metal nanocrystals are by photoirradiation.[43, 79, 144, 158, 174-179] Colloidal semiconductor nanocrystals are dispersed in solvents with metal precursors, followed by photoirradiation of reaction mixtures to induce defect sites at the surface of colloidal semiconductor nanocrystals, meanwhile initiating the nucleation and growth of metal nanocrystals. Different morphologies of metal-semiconductor heterostructured nanocrystals are achieved by controlling irradiation intensity and time. But, this method is not suitable for the precise control over number density and size of metal nanocrystals incorporated with semiconductor nanocrystals.

3.2 Tipping of Primary and Secondary Metal Nanocrystals at CdSe@CdS Nanorod Termini

This work was done under collaboration with M. M. Bull, L. J. Hill, and Prof. J. Pyun at the Department of Chemistry & Biochemistry, University of Arizona, United States.

3.2.1 Experimental Session

Materials As-synthesized CdSe@CdS nanorods and PS-COOH polymeric ligands were used after purification. Platinum acetylacetonate ($Pt(acac)_2$, 97%), cobalt carbonyl ($Co_2(CO)_8$, 90%), 1-oleic acid (OA, 90%), oleylamine (90%), 1,2-hexadecanediol (90%) and 1,2-dichlorobenzene (anhydrous, 99%) were purchased from Sigma Aldrich. Phenyl ether (90%) was purchased from TCI. Toluene and ethanol were purchased from Samchun Chemicals. All chemicals were used as purchased.

Tipping of Pt Nanocrystals onto CdSe@CdS Nanorods The synthesis of platinum tipped CdSe@CdS nanorods was adapted from the literature. To a 100 mL 3-neck round bottom flask, were added 1,2-hexadecanediol (0.043 g), 0.2 mL 1-oleic acid (0.2 mL), oleylamine (0.2 mL) and phenyl ether (10 mL), and heated to 80 °C. At 80 °C, the reaction mixture were degassed for 5 min under vacuum. Under Ar, the reaction mixture was heated to 225 °C.

Meanwhile, stock solution of as-synthesized CdSe@CdS nanorods (25 mg), platinum acetylacetonate (25 mg), both dissolved in 1,2-dichlorobenzene (1.5 mL) with gentle sonication. At 225 °C 1.5 mL of stock solution was swiftly injected, followed by the growth time of 8 min. The reaction mixture was cooled down to room temperature, while adding toluene (5 mL) to prevent solidification of the reaction mixture. Selective purification was necessary to remove free Pt nanocrystals with mild centrifuge condition. The crude product was transferred to 50 mL centrifuge tube, followed by adding toluene (35 mL) and ethanol (15 mL). Centrifugation was conducted with 2500 rpm for 12 min, 2 times. Finally, brown product was dissolved in desired solvents for further experiments.

Secondary Tipping of Cobalt Nanocrystals onto Pt-Tipped CdSe@CdS Nanorods Carboxylic acid end-functionalized polystyrene was prepared by synthetic procedure previously reported by J. Pyun et al. As-synthesized Pt-tipped CdSe@CdS nanorods (25 mg) were dissolved in 20 mL of 1,2-dichlorobenzene. PS-COOH polymeric ligands were dissolved in separate 20 mL of 1,2-dichlorobenzene. To a 100 mL 3-neck round bottom flask, were added as-prepared reaction solutions. Meanwhile, 250 mg of cobalt carbonyl ($Co_2(CO)_8$) were dissolved in 2 mL of 1,2-dichlorobenzene with gentle mixing. Sonication was strictly prohibited due to the decomposition of cobalt

precursors. The reaction mixture was heated to 160 °C under Ar, followed by the injection of cobalt precursor with the growth time of 1 hr. Purification involved one magnetic filtration step. The nanorods were precipitated via dropwise addition into vigorous stirring methanol (500 mL) to yield a black precipitate, which was collected by sedimentation using a standard AlNiCo magnet and decanting of the methanol phase.

Formation of Cobalt Oxide Tips onto Pt-CdSe@CdS Nanorods As-synthesized Pt@Co-CdSe@CdS heterostructured nanorods were dissolved in 50 mL of 1,2-dichlorobenzene, followed by transfer into 3-neck round bottom flask. The reaction mixture was heated to 173 °C, followed by bubbling with oxygen for overnight. The crude product was purified with adding excess amount of methanol.

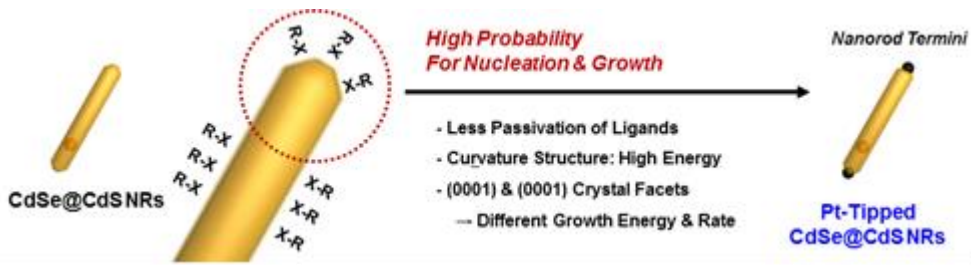

Scheme 3.2.1 Schematic illustration on Pt-tipping of CdSe@CdS semiconductor nanorods.

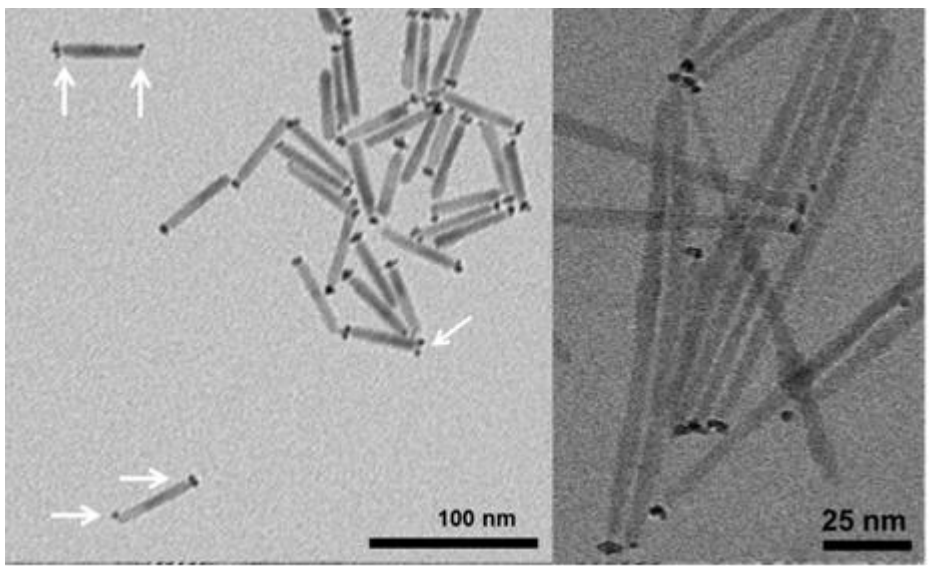

Figure 3.2.1 TEM images of Pt-tipped CdSe@CdS colloidal metal-semiconductor heterostructured nanorods.

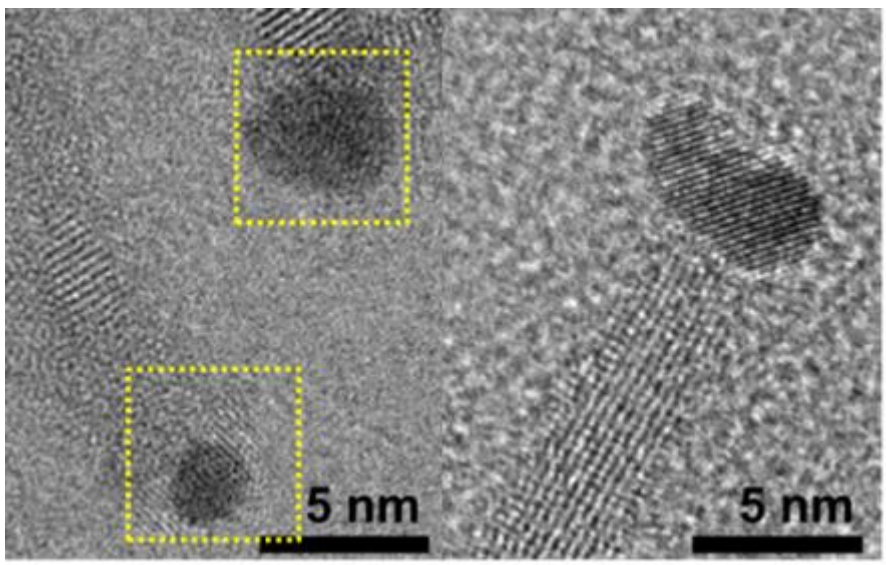

Figure 3.2.2 HR-TEM images of Pt-tipped CdSe@CdS colloidal metal-semiconductor heterostructured nanorods.

3.2.2 Results and Discussions

As-synthesized CdSe@CdS nanorods were capped with alkylphosphonic acids, which are commonly used for the shape control known to strongly bind to most crystal facets of colloidal semiconductor nanocrystals, which are explained in Scheme 3.2.1. Due to high chance for metal nanocrystals to nucleate and grow at the termini of CdSe@CdS semiconductor nanorods, platinum nanocrystals were nucleated and grown at the termini of as-synthesized CdSe@CdS nanorods, which are shown in Figure 3.2.1 and 3.2.2. By HR-TEM images, face-centered cubic Pt nanocrystals were successfully tipped at the ends of CdSe@CdS nanorods. As-synthesized Pt-tipped CdSe@CdS nanorods were then used for the secondary growth of metal nanocrystals, which in this case of cobalt. Interestingly, when Pt-CdSe@CdS nanorods were introduced for the synthesis of ferromagnetic cobalt nanoparticles with polymeric ligands, cobalt nanoparticles selectively nucleated and grown at the Pt sites of Pt-CdSe@CdS heterostructured nanocrystals, which are shown in Scheme 3.2.2. Simply by controlling the reaction temperature for the nucleation and growth of cobalt nanoparticles, the size of cobalt nanoparticles was controlled, as well as the magnetic properties changed from superpara- to ferro-. Simply by bubbling with oxygen of Pt@Co-CdSe@CdS heterostructured nanocrystals yielded cobalt oxide-tipped Pt-CdSe@CdS heterostructured nanocrystals. Here, the size of

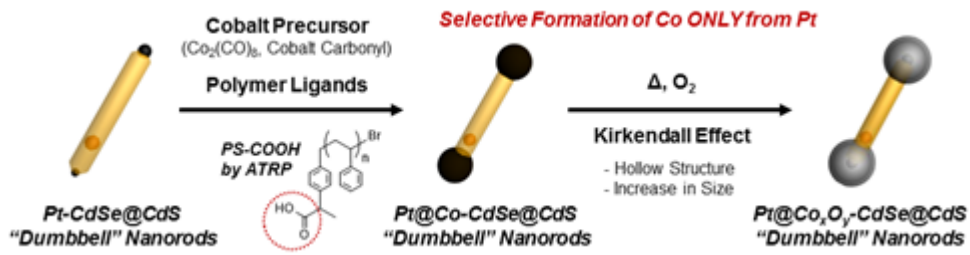

Scheme 3.2.2 Schematic illustration of primary and secondary deposition of metal nanocrystals onto semiconductor nanocrystals.

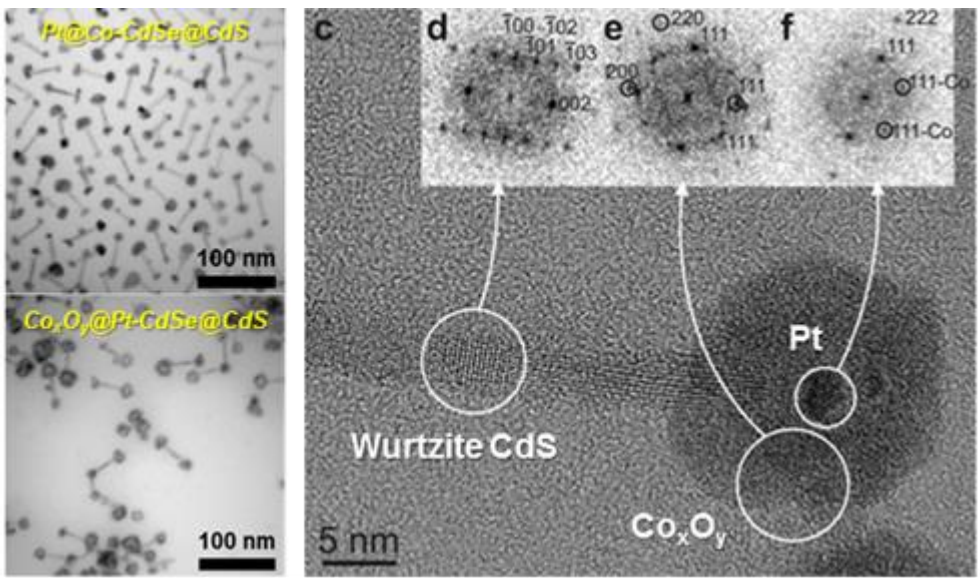

Figure 3.2.3 Normal and high-resolution TEM images of Pt@Co-CdSe@CdS and Pt@Co_xO_y-CdSe@CdS heterostructured nanocrystals.

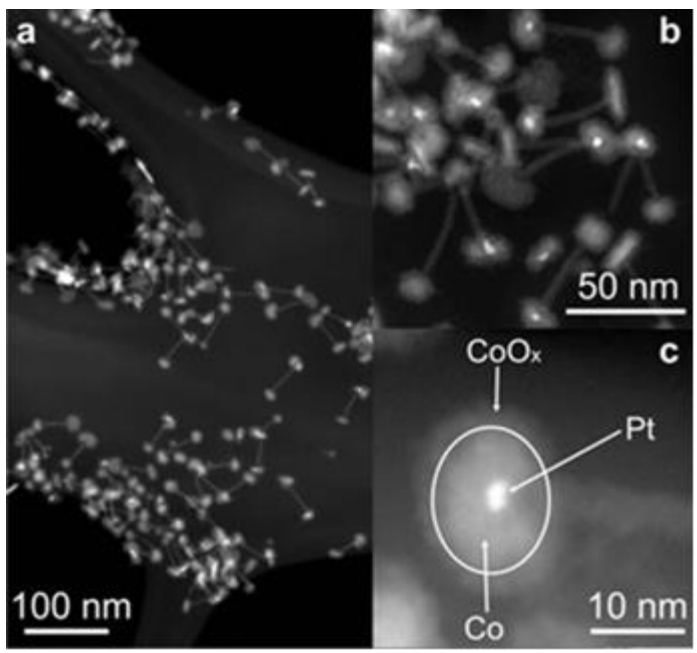

Figure 3.2.4 HAADF-STEM images of Pt@Co-CdSe@CdS and Pt@CoxOy-CdSe@CdS heterostructured nanocrystals.

cobalt oxide was slightly increased, due to the Kirkendall effect by the different diffusion rate of metal atoms consisting the metal nanoparticles, while forming hollow structures, which are shown in Figure 3.2.3 and 3.2.4. For the deposition of secondary metal nanoparticles onto metal-semiconductor heterostructured nanocrystals, primary metal-tipping step is the most important for the final morphology of metal-semiconductor heterostructured nanocrystals, which are shown in Figure 3.2.5. When no platinum tips were introduced at the surface of CdSe@CdS colloidal semiconductor nanocrystals, individual cobalt nanocrystals were synthesized instead of the formation at nanocrystals. When the reaction time was kinetically controlled for the nucleation and growth of Pt nanocrystals at termini of CdSe@CdS nanorods to exhibit one Pt tips at one end, cobalt nanoparticles were only formed at one end of Pt-CdSe@CdS heterostructured nanorods. When the nucleation and growth time for Pt nanocrystals were fully conducted, Pt nanocrystals were tipped at both ends of CdSe@CdS nanorods, followed by the formation of cobalt nanoparticles at both ends of Pt-CdSe@CdS heterostructured nanorods. Depending on the morphology of Pt@Co-CdSe@CdS heterostructured nanorods, self-assembly behavior due to ferromagnetic cobalt nanoparticles were observed, which are shown in Figure 3.2.6. When ferromagnetic cobalt nanoparticles were tipped at both ends of Pt-CdSe@CdS heterostructured nanorods, so called “dumbbell”

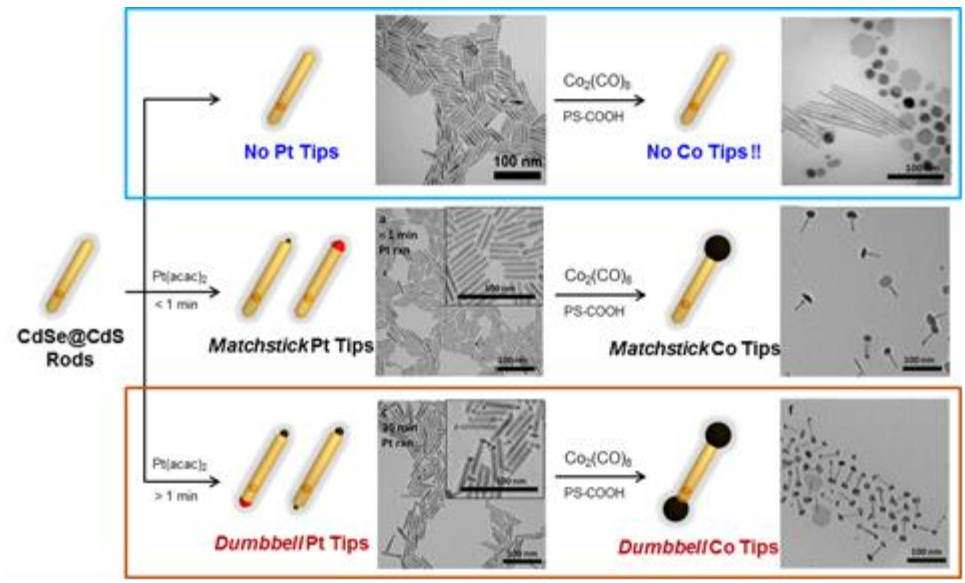

Figure 3.2.5 Nucleation and growth kinetics of primary Pt and secondary Co nanocrystals onto CdSe@CdS colloidal semiconductor nanocrystals.

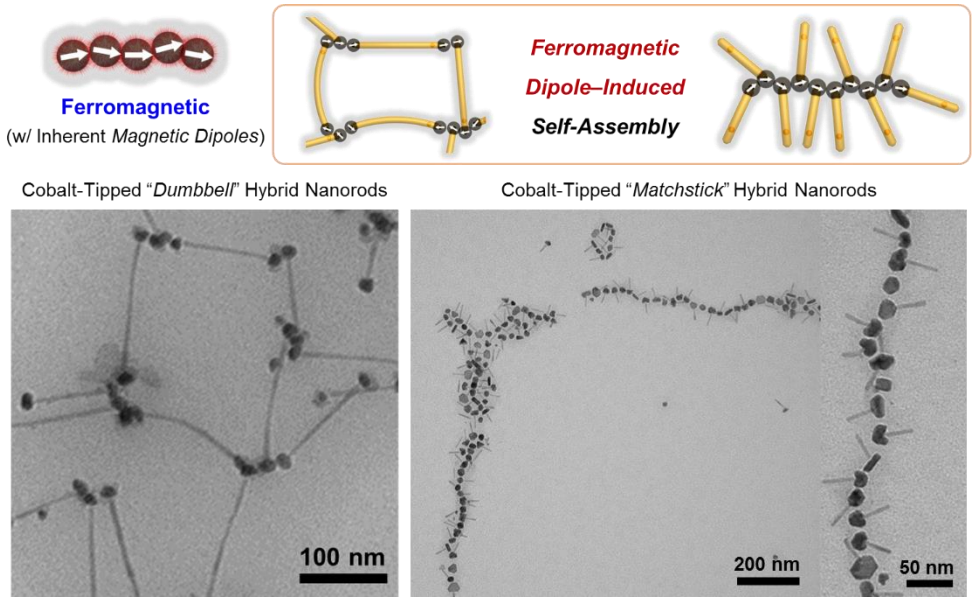

Figure 3.2.6 Self-assembly of cobalt-tipped Pt-CdSe@CdS heterostructured nanocrystals.

structures, self-assembly of network-like structured were observed.[180-184] When ferromagnetic cobalt nanoparticles were only tipped at one end of Pt-CdSe@CdS heterostructured nanocrystals, so called “matchstick” structures, Pt@Co-CdSe@CdS heterostructured nanorods showed self-assembly structures like polymeric chains, which is called colloidal polymerization technique. Oxidation of these heterostructured nanorod assemblies resulted in the formation of fixed morphologies with cobalt oxide nanoparticles, which are colloidal polymers by colloidal polymerizations of cobalt-tipped Pt-CdSe@CdS heterostructured nanocrystals.

3.2.3 Conclusions

Methods to selectively synthesize cobalt nanoparticles and cobalt oxide nanoparticle tipped CdSe@CdS nanorods with controlled matchstick or dumbbell morphologies were established via a five-step total synthesis. The morphology and connectivity of cobalt nanoparticle tips were shown to evolve as a direct consequence of the conditions used to obtain Pt-tipped nanorod precursors, which gave mixtures of matchstick and dumbbell Pt-tipped morphologies. These precursors were found to drive nearly quantitative CoNP-tipped dumbbell formation due to either chemical activation of the untipped terminus or trace amounts of platinum at the apparently untipped terminus of PtNP-tipped matchsticks. This synthetic methodology, along with detailed synthetic procedures, offers an alternative strategy to prepare heterostructured nanorods with core□shell nanoparticle tips that enable the creation of nanoscopic semiconductor or Schottky-type junctions. Future efforts will examine the electronic structure and photoelectrochemistry of these nanocomposite materials.

3.3 Direct Decoration of Metal Nanocrystals onto CdSe Tetrapods by CPI Approach

3.3.1 Experimental Session

Materials As-synthesized CdSe tetrapods by CPI approach were used after purification. Platinum acetylacetonate ($Pt(acac)_2$, 97%), 1-oleic acid (OA, 90%), oleylamine (90%), 1,2-hexadecanediol (90%) and 1,2-dichlorobenzene (anhydrous, 99%) were purchased from Sigma Aldrich. Phenyl ether (90%) was purchased from TCI. Toluene and ethanol were purchased from Samchun Chemicals. All chemicals were used as purchased.

Decoration of Pt Nanoparticles onto CdSe Tetrapods Synthetic procedure for the decoration of Pt nanoparticles onto CdSe tetrapod side walls were adopted from the literature. To a 100 mL 3-neck round flask equipped with a condenser, 43 mg 1,2-hexadecanediol, 0.2 mL OA, 0.2 mL oleylamine and 10 mL phenyl ether were loaded and heated to 80 °C under vacuum for degassing. Under Ar, the reaction mixture were heated to 225 °C for further injection. Meanwhile, 25 mg as-synthesized CdSe tetrapods along with a controlled amount of platinum precursors, which were platinum acetylacetonate, were dissolved in 1 mL 1,2-dichlorobenzene for the injection solution. At 225 °C, the injection solution was injected into the reaction mixture and reacted for 8

min, followed by cooling down to room temperature and 5 mL toluene were injected under 100 °C to prevent further solidification of the products. The crude product solution was then transferred to a centrifuge tube, and a relative amount of ethanol and toluene was added to selectively remove free Pt nanoparticles with centrifugation at 2500 rpm.

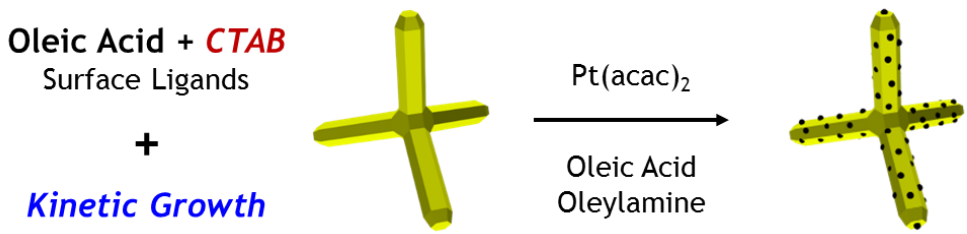

Scheme 3.3.1 Schematic illustration of the direct decoration of Pt nanocrystals onto the surface of CdSe tetrapods synthesized by CPI approach.

3.3.2 Results and Discussions

CdSe tetrapods synthesized by the continuous precursor injection (CPI) approach, previously reported by our group, showed the uniform decoration of Pt nanoparticles on the entire surface of CdSe tetrapod arms, which are shown in Scheme 3.3.1. First, the CdSe tetrapods were synthesized by using zincblende CdSe quantum dots as seeds, followed by using oleic acid and alkyl halides as mixed ligands for the growth of wurtzite CdSe tetrapod arms. Specific amount of alkyl halides, in the representative synthetic procedure (for the present case, cetyltrimethylammonium bromides were adopted as alkyl halide ligands), was necessary to maintain the growth of wurtzite CdSe arms within the kinetic growth regime. After several purification steps, as-synthesized CdSe tetrapods were used for the decoration of Pt nanoparticles with the procedure previously reported. Interestingly, we noted that Pt nanoparticles were nucleated and grown throughout the entire region of CdSe tetrapod arms, and the control of the amount of Pt precursors resulted in Pt nanoparticles of different size formed on the surface of CdSe tetrapod arms. Also, Au nanocrystals were nucleated and grown at the surface of CdSe tetrapods by CPI approach, with similar fashion to Pt decoration, which are shown in Figure 3.3.1. Typically, novel metal nanoparticles such as Au and Pt are known to nucleate at the surface sites of semiconductor nanocrystals of high energy, which are typically the termini of nanocrystals with

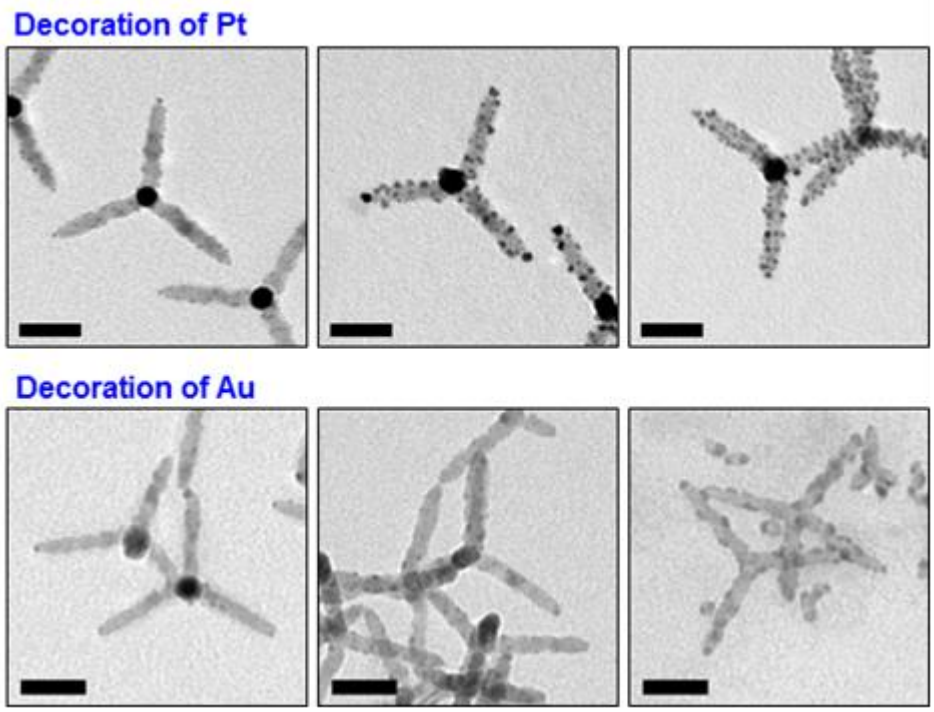

Figure 3.3.1 TEM images of Pt and Au-decorated CdSe tetrapods.

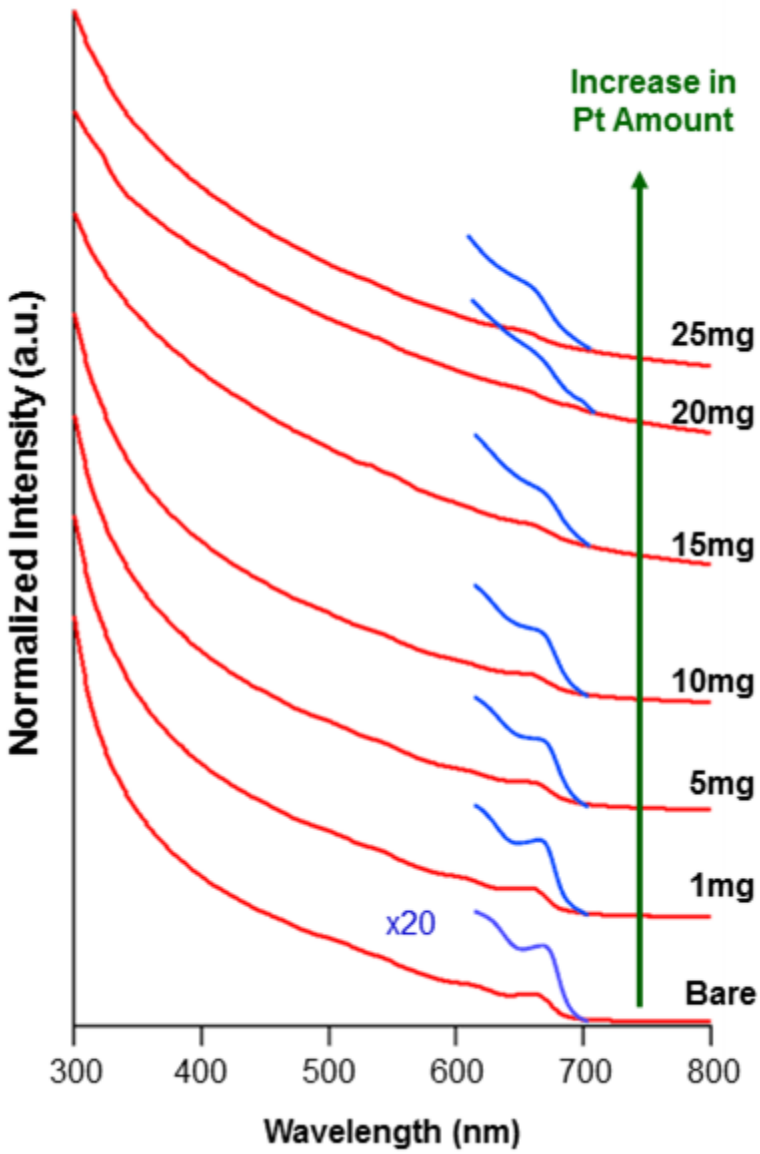

Figure 3.3.2 Absorbance spectra of Pt-decorated CdSe tetrapods with different amount of Pt precursors.

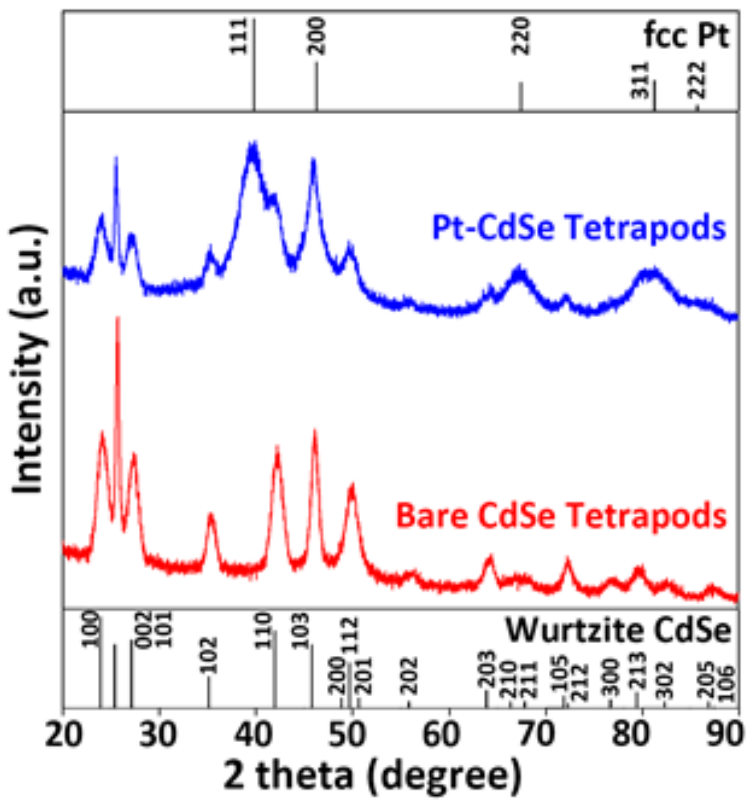

Figure 3.3.3 Powder XRD result of bare CdSe and Pt-decorated CdSe Tetrapods.

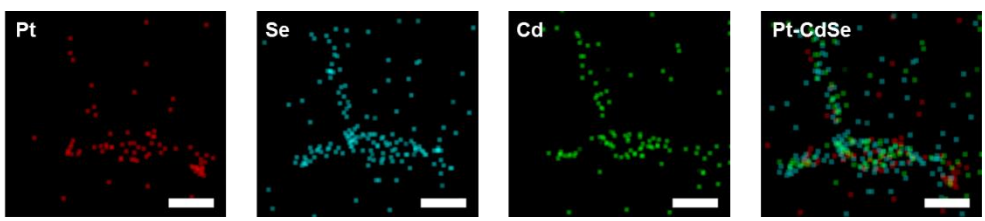

Figure 3.3.4 EDS mapping of Pt-decorated CdSe tetrapods (scalebar=20nm).

anisotropic shapes, or lattice defects generated during the synthesis. However, in the present case, uniform distribution of Pt nanoparticles decorated on the entire surface of CdSe tetrapod arms, as well as Au nanoparticles was observed. The Increase in the amount of Pt precursors resulted in the formation of larger Pt nanoparticles, yet maintaining the areal number density of Pt nanoparticles formed at the surface of CdSe tetrapods. From normal TEM images with the samples prepared with different amounts of Pt precursors, it is hard to distinguish the presence of Pt nanoparticles with extremely small size. However, the uniform decoration of Pt nanoparticles on the tetrapod arms was confirmed and will be explained later in more detail. We assume that when compared with previously reported methods to prepare CdSe nanocrystals with anisotropic shape, since a fixed amount of alkyl halides was introduced to the system during the arm growth, this procedure might lead to the surface chemical states different from other CdSe nanorods or tetrapods previously reported. We believe that the introduction of alkyl halides, which is crucial for the synthesis of CdSe tetrapods, enables the decoration of Pt nanoparticles throughout the entire surface of CdSe tetrapods due to Cd-halide ligand-free sites on the surface sidewalls of wurtzite CdSe tetrapod arms. In figure 3.3.2, by increasing the amount of Pt precursors for the nucleation and growth of Pt nanocrystals at the surface of CdSe tetrapods, while maintaining intrinsic absorption properties of CdSe tetrapods,

broadening of overall absorption spectra was observed, which is mainly due to Pt nanocrystals decorated onto CdSe tetrapod surface. Further powder XRD (Figure 3.3.3) and EDS mapping of elements confirmed the direct decoration of Pt nanocrystals at the surface of CdSe tetrapods prepared by CPI approach.

Mechanistic kinetics were taken for the direct decoration of Pt nanocrystals at the surface of CdSe tetrapods prepared by CPI approach, which are shown in Figure 3.3.5. At early stage, formation of individual free Pt nanocrystals was observed, followed by the nucleation and growth of Pt nanocrystals at the termini of CdSe tetrapods. After the certain period of growth time, finally the full decoration of Pt nanocrystals was observed. This explains that the formation of free Pt nanocrystals is faster, and there exist different surface energy for different crystal facets of CdSe tetrapods inside itself. Control experiments for the growth of second metal and previous reports by Pyun and Char et al. also support this argument that the decoration of Pt nanocrystals with extremely small size hard to figure out by microscopy techniques. During the Pt-tipping reaction with CdSe@CdS nanorods, when the reaction time for Pt to nucleate and grow was kinetically suppressed, only one Pt tip or no tip was observed by normal TEM, called the “activated” CdSe@CdS nanorods. Followed by the growth of second metal nanoparticles, which in this case were cobalt, the existence of Pt nanoparticles was indirectly

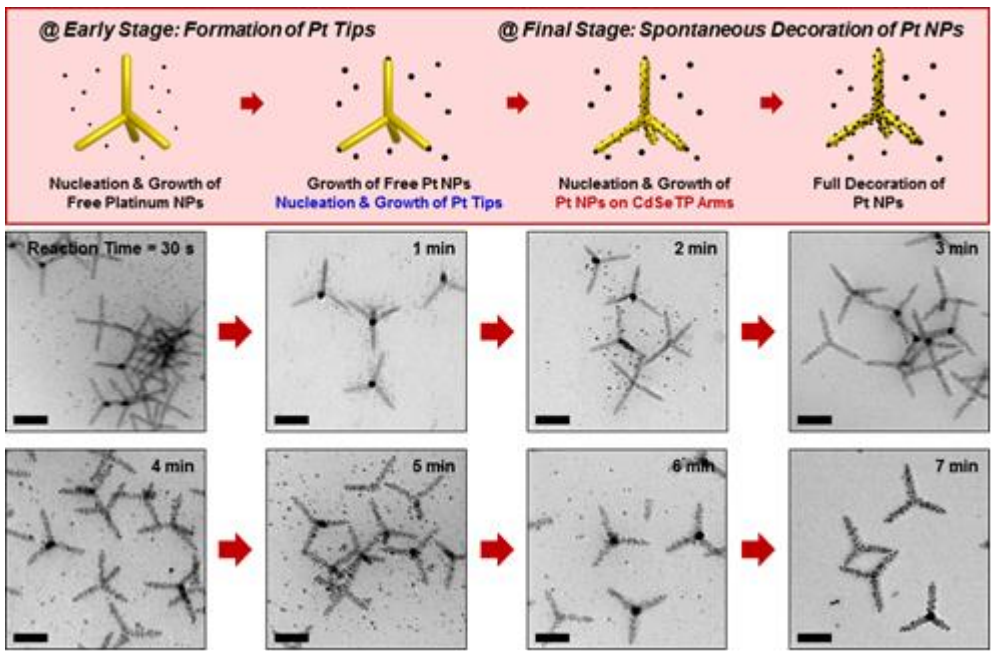

Figure 3.3.5 Nucleation and growth kinetics for the direct decoration of Pt nanocrystals onto CdSe tetrapods prepared by CPI approach (scalebar=20nm).

confirmed since cobalt nanoparticles were only formed epitaxially when Pt tips were first introduced to the ends of CdSe@CdS nanorods. Control experiment was performed by growing cobalt nanoparticles in the presence of bare CdSe tetrapods synthesized by the CPI approach and Pt-decorated CdSe tetrapods with an extremely low amount of Pt precursors. When no Pt nanoparticles were introduced to the CdSe tetrapods, no cobalt nanoparticles were formed at the surface of CdSe tetrapods. Although an extremely low amount of Pt precursors was introduced, the conformal decoration of cobalt nanoparticles on the Pt-decorated CdSe tetrapods was also observed. This result confirms the existence of Pt nanoparticles on the Pt-decorated CdSe tetrapods, but with very small in size.

3.3.3 Conclusions

CdSe colloidal semiconductor nanocrystals synthesized by CPI approach by using mixtures of oleic and alkyl halide ligands showed direct decoration of Pt nanocrystals at overall surface of CdSe tetrapods. Certain amount of CTAB ligands act as nucleation and growth sites for Pt nanocrystals. Kinetic data shows that preferential nucleation and growth of Pt nanocrystals at the termini of CdSe tetrapods exist, followed by overall decoration throughout the surface of CdSe tetrapods. This direct decoration is due to different surface chemistry from the synthesis of anisotropic shapes of colloidal semiconductor nanocrystals, and expected to guide to design novel structured of metal-semiconductor heterostructured nanocrystals for proper applications.

Chapter 4. Effect of Metal Cocatalysts on Photocatalytic Hydrogen Generation

4.1 Introduction

Colloidal metal-semiconductor heterostructured nanocrystals, in particular platinum-incorporated cadmium chalcogenide heterostructured nanocrystals are the most well-studied model system for photocatalysts in photocatalytic hydrogen generation reaction. Platinum has been used as catalysts in many research area as in the form of either nanocrystals or electrodes with proper energy level to quench electrons generated by various functional nanomaterials.[50, 52, 173, 185-192] In colloidal Pt-incorporated semiconductor nanocrystals, as-generated charge carriers are separated, and electrons are quenched in platinum sites due to their high electron density as well as proper energy level. Therefore, effect of metal cocatalysts in photocatalysts for photocatalytic hydrogen generation is important issue to be considered for the design of high-performance heterostructured photocatalysts.[43, 47, 86, 170, 175-178, 193-194]

Bang et al. reported on the geometric effect of single and double-tipped Pt onto CdSe semiconductor nanocrystals and their effect on photocatalytic hydrogen generation reaction.[170] Geometry of tipping of Pt nanocrystals at

the termini of CdSe nanorods to have either one or two Pt tips were controlled by controlling reaction parameters during the synthesis, such as the amount of Pt precursors and reaction time. As a result, two different Pt-CdSe heterostructured nanocrystals with different geometry, which majority of the morphology is single Pt-tipped CdSe nanorods or double Pt-tipped CdSe nanorods, showed different photocatalytic hydrogen generation behavior. Pt-CdSe heterostructured nanorods with less Pt nanocrystals showed higher photocatalytic efficiency. Moreover, Amirav et al., also demonstrated the number density effect of Pt metal cocatalysts onto CdSe@CdS core@shell nanorods, that less Pt nanocrystals show higher photocatalytic efficiency.[173] However, by carrier dynamics of Pt-decorated CdSe@CdS octapods by Conca et al., showed faster electron quenching properties with high number density of Pt-decorated CdSe@CdS octapods.

More recently, studies on the morphological effect of metal cocatalysts, such as Pt, Ni or Pd, on the performance of photocatalytic hydrogen generation have been reported. Metal cocatalysts with higher chance for the exposure of certain crystal facets show different photocatalytic behavior, as well as size of metal cocatalyst. Therefore, study on the effect of metal cocatalysts on colloidal metal-semiconductor heterostructured nanocrystals as photocatalysts in photocatalytic hydrogen generation reaction is essential.

4.2 Effect of Pt Nanocrystal Size on Photocatalytic Hydrogen Generation

In this work, carrier dynamics of Pt-decorated CdSe tetrapods were done under collaboration with M. Karakus and Dr. E. Canovas at Max Planck Institute for Polymer Research, Germany.

4.2.1 Experimental Session

Materials Cadmium oxide (CdO, 99.95%) was purchased from Alfa Aesar. Selenium (99.99%, powder), n-triocytylphosphine (TOP, 90%), oleic acid (OA, 90%), 1-octadecene (ODE, 90%), 1,2-hexadecanediol (90%), oleylamine (70%), platinum(II) acetylacetonate (Pt(acac)2, 97%), 1,2-dicholrobenzene (anhydrous, 99%), 11-mercaptoundecanoit acid (MUA, 95%), tetramethylammoniumhydroxide pentahydrate salt (>97%) and cetyltrimethylammonium bromide (CTAB, 99+%) were purchased from Sigma Aldrich. Phenyl ether (90%) was purchased from TCI. Toluene, methanol and ethanol were purchased from Samchun Chemicals. All chemicals were used as purchased.

Decoration of Pt Nanoparticles onto CdSe Tetrapods Synthetic procedure for the decoration of Pt nanoparticles onto CdSe tetrapod side walls were adopted from the literature. To a 100 mL 3-neck round flask equipped with a

condenser, 43 mg 1,2-hexadecanediol, 0.2 mL OA, 0.2 mL oleylamine and 10 mL phenyl ether were loaded and heated to 80 °C under vacuum for degassing. Under Ar, the reaction mixture were heated to 225 °C for further injection. Meanwhile, 25 mg as-synthesized CdSe tetrapods along with a controlled amount of platinum precursors, which were platinum acetylacetonate, were dissolved in 1 mL 1,2-dichlorobenzene for the injection solution. At 225 °C, the injection solution was injected into the reaction mixture and reacted for 8 min, followed by cooling down to room temperature and 5 mL toluene were injected under 100 °C to prevent further solidification of the products. The crude product solution was then transferred to a centrifuge tube, and a relative amount of ethanol and toluene was added to selectively remove free Pt nanoparticles with centrifugation at 2500 rpm.

Photocatalytic Hydrogen Generation Experiments First, as-prepared Pt-decorated CdSe tetrapods were precipitated by adding an excess amount of methanol. Next, 250 mg 11-mercaptoundecanoic acid (MUA) were dissolved in 20 g methanol. Tetramethylammonium hydroxidepentahydrate salt was added until the solution pH of 11 was obtained. This solution was added to the precipitates of Pt-decorated CdSe tetrapods and sonicated for a few seconds, followed by adding toluene and centrifugation at 4000 rpm for the precipitation of the products. Finally, Pt-decorated CdSe tetrapods passivated with MUA were dispersed in water.

For the photocatalytic H_2 generation reaction, the as-prepared Pt-decorated CdSe tetrapod photocatalyst solution was mixed with 0.35 M Na_2SO_3 / 0.25 M Na_2S aqueous solution (10 mL). The amount of the photocatalysts was set at 2.5 mg considering the concentration of solution and head space. The reaction mixture was loaded to a homemade quartz tube with a total volume of 19 mL and sealed with a rubber septum, and purged with Ar for 30 min prior to the reaction, followed by illumination with AM 1SUN condition by a solar simulator (ABET Technologies). The aliquot of the reaction mixture was collected by a syringe from the head space in every 30 min. The amount of H_2 generated was measured by a gas chromatograph (GC, YL6100).

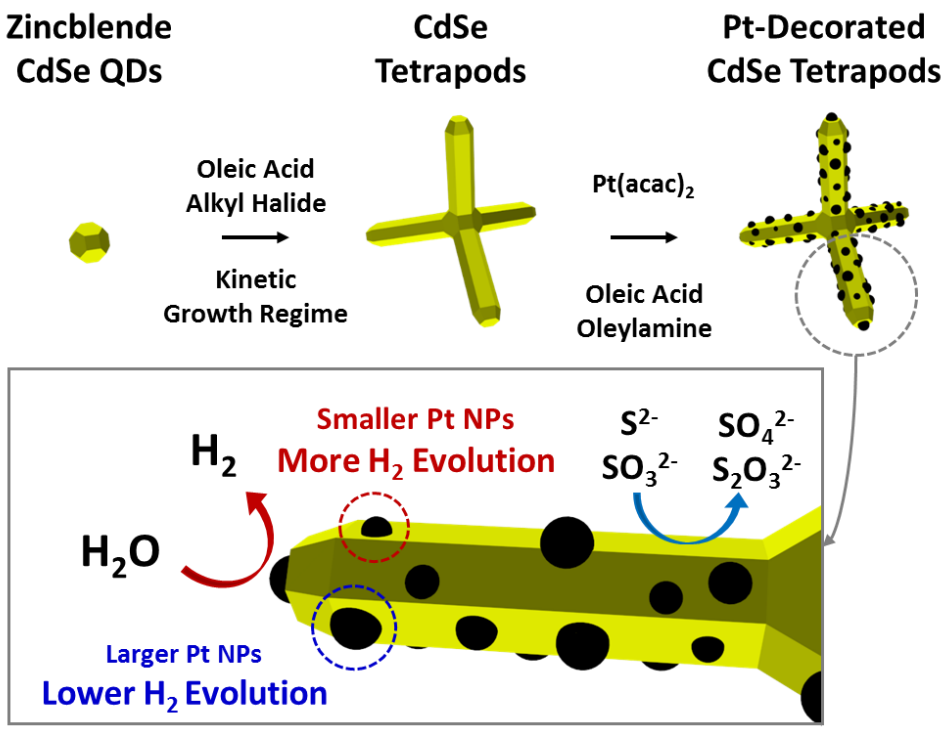

Scheme 4.2.1 Schematic illustration for the direct decoration of Pt nanocrystals on the surface of CdSe tetrapods synthesized by CPI approach and their photocatalytic H_2 generation.

4.2.2 Results and Discussions

As mentioned earlier, CdSe tetrapods prepared by CPI approach with using mixture of ligands, which are oleic acids and CTAB, showed direct decoration of Pt nanocrystals onto overall surface of CdSe tetrapod arms. Simply by controlling the amount of Pt precursors for the direct decoration of Pt nanocrystals onto CdSe tetrapodsd by CPI, controlled size of Pt nanocrystals decorated onto the surface of CdSe tetrapod arms were observed. As a result, Pt-decorated CdSe tetrapods with smaller size of Pt nanocrystals showed higher photocatalytic hydrogen generation behavior in the presence of hole scavengers (Scheme 4.2.1).

In Figure 4.2.1., Pt-decorated CdSe tetrapods with controlled size of Pt nanocrystals were successfully synthesized. By normal TEM images, it is hard to distinguish the existence of Pt nanocrystals at the surface of CdSe tetrapods, when little amount of Pt precursors were introduced during the synthesis. Therefore, detailed structural analyses were conducted with HR-TEM and HAADF-STEM techniques. In Figure 4.2.2, successful decoration of Pt nanocrystals was confirmed by diffraction patterns of face-centered cubic Pt, and increasing the amount of Pt precursors resulted in direct decoration of larger and distinct Pt nanocrystals. Nucleation and growth lattice directions of Pt nanocrystals onto the surface of CdSe tetrapods were random. From normal TEM images with the samples prepared with different

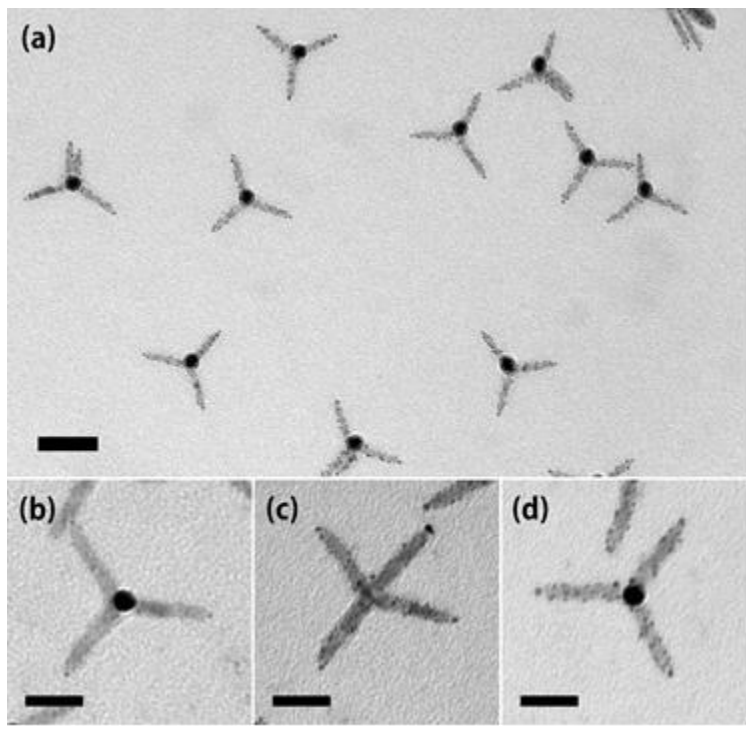

Figure 4.2.1 TEM images of Pt-decorated CdSe tetrapods with different size of Pt nanocrystals.

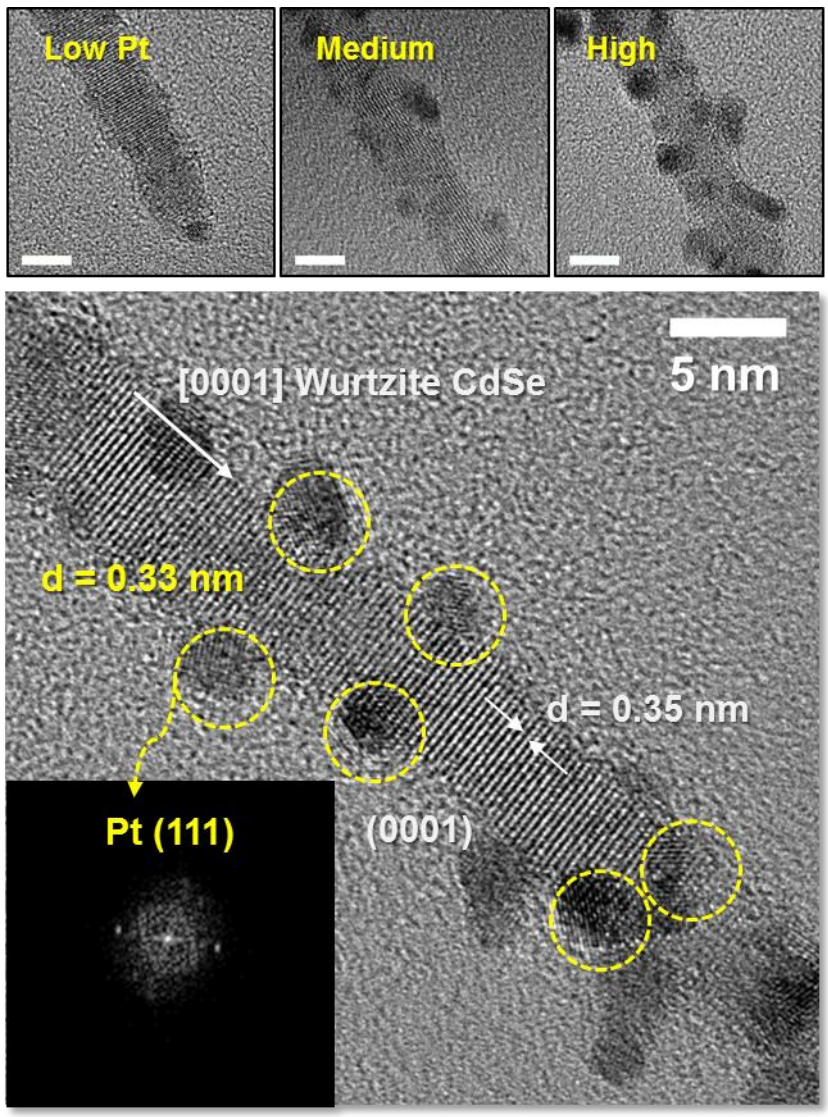

Figure 4.2.2 HR-TEM images of Pt-decorated CdSe tetrapods with different size of Pt nanocrystals. © Royal Society of Chemistry.

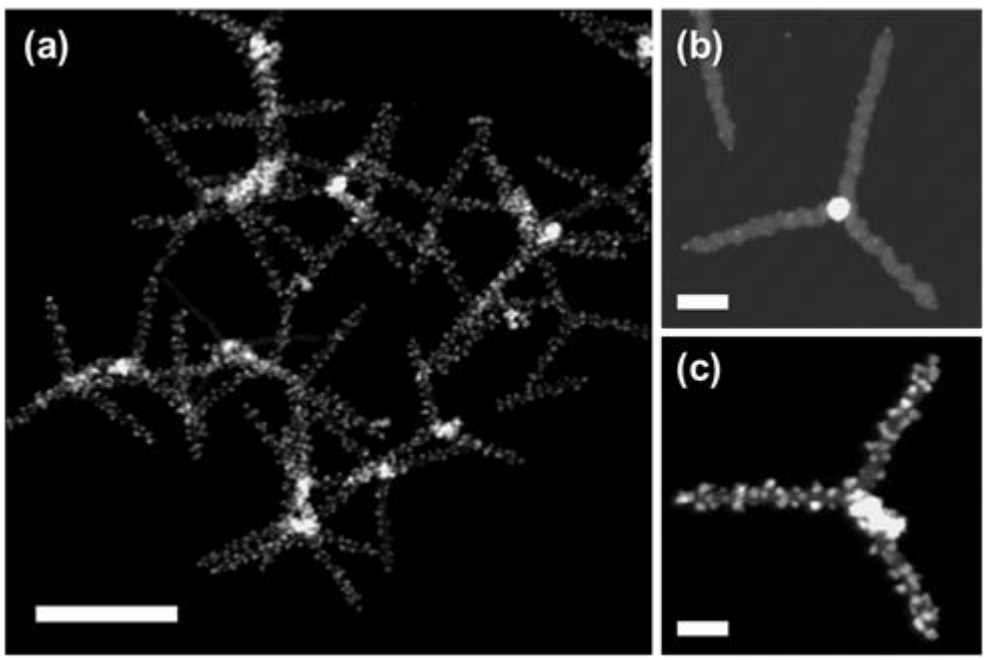

Figure 4.2.3 HAADF-STEM images of Pt-decorated CdSe tetrapods with different size of Pt nanocrystals.

amounts of Pt precursors, it is hard to distinguish the presence of Pt nanoparticles with extremely small size. However, the uniform decoration of Pt nanoparticles on the tetrapod arms was confirmed. We assume that when compared with previously reported methods to prepare CdSe nanocrystals with anisotropic shape, since a fixed amount of alkyl halides was introduced to the system during the arm growth, this procedure might lead to the surface chemical states different from other CdSe nanorods or tetrapods previously reported. We believe that the introduction of alkyl halides, which is crucial for the synthesis of CdSe tetrapods, enables the decoration of Pt nanoparticles throughout the entire surface of CdSe tetrapods due to Cd-halide ligand-free sites on the surface sidewalls of wurtzite CdSe tetrapod arms. Further detailed mechanistic studies along with structural analysis are currently under progress.

In Figure 4.2.3, from the HAADF-STEM images, the bright region corresponds to Pt nanoparticles with higher electron density when compared with semiconducting CdSe tetrapods. As mentioned earlier, normal TEM could not clearly confirm the existence of Pt nanoparticles formed on the CdSe tetrapods when an extremely low amount of Pt precursors was introduced. But, by the HAADF-STEM images, the existence of Pt nanoparticles even with very small size (~ 1 nm) was observed (Figure 3(a)). Moreover, control experiments for the growth of second metal and previous

Amount of CdSe	Amount of Pt	Cd	Se	Pt
25 mg	1 mg	42.70 %	29.58 %	1.61 %
25 mg	5 mg	45.03 %	30.93 %	8.73 %
25 mg	15 mg	40.33 %	30.93 %	15.59 %
25 mg	25 mg	26.08 %	20.38 %	41.62 %

Table 4.2.1 ICP-AES results of Pt-decorated CdSe tetrapods with different amount of Pt precursors.

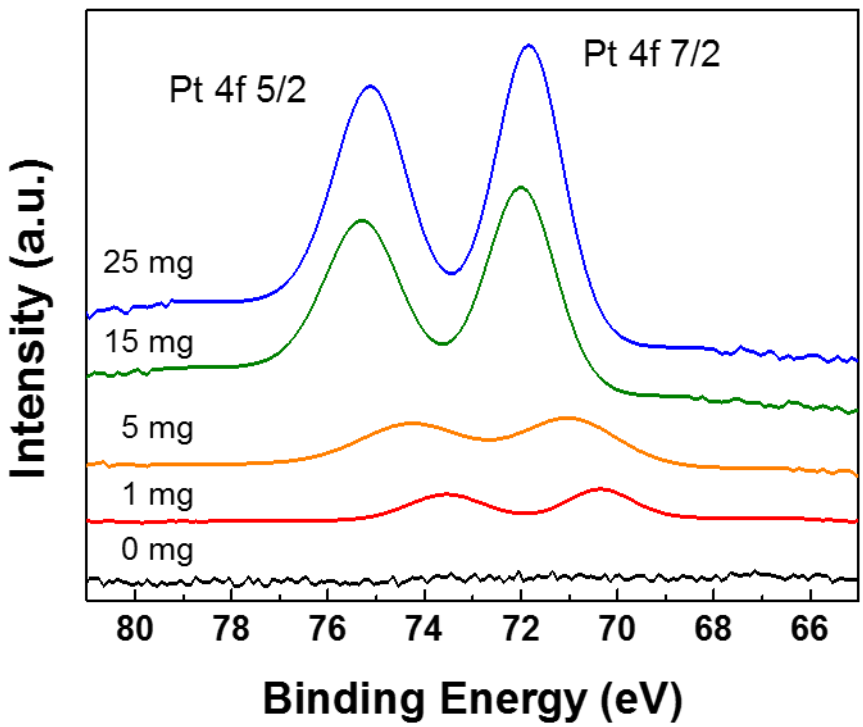

Peak Area	0 mg	1 mg	5 mg	15 mg	25 mg
Pt 4f 5/2	0	327.74	423.27	1953.91	2825.87
Pt 4f 7/2	0	326.53	419.76	2320.60	3280.82

Figure 4.2.4 XPS results of Pt-decorated CdSe tetrapods with different amount of Pt precursors.

reports by Pyun and Char et al. also support this argument. During the Pt-tipping reaction with CdSe@CdS nanorods, when the reaction time for Pt to nucleate and grow was kinetically suppressed, only one Pt tip or no tip was observed by normal TEM, called the "activated" CdSe@CdS nanorods. Followed by the growth of second metal nanoparticles, which in this case were cobalt, the existence of Pt nanoparticles was indirectly confirmed since cobalt nanoparticles were only formed epitaxially when Pt tips were first introduced to the ends of CdSe@CdS nanorods. Control experiment was performed by growing cobalt nanoparticles in the presence of bare CdSe tetrapods synthesized by the CPI approach and Pt-decorated CdSe tetrapods with an extremely low amount of Pt precursors (FigureS2). When no Pt nanoparticles were introduced to the CdSe tetrapods, no cobalt nanoparticles were formed at the surface of CdSe tetrapods. Although an extremely low amount of Pt precursors was introduced, the conformal decoration of cobalt nanoparticles on the Pt-decorated CdSe tetrapods was also observed. This result confirms the existence of Pt nanoparticles on the Pt-decorated CdSe tetrapods, but with very small in size.

Further ICP-AES analysis also confirmed the increase in Pt concentration on the tetrapod arms with the increase in the amount of Pt precursors added, which are shown in Table 4.2.1. By XPS analysis in Figure 4.2.4, when Pt nanocrystals were directly decorated with increased amount of Pt precursors

versus the amount of CdSe tetrapods during the synthesis, increased peak area of XPS binding energies were observed, meaning that the larger amount of Pt nanocrystals or larger size were decorated onto CdSe tetrapods. Here, peak shift of XPS corresponds to the formation of alloy structures, which matches with the decoration of Pt nanocrystals with larger size by larger amount of Pt precursors.

As-synthesized Pt-decorated CdSe tetrapods with different amount of Pt precursors were then used to examine the photocatalytic H2 generation efficiency. A series of Pt-decorated CdSe tetrapods were prepared by controlling the amount of Pt precursors and used as photocatalysts. The amount of CdSe tetrapods used for the decoration of Pt nanoparticles was fixed at 25 mg, whereas the amount of Pt precursors was varied from 1 to 25 mg. Simply by the ligand exchange of Pt-decorated CdSe tetrapods with mercaptoundecanoic acids, the Pt-decorated CdSe tetrapods were well-dispersed in hydrophilic solvents (i.e., water) without any structural transformation or aggregation. The amount of Pt-CdSe hybrid tetrapod photocatalysts was fixed at 2.5 mg and dispersed in 0.35 M Na_2SO_3 / 0.25 M Na_2S aqueous solution under the 1SUN illumination condition. Figure 4(a) shows the amount of H_2 evolved by the Pt-decorated CdSe tetrapods with different amount of Pt precursors plotted against time for a period of 30 min. All the Pt-decorated CdSe tetrapods tested in the present study showed the

photocatalytic H_2 generation behavior with relatively the linear increase with time. Interestingly, when the extremely low amount of Pt precursors was introduced into the CdSe tetrapods, much higher amount of H_2 was generated when compared with other tetrapods with larger size of Pt nanoparticles decorated (Figure 4.2.5). When 1 mg of Pt precursors was used for the decoration of Pt nanoparticles on the surfaces of the CdSe tetrapods, the average size of the Pt nanoparticles was hard to measure, but approximately less than 1.5 nm, which is the smallest size possible to identify with our TEM. The Increase in the amount of Pt precursors resulted in Pt nanoparticles with distributions of particle size, implying that both small (less than 1.5 nm) and larger (~ 2.5 nm) Pt nanoparticles coexist. The result that the CdSe tetrapods containing less than 1.5 nm Pt nanoparticles show higher efficiency could be explained from the literature, which the Pt cluster size significantly affects the photocatalytic activity of metal-semiconductor heterostructured nanomaterials. The LUMO of Pt nanoparticles should be located between the conduction band of semiconductors and the H^+/H_2 reduction potential in order to promote the electron transfer. In our system, the controlled amount of Pt precursors resulted in the different size of Pt nanoparticles formed on the surfaces of CdSe tetrapods. Meanwhile, the number density for the nucleation sites for Pt formation on the CdSe tetrapods is, more or less, fixed by the amount of CTAB ligands in the mixed ligands. Therefore, the formation of Pt

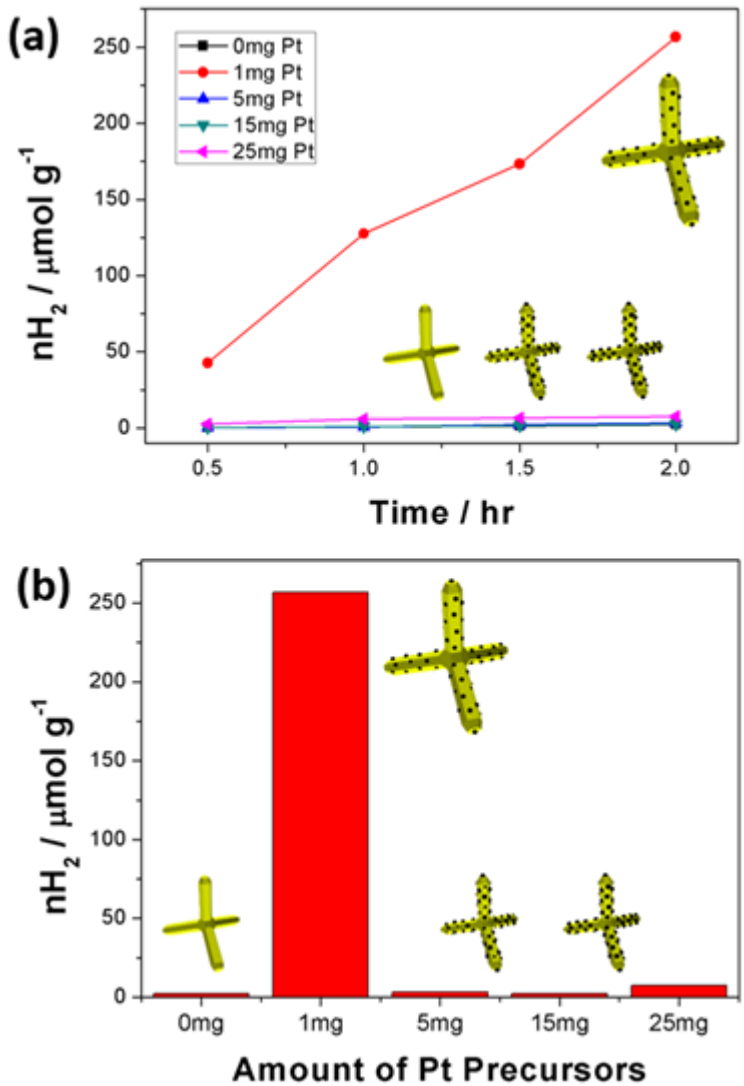

Figure 4.2.5 Photocatalytic H_2 generation results of Pt-decorated CdSe tetrapods with different size of Pt nanocrystals.

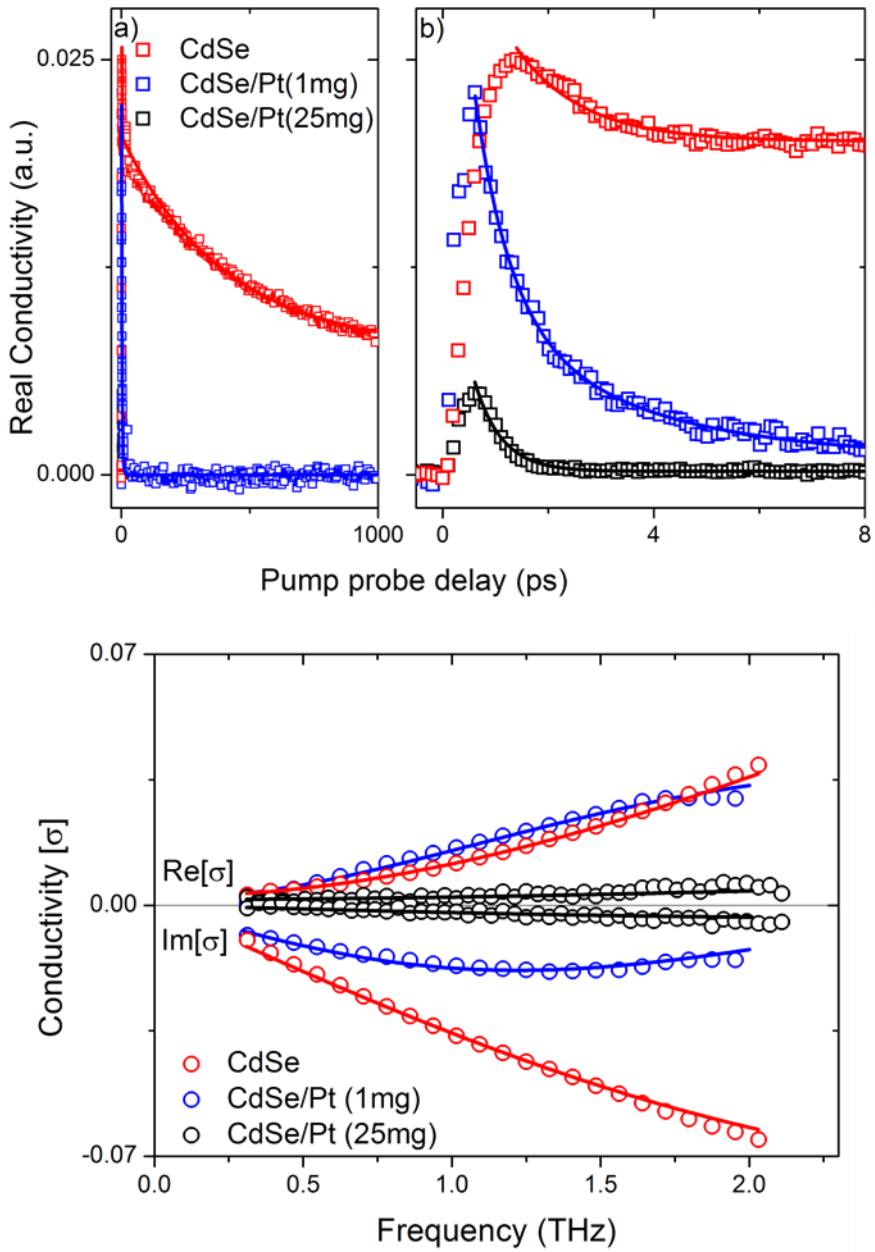

Figure 4.2.6 Carrier dynamics of Pt-decorated CdSe tetrapods with different amount of Pt precursors by time-resolved terahertz spectroscopy.

nanoparticles of different size simply by controlling the amount of Pt precursors, with a fixed number density of Pt nanoparticles formed on the surface of CdSe tetrapods, was observed. This is believed to change the LUMO energy level of Pt nanoparticles and when larger Pt nanoparticles, of which the LUMO energy level is misplaced for the photocatalytic H_2 generation, showed significantly low photocatalytic activity. Further carrier dynamics of Pt-decorated CdSe tetrapods with different size of Pt nanocrystals were analyzed by terahertz spectroscopy technique. In bare CdSe tetrapods, conductivity with respect to pump probe delay time, which corresponds to the electron population in the nanocrystals, showed slow decay curve. On the other hand, Pt-decorated CdSe tetrapods showed faster decay curve in conductivity, which is due to the presence of metal nanocrystals with electron-quenching properties. However, different size of Pt nanocrystals onto CdSe tetrapods, which are directly decorated onto CdSe tetrapods by controlling the amount of Pt precursors, showed different decay time in conductivity of Pt-decorated CdSe tetrapods. Pt-decorated CdSe tetrapods with larger size of Pt nanocrystals showed extremely fast decay behavior, but Pt-decorated CdSe tetrapods with small sizes of Pt nanocrystals showed delayed decay curve than previous one.

4.2.3 Conclusions

Pt-decorated CdSe tetrapods with controlled size of Pt nanocrystals were successfully synthesized. CdSe tetrapods prepared in the presence of alkyl halide ligands led to the direct incorporation of Pt nanoparticles without post treatment. These heterostructured tetrapods had a fixed number density for nucleation sites, enabling to assess the size effect of Pt nanoparticles formed uniformly on the CdSe tetrapods on the photocatalytic activity of H_2 generation reaction. An extremely low amount of Pt precursors employed for Pt nanoparticle synthesis resulted in the uniform incorporation of Pt nanoparticles with very small size, which in turn, well matches with the energy levels of CdSe semiconductor arms and the H^+/H_2 reduction potential, showed the highest photocatalytic efficiency. The result shown in the present study opens another avenue for the rational design of new types of metal-semiconductor heterostructured nanomaterials to further increase the photoconversion efficiency in the photocatalytic water splitting reaction.

Chapter 5. Morphological Effect of Semiconductor Nanocrystals on Photocatalytic Hydrogen Generation

5.1 Introduction

As mentioned in the previous chapter, colloidal semiconductor nanocrystals show different optoelectronic properties depending on the shape of nanocrystals, and this is also same with colloidal metal-semiconductor heterostructured nanocrystals with various combinations of morphologies and compositions since semiconductor nanocrystals will remain their intrinsic properties even after hybridization with metal nanocrystals.[17, 103, 114, 128, 195-200] Colloidal semiconductor nanocrystals with different shapes show improved absorption cross-section than quantum dots due to volume difference from morphological difference as well as density of states.[40, 48, 76, 135, 144, 171, 201-207] This phenomena supports the idea of systematic study for the rational design of colloidal metal-semiconductor heterostructured nanocrystal photocatalysts in photocatalytic hydrogen generation, where specific shapes with larger absorption cross-section will improve photocatalytic efficiency.[7, 208-216]

Also, as the dimension of colloidal semiconductor nanocrystals increase, electrons and holes wavefunctions within nanocrystals are hugely affected. This is also very important issue to be considered when designing colloidal

metal-semiconductor heterostructured nanocrystal photocatalysts since efficient management of electrons and holes for better charge transport by control over morphologies of semiconductor nanocrystals could be applied.[51-52, 148, 217-220] If systematic study on the influence of morphological effect of semiconductor nanocrystals from colloidal metal-semiconductor heterostructured nanocrystals as photocatalysts in photocatalytic hydrogen generation reaction were performed, this will guide to rational design of novel colloidal metal-semiconductor heterostructured photocatalysts in further overall photocatalytic water splitting reaction.[21, 23, 221-225]

5.2 Arm Length Dependency of Pt-Decorated CdSe Tetrapods on the Performance of Photocatalytic Hydrogen Generation

5.2.1 Experimental Session

Materials Cadmium oxide (CdO, 99.95%) was purchased from Alfa Aesar. Selenium (99.99%, powder), n-triocytylphosphine (TOP, 90%), oleic acid (OA, 90%), 1-octadecene (ODE, 90%), 1,2-hexadecanediol (90%), oleylamine (70%), platinum(II) acetylacetonate (Pt(acac)2, 97%), 1,2-dicholrobenzene (anhydrous, 99%), 11-mercaptoundecanoit acid (MUA, 95%), tetramethylammoniumhydroxide pentahydrate salt (>97%) and cetyltrimethylammonium bromide (CTAB, 99+%) were purchased from Sigma Aldrich. Phenyl ether (90%) was purchased from TCI. Toluene, methanol and ethanol were purchased from Samchun Chemicals. All chemicals were used as purchased.

Preparation of Injection Solution For the preparation of cadmium oleate ($Cd(OA)_2$) solution, 12 mmol CdO, 10.8 mL OA and 6 mL ODE were placed in an 100mL 3-neck round flask equipped with a condenser. The reaction mixture was degassed under vacuum at 100 °C for degassing, followed by heating to 280 °C under Ar for 20 min to form an optically clear solution. The mixture was then cooled down to room temperature for further use. Separately,

12 mmol Se and 6 ml TOP were mixed in a 50 mL 3-neck round flask with a condenser and heated to 200 °C until powdered Se fully dissolved. After SeTOP was cooled down to room temperature, 6 mL SeTOP solution was mixed with 14 mL $Cd(OA)_2$ solution for further injection.

Zincblende CdSe Quantum Dots Procedure for the synthesis of zincblende CdSe quantum dot seeds was adopted with a slight modification from the literature. First, to a 100 mL 3-neck round flask equipped with a condenser, 1 mmol Se and 10 mL ODE were loaded and heated to 100 °C for degassing under vacuum. Under Ar, the reaction mixture was heated to 300°C for the injection of as-prepared $Cd(OA)_2$. At 300°C, 2.8 mL Cd(OA)2 and 7.2 mL ODE were injected to make the total volume of 20 mL and the reaction solution was reacted at 270 °C for 15 min. In common, spherical zincblende CdSe quantum dot seeds with ~5 nm diameter (1st exciton peak ~630 nm) were obtained, and this crude solution was used without further purification.

CdSe Tetrapods with Different Arm Length by Continuous Precursor Injection (CPI) Approach To a 100 mL 3-neck round flask equipped with a condenser, 5 mL zincblende CdSe seed solution, 2.25 mL OA, 1.5 mL TOP, 21.25 mL ODE and 0.21 mmol CTAB were loaded and heated to 100 °C under vacuum for degassing. Under Ar, the reaction mixture was heated to desired temperature for target arm length. In the case of shorter CdSe tetrapods,

injection temperature was set as 260 °C with lower growth rate. For the synthesis of medium and long CdSe tetrapod arms, injection temperature was set to 270 °C for the injection of as-prepared $Cd(OA)_2$ and SeTOP injection solution, with the injection rate of 0.4 mL / min and 0.8 mL / min by syringe pump. After the reaction, the crude mixture was loaded to centrifuge tube and equal amount of toluene and ethanol were added repeatedly for the precipitation of the products by centrifugation at 4000 rpm.

Decoration of Pt Nanoparticles onto CdSe Tetrapods To a 100 mL 3-neck round flask equipped with a condenser, 43 mg 1,2-hexadecanediol, 0.2 mL OA, 0.2 mL oleylamine and 10 mL phenyl ether were loaded and heated to 80 °C under vacuum for degassing. Under Ar, the reaction mixture was heated to 225 °C for further injection. Meanwhile, 25 mg as-synthesized CdSe tetrapods along with 1 mg of platinum precursors, which were platinum acetylacetonate, were dissolved in 1 mL 1,2-dichlorobenzene for the injection solution. At 225 °C, the injection solution was injected into the reaction mixture and reacted for 8 min, followed by cooling down to room temperature and 5 mL toluene were injected under 100 °C to prevent further solidification of the products. The crude product solution was then transferred to a centrifuge tube, and a relative amount of ethanol and toluene was added to selectively remove free Pt nanoparticles with centrifugation at 2500 rpm.

Photocatalytic Hydrogen Generation Experiments First, as-prepared Pt-decorated CdSe tetrapods were precipitated by adding an excess amount of methanol. Next, 250 mg 11-mercaptoundecanoic acid (MUA) were dissolved in 20 g methanol. Tetramethylaamonium hydroxidepentahydrate salt was added until the solution pH of 11 was obtained. This solution was added to the precipitates of Pt-decorated CdSe tetrapods and sonicated for a few seconds, followed by adding toluene and centrifugation at 4000 rpm for the precipitation of the products. Finally, Pt-decorated CdSe tetrapods passivated with MUA were dispersed in water.

For the photocatalytic H_2 generation reaction, the as-prepared Pt-decorated CdSe tetrapod photocatalyst solution was mixed with 0.35 M Na_2SO_3 / 0.25 M Na_2S aqueous solution (10 mL). The amount of the photocatalysts was set at 2.5 mg considering the concentration of solution and head space. The reaction mixture was loaded to a homemade quartz tube with a total volume of 19 mL and sealed with a rubber septum, and purged with Ar for 30 min prior to the reaction, followed by illumination with AM 1SUN condition by a solar simulator (ABET Technologies). The aliquot of the reaction mixture was collected by a syringe from the head space in every 30 min. The amount of H_2 generated was measured by a gas chromatograph (GC, YL6100).

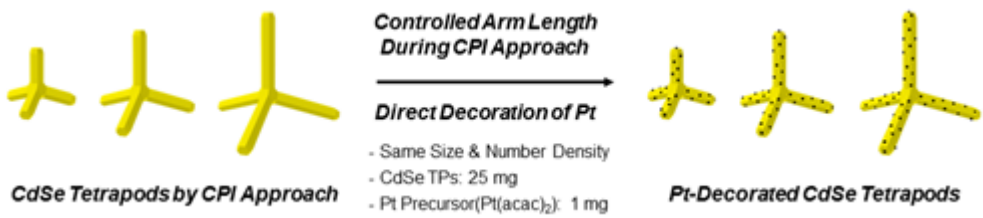

Scheme 5.2.1 Schematic illustration on the preparation of Pt-decorated CdSe tetrapods with controlled arm length.

5.2.2 Results and Discussions

CdSe tetrapods were synthesized by the CPI approach with zincblende CdSe quantum dots as seeds to grow wurtzite CdSe tetrapod arms. During the synthesis of CdSe tetrapods, certain amount of alkyl halide ligands with 1-oleic acid, which, in the present case, are cetyltrimethylammonium bromide (CTAB), is necessary to maintain the crystal structures of zincblende CdSe seeds as well as wurtzite CdSe tetrapod arms. During the CPI to grow the wurtzite CdSe tetrapod arms, injection solutions containing cadmium oleate and SeTOP were injected with syringe pumps by monitoring first excitonic peaks from the absorption spectra of reaction mixtures in real-time. Since the growth of wurtzite CdSe tetrapod arms with the CPI method is mostly governed by monomer concentrations of Cd and Se within the kinetic growth regime, the control over injection rate and temperature is important to obtain desired arm length and diameter, which are described in Scheme 5.2.1. The growth of wurtzite CdSe tetrapod arms occurs primarily along the length direction, followed by the growth of the diameter, therefore when the diameter of CdSe tetrapods reached at a desired point, reactions were immediately quenched. With this synthetic strategy, the length of wurtzite CdSe tetrapod arms was varied from ~15 to ~90 nm, while the diameter remained the same as the target value of ~6 nm (Figure 5.2.1).

The direct decoration of Pt nanocrystals on overall surfaces of CdSe

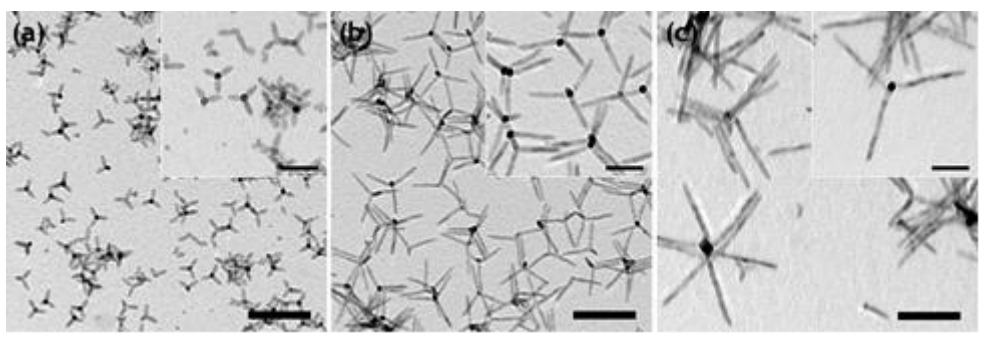

Figure 5.2.1 TEM images of Pt-decorated CdSe tetrapods with controlled arm length (scalebar=50nm).

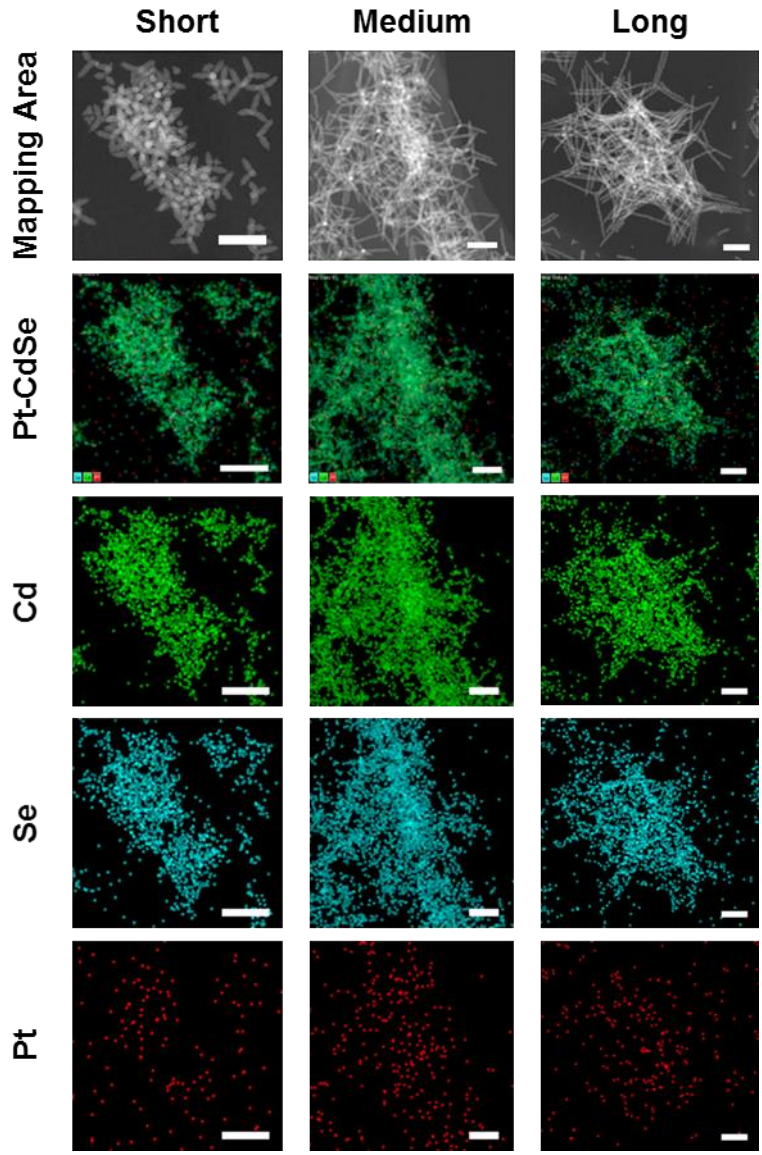

Figure 5.2.2 EDS mapping of Pt-decorated CdSe tetrapods with controlled arm length.

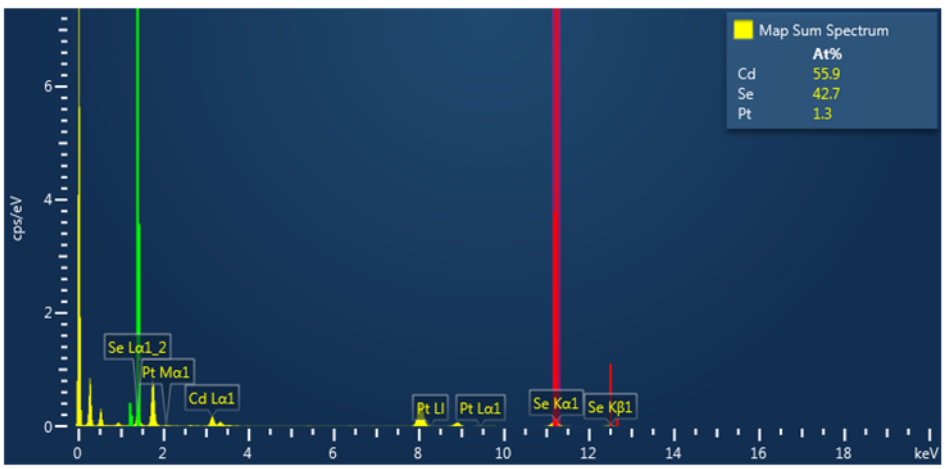

Arm Length	Amount of CdSe	Amount of Pt	Cd	Se	Pt
Short	25 mg	1 mg	55.43 %	39.09 %	2.67 %
Medium	25 mg	1 mg	55.36 %	39.15 %	2.56 %
Long	25 mg	1 mg	53.34 %	39.05 %	2.44 %

Figure 5.2.3 Elemental analysis of Pt-decorated CdSe tetrapods with controlled arm length by EDS and ICP-AES.

tetrapods was performed by the procedure from literature. From the previous study, with CdSe tetrapods prepared by the CPI approach, we observed that controlling the amount of Pt precursor resulted in the decoration of Pt nanocrystals with different size. The effect of the size of Pt nanocrystals on the photocatalytic hydrogen generation reaction has been studied by our group, in which smaller size of Pt nanocrystals has shown the highest efficiency. As a result, in the present study, CdSe tetrapods with different arm lengths were decorated with Pt nanocrystals with a size of around 1 nm. To confirm the uniform decoration of Pt nanocrystals at the surface of CdSe tetrapod arms, high-angle annual dark field scanning transmission electron microscopy (HAADF-STEM) with energy-dispersive spectrometry (EDS) was conducted (Figure 5.2.2). From Figure 5.2.3, by the elemental mapping of Pt-decorated CdSe tetrapods with different arm lengths, the existence of Pt nanocrystals was confirmed. All the mapping images showed the atomic ratio of Cd, Se and Pt as 56:43:1, which almost matches with the amount of Pt precursors used for the decoration of Pt nanocrystals with respect to the amount of CdSe tetrapods. As mentioned above, the size of Pt nanocrystals was mainly controlled by the amount of Pt precursors. Therefore, we can assume that different numbers of CdSe tetrapods with different arm lengths with respect to the same amount of Pt precursors could be introduced during the decoration of Pt nanocrystals. Inductively-coupled plasma atomic

emission spectroscopy (ICP-AES) was conducted to analyze the amount of Cd, Se, and Pt for the same weight percent. As a consequence, regardless of the arm length of Pt-decorated CdSe tetrapods, the amount of Pt nanocrystals remained almost the same. This result explains that when the same amount of Pt-decorated CdSe tetrapods with different arm lengths is present, the total amount of Pt nanocrystals with respect to CdSe tetrapods are the same, implying that the number densities of Pt nanocrystals are similar for Pt-decorated CdSe tetrapods with different arm lengths.

Pt-decorated CdSe tetrapods with different arm lengths were ligand-exchanged with 11-mercaptoundecanoic acid under pH11 condition according to the literature. These heterostructured photocatalysts were dispersed in water for further photocatalytic hydrogen generation. Photocatalyst solutions containing 0.35 M Na_2SO_3 / 0.25 M Na_2S as hole scavengers were transferred to a homemade quartz tube sealed with a vacuum rubber septum. Samples were irradiated with a solar simulator (Sun 2000, ABET Technologies) under 1 SUN condition for 2 hrs. Certain amount of gas was collected directly from the head space with a gas-tight microsyringe for every 30 min., followed by the injection to a gas chromatograph equipped with a pulsed discharge ionization detector (YL6500, YL Instruments). Figure 5.2.4 shows the photocatalytic hydrogen generation of Pt-decorated CdSe tetrapods with different arm lengths after 2 hrs of irradiation. We note that Pt-

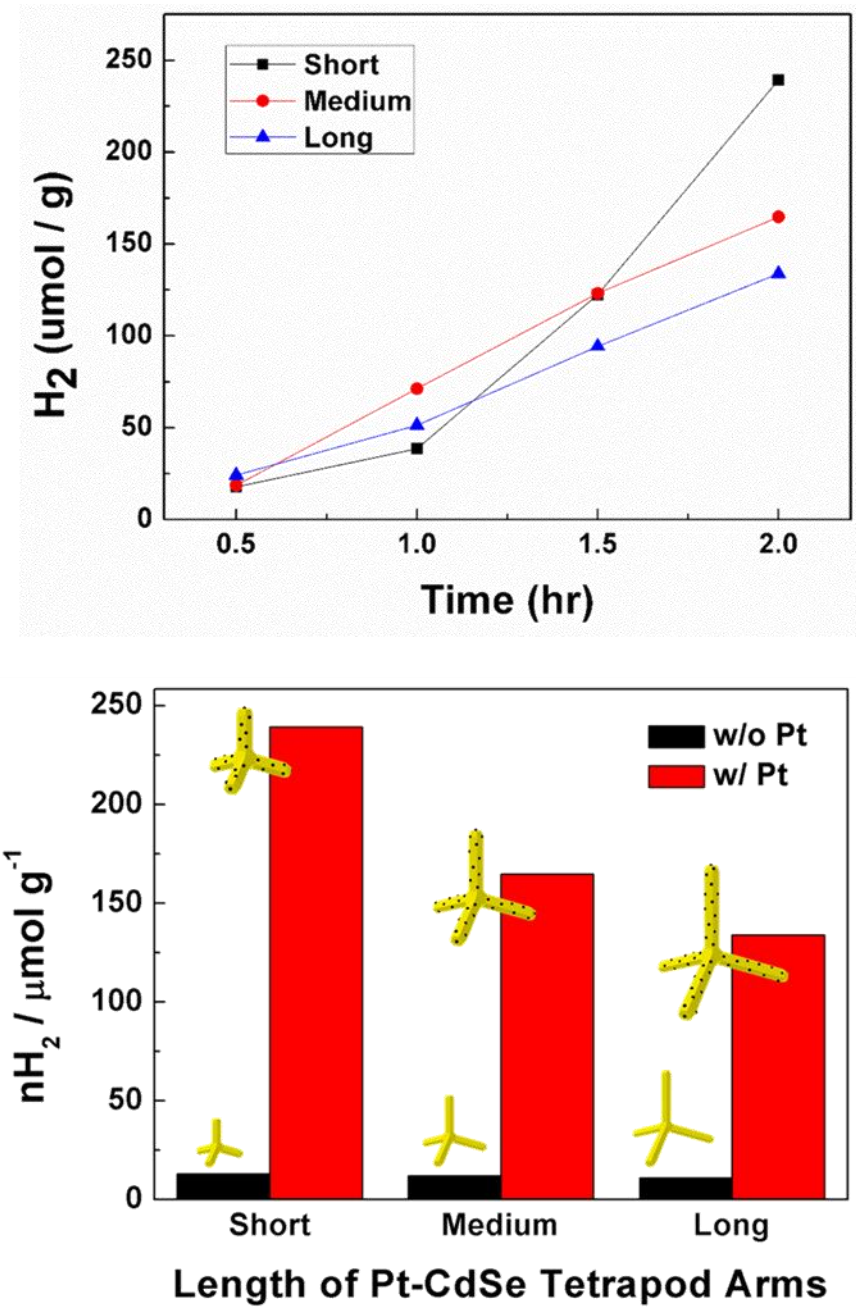

Figure 5.2.4 Photocatalytic H_2 generation results of Pt-decorated CdSe tetrapods with controlled arm length.

decorated CdSe tetrapods with shorter arm length showed the highest photocatalytic hydrogen generation efficiency. Bare CdSe tetrapods without Pt nanocrystals showed the lowest photocatalytic efficiency when compared with Pt-decorated CdSe tetrapods regardless of the different arm length. As the length of the wurtzite CdSe arms is increased, the photocatalytic efficiency gradually decreases (Figure 5.2.4). We assume that this result could be explained based on the previous study from the literature that excitons generated by the CdSe tetrapods mostly remains at the zincblende CdSe quantum dot cores due to the quasi type-II band alignment. This argument supports our results that shorter CdSe tetrapods have higher probability for excitons to separate charges, given the fact that the amount of Pt with respect to CdSe is the same for different arm lengths of Pt-decorated CdSe tetrapods.

5.2.3 Conclusions

Pt-decorated CdSe tetrapods with different arm lengths were successfully prepared. Pt-decorated CdSe tetrapods with shorter arm length showed the highest hydrogen generation efficiency, while the densities of Pt nanocrystals per surface area of CdSe tetrapods remained almost the same. This indicates that the photocatalytic hydrogen generation behavior of Pt-decorated CdSe tetrapods with different arm lengths mainly depends on the length of wurtzite CdSe tetrapod arms, which we assume, due to higher probability for as-generated excitons to separate charges.

Chapter 6. Conclusion and Outlook

Demands on exploring new renewable energy resources are inevitable since natural resources in earth is limited. Conventional technologies to generate energy such as fossil fuels and petroleum gas fuels are also major reasons for pollution, which then leads to global warming to destroy nature that human mankind are living. Colloidal metal-semiconductor heterostructured nanocrystals as photocatalysts in photocatalytic water splitting reaction to generate hydrogen fuel is promising research area for renewable energy. Fuel cell cars and fuel cell technologies have been extensively studied and developed both in academia and industry. Therefore, rational design of high-performance photocatalysts is remained problem to be solved. Since the first discovery of colloidal semiconductor nanocrystals, which is well known as quantum dots, many research scientists have studied the development of new synthetic chemistry, and to understand the optoelectronic properties and phenomena by analyzing carrier dynamics with state-of-the-art spectroscopy techniques. Therefore, designing and synthesizing novel colloidal metal-semiconductor heterostructured photocatalysts with principles is not impossible.

In this context above, this thesis describes strategies to design and synthesize

high-performance colloidal metal-semiconductor heterostructured nanocrystals as photocatalysts in photocatalytic hydrogen generation reaction. In particular, by systematic study of the influence of each component, which in this case is metal as Pt and semiconductor as CdSe, methodologies and design principles are introduced.

Colloidal semiconductor nanocrystals have been extensively studied due to their unique optoelectronic properties from control over compositions and shapes. There are certain strategies to control the shape of colloidal semiconductor nanocrystals: 1) choice of seed crystal structure 2) choice of organic binding ligands 3) choice of growth mechanism. Typical synthetic methods to control the shape of colloidal semiconductor nanocrystals use colloidal semiconductor nanocrystals with spherical shapes called quantum dots as seeds to further grow anisotropic shapes. Wurtzite CdSe quantum dots have fast growth rate along (0001) directions, which finally leads to the formation of 1-dimensional structured such as nanorodsd. Zincblende CdSe quantum dots are more suitable for multibranched nanocrystals such as tetrapods and octapods. Alkylphosphonic acids with combinations of different number of carbon chains are typically used for the shape control of colloidal semiconductor nanocrystals, as they suppress certain crystal facets for the growth of semiconductors. Alkyl halide ligands with typical oleic acid ligands also enabled the shape control of colloidal semiconductor

nanocrystals into 3-dimensional shapes such as tetrapods, but the precise control over ratio between oleic acids and alkyl halides is very important. Most of the colloidal semiconductor nanocrystals are synthesized within thermodynamic growth regime by hot injection method, where burst nucleation happens with extremely high temperature for precursors to thermally decompose to nucleate, followed by control over growth rate. In this mechanism, alkylphosphonic acids that are known to strongly bind to certain crystal facets of colloidal semiconductor nanocrystals are necessary since the nucleation and growth rate are extremely fast. However, in the case of kinetic growth regime, monomer concentration is the key factor that governs the nucleation and growth rate of colloidal semiconductor nanocrystals. By maintain seed crystal structures of colloidal semiconductor nanocrystals, by controlling the monomer concentration different morphologies of colloidal semiconductor nanocrystals have been synthesized. Continuous precursor injection (CPI) approach is well suited for the precise control over monomer concentrations during the synthesis, for final engineering of surface properties and morphologies of colloidal semiconductor nanocrystals. Simply by controlling the injection rate and temperature with precise control over the ration between carboxylic acid ligands and alkyl halide ligands, precise control over arm length and diameter of CdSe tetrapods were observed.

As mentioned above, different strategies for the shape control of colloidal semiconductor nanocrystals result in different surface chemistry and properties. This is important for the preparation of colloidal metal-semiconductor heterostructured nanocrystals. For the incorporation of metal nanocrystals with colloidal semiconductor nanocrystals, it is well studied that metal nanocrystals are nucleated and grown from surface sites of colloidal semiconductor nanocrystals with high surface energy such as lattice defects and less passivated ligand sites. Therefore, type of ligands passivating overall surface of colloidal semiconductor nanocrystals, density and lattice defects generated during the different nucleation and growth regime for colloidal semiconductor nanocrystals are very important. Alkylphosphonic acid-capped anisotropic shapes such as CdSe@CdS nanorods showed tipping of metal nanocrystals only at the termini of colloidal semiconductor nanocrystals, which is due to strongly binding alkylphosphonic acid ligands at sidewalls of nanorods. By controlling the nucleation and growth kinetics for Pt with CdSe@CdS nanorods, control over geometries such as one metal tip called “matchstick” or double metal tips at both ends of nanorods called “dumbbell” were studied. Also, secondary deposition of metal nanocrystals was affected by the primary deposition of metal nanocrystals onto colloidal semiconductor nanocrystals. Polymer-coated cobalt nanoparticles were selectively nucleated and grown only from Pt sites of Pt-CdSe@CdS colloidal

metal-semiconductor heterostructured nanocrystals with matchstick and dumbbell dyads. Due to ferromagnetic properties of cobalt nanoparticles, Pt@Co-CdSe@CdS colloidal heterostructured nanocrystals showed self-assembly behavior like colloidal polymers by colloidal polymerization. Simple oxidation yielded cobalt oxide-tipped Pt-CdSe@CdS colloidal heterostructured nanocrystals. On the other hand, CdSe tetrapod synthesized by CPI approach with using oleic acid and CTAB as ligands to nucleate and grow within kinetic growth regime resulted in overall direct decoration of Pt nanocrystals at the surface of CdSe tetrapods. From kinetics for the nucleation and growth of Pt nanocrystals at the surface of CdSe tetrapods by CPI approach, free Pt nanocrystals were first formed, followed by the nucleation and growth at termini of CdSe tetrapods, and finally overall decoration throughout the surface of CdSe tetrapods. We believe that the direct decoration of Pt nanocrystals is due to the certain amount of CTAB ligands at the surface of CdSe tetrapods by CPI approach. Certain amount of CTAB is very important to both maintain zincblende CdSe quantum dot seeds as well as the growth of wurtzite CdSe tetrapod arms without alkylphosphonic acids. When CTAB is introduced during the synthesis, certain amount of as-prepared $Cd(OA)_2$ are replaced with Cd-halides, thus generating ligand-free sites for high probabilities for the nucleation and growth of Pt nanocrystals. These CdSe tetrapods by CPI approach with new surface chemistry allow to

decorate metal nanocrystals without photoirradiation with control over morphologies of metal nanocrystals.

With these methodologies to design and synthesize colloidal metal-semiconductor heterostructured nanocrystals with different compositions and morphologies, systematic study on the influence of each component, which in this case is metal and semiconductor, on the final performance of photocatalytic hydrogen generation reaction, is conducted. First, control over sizes of Pt nanocrystals directly decorated at the surface of CdSe tetrapods by CPI approach was examined simply by controlling the amount of Pt precursors. Photocatalytic hydrogen generation results show that when Pt nanocrystals with extremely small size around 1.5 nm are decorated at the surface of CdSe tetrapods, showed better performance than bare or CdSe tetrapods decorated with larger Pt nanocrystals. We believe that this is due to the control over LUMO of Pt nanocrystals by controlling the size of Pt nanocrystals. When LUMO of Pt exactly positions between conduction band of colloidal semiconductor nanocrystals and hydrogen reduction potential, photocatalysts show higher efficiency. Moreover, with the precise control over morphologies of CdSe tetrapods by CPI approach, CdSe tetrapods with controlled arm length were prepared. These tetrapods showed same decoration densities for Pt nanocrystals, and interestingly shorter Pt-decorated CdSe tetrapods showed higher photocatalytic hydrogen generation

efficiency. We believe that this is due to the different number of zincblende CdSe tetrapod cores. When series of photocatalysts are tested for photocatalytic hydrogen generation experiments, same weight amount of photocatalysts are introduced. By elemental analyses, all series of Pt-decorated CdSe tetrapods with controlled arm length are consist of similar amount of Cd, Se and Pt. Therefore, we can conclude that the total amount of Pt versus CdSe is the same for all samples, but there is only difference in the number of Pt-decorated CdSe tetrapods with controlled arm length, which is different number of Pt-CdSe tetrapod cores introduced. From the literature, it is well-studied that as-generated electrons and holes in CdSe tetrapods are either migrate to core region or surface sites, and both pathways are always competing but migration to core region are faster. Therefore, larger number of CdSe tetrapod cores will result in higher chance for electrons and holes to charge separate, and also reports on the faster hole removal rate determines the final performance of photocatalysts supports this idea.

Although this thesis has focused on the photocatalysts in photocatalytic hydrogen generation reaction, the underlying principle discussed here can be widely applied to the other applications based on the novel nanomaterials and offer reasonable guidelines. It is believed that interdisciplinary approach and ceaseless devotions will make a success on the realization of nanoscience into the practical applications.

Bibliography

[1] Costi, R.; Saunders, A. E.; Banin, U., *Angew. Chem. Int. Ed.* **2010,** *49* (29), 4878-97.

[2] Banin, U.; Ben-Shahar, Y.; Vinokurov, K., *Chem. Mater.* **2014,** *26* (1), 97-110.

[3] Nanayakkara, S. U.; van de Lagemaat, J.; Luther, J. M., *Chem. Rev.* **2015,** *115* (16), 8157-81.

[4] Mastria, R.; Rizzo, A., *J. Mater. Chem. C* **2016**.

[5] Kershaw, S. V.; Susha, A. S.; Rogach, A. L., *Chem. Soc. Rev.* **2013,** *42* (7), 3033-87.

[6] Rivest, J. B.; Jain, P. K., *Chem. Soc. Rev.* **2013,** *42* (1), 89-96.

[7] Sitt, A.; Hadar, I.; Banin, U., *Nano Today* **2013,** *8* (5), 494-513.

[8] Justo, Y.; Sagar, L. K.; Flamee, S.; Zhao, Q.; Vantomme, A.; Hens, Z., *ACS Nano* **2014,** *8* (8), 7948-57.

[9] Baghani, E.; O'Leary, S. K.; Fedin, I.; Talapin, D. V.; Pelton, M., *J. Phys. Chem. Lett.* **2015,** *6* (6), 1032-6.

[10] Dutta, S. K.; Mehetor, S. K.; Pradhan, N., *J. Phys. Chem. Lett.* **2015,** *6* (6), 936-44.

[11] Rowland, C. E.; Fedin, I.; Zhang, H.; Gray, S. K.; Govorov, A. O.; Talapin, D. V.; Schaller, R. D., *Nat. Mater.* **2015,** *14* (5), 484-489.

[12] Schnitzenbaumer, K. J.; Labrador, T.; Dukovic, G., *J. Phys. Chem. C* **2015,** *119* (23), 13314-13324.

[13] Singh, S.; Ryan, K. M., *J. Phys. Chem. Lett.* **2015,** *6* (16), 3141-3148.

[14] van Embden, J.; Chesman, A. S. R.; Jasieniak, J. J., *Chem. Mater.* **2015,** *27* (7), 2246-2285.

[15] Dabbousi, B. O.; Rodriguez-Viejo, J.; Mikulec, F. V.; Heine, J. R.; Mattoussi, H.; Ober, R.; Jensen, K. F.; Bawendi, M. G., *J. Phys. Chem. B* **1997,** *101* (46), 9463-9475.

[16] Talapin, D. V.; Rogach, A. L.; Kornowski, A.; Haase, M.; Weller, H., *Nano Lett.* **2001,** *1* (4), 207-211.

[17] Peng, P.; Milliron, D. J.; Hughes, S. M.; Johnson, J. C.; Alivisatos, A. P.; Saykally, R. J., *Nano Lett.* **2005,** *5* (9), 1809-13.

[18] Cozzoli, P. D.; Pellegrino, T.; Manna, L., *Chem. Soc. Rev.* **2006,** *35* (11), 1195-208.

[19] Lee, D.; Kim, W. D.; Lee, S.; Bae, W. K.; Lee, S.; Lee, D. C., *Chem. Mater.* **2015,** *27* (15), 5295-5304.

[20] Tessier, M. D.; Dupont, D.; De Nolf, K.; De Roo, J.; Hens, Z., *Chem. Mater.* **2015,** *27* (13), 4893-4898.

[21] Wu, K.; Hill, L. J.; Chen, J.; McBride, J. R.; Pavlopolous, N. G.; Richey, N. E.; Pyun, J.; Lian, T., *ACS Nano* **2015,** *9* (4), 4591-9.

[22] Kelestemur, Y.; Guzelturk, B.; Erdem, O.; Olutas, M.; Gungor, K.; Demir,

H. V., *Adv. Funct. Mater.* **2016,** *26* (21), 3570-3579.

[23] Li, Q.; Wu, K.; Chen, J.; Chen, Z.; McBride, J. R.; Lian, T., *ACS Nano* **2016,** *10* (3), 3843-51.

[24] Kriegel, I.; Wisnet, A.; Kandada, A. R. S.; Scotognella, F.; Tassone, F.; Scheu, C.; Zhang, H.; Govorov, A. O.; Rodriguez-Fernandez, J.; Feldmann, J., *J. Mater. Chem. C* **2014,** *2* (17), 3189-3198.

[25] Lian, J.; Anggara, K.; Lin, M.; Chan, Y., *Small* **2014,** *10* (4), 667-73.

[26] Amirav, L.; Oba, F.; Aloni, S.; Alivisatos, A. P., *Angew. Chem. Int. Ed.* **2015,** *54* (24), 7007-11.

[27] Christodoulou, S.; Rajadell, F.; Casu, A.; Vaccaro, G.; Grim, J. Q.; Genovese, A.; Manna, L.; Climente, J. I.; Meinardi, F.; Raino, G.; Stoferle, T.; Mahrt, R. F.; Planelles, J.; Brovelli, S.; Moreels, I., *Nat. Commun.* **2015,** *6*, 7905.

[28] Ehamparam, R.; Pavlopoulos, N. G.; Liao, M. W.; Hill, L. J.; Armstrong, N. R.; Pyun, J.; Saavedra, S. S., *ACS Nano* **2015,** *9* (9), 8786-800.

[29] Talapin, D. V.; Nelson, J. H.; Shevchenko, E. V.; Aloni, S.; Sadtler, B.; Alivisatos, A. P., *Nano Lett.* **2007,** *7* (10), 2951-9.

[30] Bae, W. K.; Char, K.; Hur, H.; Lee, S., *Chem. Mater.* **2008,** *20* (2), 531-539.

[31] Bae, W. K.; Nam, M. K.; Char, K.; Lee, S., *Chem. Mater.* **2008,** *20* (16), 5307-5313.

[32] Hewa-Kasakarage, N. N.; Gurusinghe, N. P.; Zamkov, M., *J. Phys. Chem. C* **2009,** *113* (11), 4362-4368.

[33] Zhong, H.; Scholes, G. D., *J. Am. Chem. Soc.* **2009,** *131* (26), 9170-1.

[34] Carbone, L.; Cozzoli, P. D., *Nano Today* **2010,** *5* (5), 449-493.

[35] Hewa-Kasakarage, N. N.; El-Khoury, P. Z.; Tarnovsky, A. N.; Kirsanova, M.; Nemitz, I.; Nemchinov, A.; Zamkov, M., *ACS Nano* **2010,** *4* (4), 1837-44.

[36] Lian, J.; Xu, Y.; Lin, M.; Chan, Y., *J. Am. Chem. Soc.* **2012,** *134* (21), 8754-7.

[37] Lim, J.; Bae, W. K.; Kwak, J.; Lee, S.; Lee, C.; Char, K., *Opt. Mater. Express* **2012,** *2* (5), 594-628.

[38] Adel, P.; Wolf, A.; Kodanek, T.; Dorfs, D., *Chem. Mater.* **2014,** *26* (10), 3121-3127.

[39] Christodoulou, S.; Vaccaro, G.; Pinchetti, V.; De Donato, F.; Grim, J. Q.; Casu, A.; Genovese, A.; Vicidomini, G.; Diaspro, A.; Brovelli, S.; Manna, L.; Moreels, I., *J. Mater. Chem. C* **2014,** *2* (17), 3439-3447.

[40] Acharya, K. P.; Khnayzer, R. S.; O'Connor, T.; Diederich, G.; Kirsanova, M.; Klinkova, A.; Roth, D.; Kinder, E.; Imboden, M.; Zamkov, M., *Nano Lett.* **2011,** *11* (7), 2919-26.

[41] Chakrabortty, S.; Xing, G.; Xu, Y.; Ngiam, S. W.; Mishra, N.; Sum, T. C.; Chan, Y., *Small* **2011,** *7* (20), 2847-52.

[42] Vaneski, A.; Susha, A. S.; Rodriguez-Fernandez, J.; Berr, M.; Jackel, F.;

Feldmann, J.; Rogach, A. L., *Adv. Funct. Mater.* **2011,** *21* (9), 1547-1556.

[43] Berr, M. J.; Vaneski, A.; Mauser, C.; Fischbach, S.; Susha, A. S.; Rogach, A. L.; Jackel, F.; Feldmann, J., *Small* **2012,** *8* (2), 291-7.

[44] Hu, W. W.; Liu, H.; Ye, F.; Ding, Y. L.; Yang, J., *CrystEngComm* **2012,** *14* (20), 7049-7054.

[45] Khanal, B. P.; Pandey, A.; Li, L.; Lin, Q.; Bae, W. K.; Luo, H.; Klimov, V. I.; Pietryga, J. M., *ACS Nano* **2012,** *6* (5), 3832-40.

[46] O'Connor, T.; Panov, M. S.; Mereshchenko, A.; Tarnovsky, A. N.; Lorek, R.; Perera, D.; Diederich, G.; Lambright, S.; Moroz, P.; Zamkov, M., *ACS Nano* **2012,** *6* (9), 8156-65.

[47] Conca, E.; Aresti, M.; Saba, M.; Casula, M. F.; Quochi, F.; Mula, G.; Loche, D.; Kim, M. R.; Manna, L.; Corrias, A.; Mura, A.; Bongiovanni, G., *Nanoscale* **2014,** *6* (4), 2238-43.

[48] Vaneski, A.; Schneider, J.; Susha, A. S.; Rogach, A. L., *J. Photochem. Photobiol. C: Photochem. Rev.* **2014,** *19* (0), 52-61.

[49] Read, C. G.; Gordon, T. R.; Hodges, J. M.; Schaak, R. E., *J. Am. Chem. Soc.* **2015,** *137* (39), 12514-7.

[50] Song, H., *Acc. Chem. Res.* **2015,** *48* (3), 491-9.

[51] Wu, K.; Zhu, H.; Lian, T., *Acc. Chem. Res.* **2015,** *48* (3), 851-9.

[52] Wu, K.; Lian, T., *Chem. Soc. Rev.* **2016**.

[53] Sun, B. Q.; Marx, E.; Greenham, N. C., *Nano Lett.* **2003,** *3* (7), 961-963.

[54] Sandberg, R. L.; Padilha, L. A.; Qazilbash, M. M.; Bae, W. K.; Schaller, R. D.; Pietryga, J. M.; Stevens, M. J.; Baek, B.; Nam, S. W.; Klimov, V. I., *ACS Nano* **2012,** *6* (11), 9532-40.

[55] Lim, J.; Borg, L.; Dolezel, S.; Schmid, F.; Char, K.; Zentel, R., *Macromol. Rapid Commun.* **2014,** *35* (19), 1685-91.

[56] Lim, J.; Lee, D.; Park, M.; Song, J.; Lee, S.; Kang, M. S.; Lee, C.; Char, K., *J. Phys. Chem. C* **2014,** *118* (8), 3942-3952.

[57] Song, J.; Lim, J.; Lee, D.; Thambidurai, M.; Kim, J. Y.; Park, M.; Song, H. J.; Lee, S.; Char, K.; Lee, C., *ACS Appl. Mater. Interfaces* **2015,** *7* (33), 18460-6.

[58] Taniguchi, Y.; Takishita, T.; Kawai, T.; Nakashima, T., *Angew. Chem. Int. Ed.* **2016,** *55* (6), 2083-6.

[59] Yang, J.; Choi, M. K.; Kim, D. H.; Hyeon, T., *Adv. Mater.* **2016,** *28* (6), 1176-207.

[60] Cui, Y.; Banin, U.; Bjork, M. T.; Alivisatos, A. P., *Nano Lett.* **2005,** *5* (7), 1519-1523.

[61] Bae, W. K.; Kwak, J.; Park, J. W.; Char, K.; Lee, C.; Lee, S., *Adv. Mater.* **2009,** *21* (17), 1690-+.

[62] Bae, W. K.; Kwak, J.; Lim, J.; Lee, D.; Nam, M. K.; Char, K.; Lee, C.; Lee, S., *Nano Lett.* **2010,** *10* (7), 2368-73.

[63] Franchini, I. R.; Cola, A.; Rizzo, A.; Mastria, R.; Persano, A.; Krahne,

R.; Genovese, A.; Falqui, A.; Baranov, D.; Gigli, G.; Manna, L., *Nanoscale* **2010,** *2* (10), 2171-9.

[64] Lim, J.; Bae, W. K.; Lee, D.; Nam, M. K.; Jung, J.; Lee, C.; Char, K.; Lee, S., *Chem. Mater.* **2011,** *23* (20), 4459-4463.

[65] Kwak, J.; Bae, W. K.; Lee, D.; Park, I.; Lim, J.; Park, M.; Cho, H.; Woo, H.; Yoon do, Y.; Char, K.; Lee, S.; Lee, C., *Nano Lett.* **2012,** *12* (5), 2362-6.

[66] Lim, J.; Park, M.; Bae, W. K.; Lee, D.; Lee, S.; Lee, C.; Char, K., *ACS Nano* **2013,** *7* (10), 9019-26.

[67] Bae, W. K.; Lim, J.; Lee, D.; Park, M.; Lee, H.; Kwak, J.; Char, K.; Lee, C.; Lee, S., *Adv. Mater.* **2014,** *26* (37), 6387-93.

[68] Brovelli, S.; Bae, W. K.; Galland, C.; Giovanella, U.; Meinardi, F.; Klimov, V. I., *Nano Lett.* **2014,** *14* (2), 486-94.

[69] Oh, N.; Nam, S.; Zhai, Y.; Deshpande, K.; Trefonas, P.; Shim, M., *Nat. Commun.* **2014,** *5*, 3642.

[70] Castelli, A.; Meinardi, F.; Pasini, M.; Galeotti, F.; Pinchetti, V.; Lorenzon, M.; Manna, L.; Moreels, I.; Giovanella, U.; Brovelli, S., *Nano Lett.* **2015,** *15* (8), 5455-64.

[71] Kwak, J.; Lim, J.; Park, M.; Lee, S.; Char, K.; Lee, C., *Nano Lett.* **2015,** *15* (6), 3793-9.

[72] Salant, A.; Amitay-Sadovsky, E.; Banin, U., *J. Am. Chem. Soc.* **2006,** *128* (31), 10006-7.

[73] Costi, R.; Saunders, A. E.; Elmalem, E.; Salant, A.; Banin, U., *Nano Lett.* **2008,** *8* (2), 637-41.

[74] Kudo, A.; Miseki, Y., *Chem. Soc. Rev.* **2009,** *38* (1), 253-78.

[75] Zhao, N.; Liu, K.; Greener, J.; Nie, Z.; Kumacheva, E., *Nano Lett.* **2009,** *9* (8), 3077-81.

[76] Amirav, L.; Alivisatos, A. P., *J. Phys. Chem. Lett.* **2010,** *1* (7), 1051-1054.

[77] Maeda, K.; Domen, K., *J. Phys. Chem. Lett.* **2010,** *1* (18), 2655-2661.

[78] Shemesh, Y.; Macdonald, J. E.; Menagen, G.; Banin, U., *Angew. Chem. Int. Ed.* **2011,** *50* (5), 1185-9.

[79] Berr, M. J.; Wagner, P.; Fischbach, S.; Vaneski, A.; Schneider, J.; Susha, A. S.; Rogach, A. L.; Jackel, F.; Feldmann, J., *Appl. Phys. Lett.* **2012,** *100* (22), 223903.

[80] Brown, K. A.; Wilker, M. B.; Boehm, M.; Dukovic, G.; King, P. W., *J. Am. Chem. Soc.* **2012,** *134* (12), 5627-36.

[81] Gao, P.; Liu, J. C.; Lee, S.; Zhang, T.; Sun, D. D., *J. Mater. Chem.* **2012,** *22* (5), 2292-2298.

[82] Haldar, K. K.; Sinha, G.; Lahtinen, J.; Patra, A., *ACS Appl. Mater. Interfaces* **2012,** *4* (11), 6266-72.

[83] Kraus-Ophir, S.; Ben-Shahar, Y.; Banin, U.; Mandler, D., *Adv. Mater. Interf.* **2014,** *1* (1).

[84] Schneider, J.; Vaneski, A.; Pesch, G. R.; Susha, A. S.; Yang Teoh, W.;

Rogach, A. L., *APL Mater.* **2014,** *2* (12), 126102.

[85] Simon, T.; Bouchonville, N.; Berr, M. J.; Vaneski, A.; Adrovic, A.; Volbers, D.; Wyrwich, R.; Doblinger, M.; Susha, A. S.; Rogach, A. L.; Jackel, F.; Stolarczyk, J. K.; Feldmann, J., *Nat. Mater.* **2014,** *13* (11), 1013-8.

[86] Soni, U.; Tripathy, P.; Sapra, S., *J. Phys. Chem. Lett.* **2014,** *5* (11), 1909-16.

[87] Ben-Shahar, Y.; Scotognella, F.; Waiskopf, N.; Kriegel, I.; Dal Conte, S.; Cerullo, G.; Banin, U., *Small* **2015,** *11* (4), 462-71.

[88] Chauviré, T.; Mouesca, J.-M.; Gasparutto, D.; Ravanat, J.-L.; Lebrun, C.; Gromova, M.; Jouneau, P.-H.; Chauvin, J.; Gambarelli, S.; Maurel, V., *J. Phys. Chem. C* **2015,** *119* (31), 17857-17866.

[89] Kalisman, P.; Kauffmann, Y.; Amirav, L., *J. Mater. Chem. A* **2015,** *3* (7), 3261-3265.

[90] Kim, D.; Kim, W. D.; Kang, M. S.; Kim, S. H.; Lee, D. C., *Nano Lett.* **2015,** *15* (1), 714-20.

[91] Li, X.; Yu, J. G.; Low, J. X.; Fang, Y. P.; Xiao, J.; Chen, X. B., *J. Mater. Chem. A* **2015,** *3* (6), 2485-2534.

[92] Liu, Y.; Zhang, P.; Tian, B.; Zhang, J., *ACS Appl. Mater. Interfaces* **2015,** *7* (25), 13849-58.

[93] Razgoniaeva, N.; Moroz, P.; Lambright, S.; Zamkov, M., *J. Phys. Chem. Lett.* **2015,** *6* (21), 4352-9.

[94] Sahasrabudhe, A.; Bhattacharyya, S., *Chem. Mater.* **2015,** *27* (13), 4848-4859.

[95] Wong, A. B.; Brittman, S.; Yu, Y.; Dasgupta, N. P.; Yang, P., *Nano Lett.* **2015,** *15* (6), 4096-101.

[96] Yu, X.; An, X.; Genç, A.; Ibáñez, M.; Arbiol, J.; Zhang, Y.; Cabot, A., *J. Phys. Chem. C* **2015,** *119* (38), 21882-21888.

[97] Jiang, D.; Sun, Z.; Jia, H.; Lu, D.; Du, P., *J. Mater. Chem. A* **2016,** *4* (2), 675-683.

[98] Nusimovi.Ma; Birman, J. L., *Phys. Rev.* **1967,** *156* (3), 925.

[99] Chang, K. J.; Froyen, S.; Cohen, M. L., *Phys. Rev. B* **1983,** *28* (8), 4736-4743.

[100] Murray, C. B.; Norris, D. J.; Bawendi, M. G., *J. Am. Chem. Soc.* **1993,** *115* (19), 8706-8715.

[101] Peng, Z. A.; Peng, X. G., *J. Am. Chem. Soc.* **2001,** *123* (1), 183-184.

[102] Kucur, E.; Riegler, J.; Urban, G. A.; Nann, T., *J. Chem. Phys.* **2003,** *119* (4), 2333-2337.

[103] Peng, X. G., *Adv. Mater.* **2003,** *15* (5), 459-463.

[104] Yu, W. W.; Qu, L. H.; Guo, W. Z.; Peng, X. G., *Chem. Mater.* **2003,** *15* (14), 2854-2860.

[105] Yin, Y.; Alivisatos, A. P., *Nature* **2005,** *437* (7059), 664-70.

[106] Cao, H.; Wang, G.; Zhang, S.; Zhang, X.; Rabinovich, D., *Inorg. Chem.*

2006, *45* (13), 5103-8.

[107] Liu, H.; Owen, J. S.; Alivisatos, A. P., *J. Am. Chem. Soc.* **2007,** *129* (2), 305-12.

[108] Owen, J. S.; Park, J.; Trudeau, P. E.; Alivisatos, A. P., *J. Am. Chem. Soc.* **2008,** *130* (37), 12279-81.

[109] Reiss, P.; Protiere, M.; Li, L., *Small* **2009,** *5* (2), 154-68.

[110] Peng, X. G.; Wickham, J.; Alivisatos, A. P., *J. Am. Chem. Soc.* **1998,** *120* (21), 5343-5344.

[111] Manna, L.; Scher, E. C.; Alivisatos, A. P., *J. Am. Chem. Soc.* **2000,** *122* (51), 12700-12706.

[112] Peng, X.; Manna, L.; Yang, W.; Wickham, J.; Scher, E.; Kadavanich, A.; Alivisatos, A. P., *Nature* **2000,** *404* (6773), 59-61.

[113] Peng, Z. A.; Peng, X. G., *J. Am. Chem. Soc.* **2002,** *124* (13), 3343-53.

[114] Kan, S.; Mokari, T.; Rothenberg, E.; Banin, U., *Nat. Mater.* **2003,** *2* (3), 155-8.

[115] Manna, L.; Milliron, D. J.; Meisel, A.; Scher, E. C.; Alivisatos, A. P., *Nat. Mater.* **2003,** *2* (6), 382-5.

[116] Talapin, D. V.; Koeppe, R.; Gotzinger, S.; Kornowski, A.; Lupton, J. M.; Rogach, A. L.; Benson, O.; Feldmann, J.; Weller, H., *Nano Lett.* **2003,** *3* (12), 1677-1681.

[117] Bullen, C.; van Embden, J.; Jasieniak, J.; Cosgriff, J. E.; Mulder, R. J.;

Rizzardo, E.; Gu, M.; Raston, C. L., *Chem. Mater.* **2010,** *22* (14), 4135-4143.

[118] Karel Čapek, R.; Moreels, I.; Lambert, K.; De Muynck, D.; Zhao, Q.; Van Tomme, A.; Vanhaecke, F.; Hens, Z., *J. Phys. Chem. C* **2010,** *114* (14), 6371-6376.

[119] Kovalenko, M. V.; Bodnarchuk, M. I.; Talapin, D. V., *J. Am. Chem. Soc.* **2010,** *132* (43), 15124-6.

[120] Owen, J. S.; Chan, E. M.; Liu, H.; Alivisatos, A. P., *J. Am. Chem. Soc.* **2010,** *132* (51), 18206-13.

[121] Seongmi, H.; Youngmin, C.; Sunho, J.; Hakyun, J.; Chang Gyoun, K.; Teak-Mo, C.; Beyong-Hwan, R., *Jpn. J. Appl. Phys.* **2010,** *49* (5S1), 05EA03.

[122] Nag, A.; Kovalenko, M. V.; Lee, J. S.; Liu, W.; Spokoyny, B.; Talapin, D. V., *J. Am. Chem. Soc.* **2011,** *133* (27), 10612-20.

[123] Rupich, S. M.; Talapin, D. V., *Nat. Mater.* **2011,** *10* (11), 815-6.

[124] Moghaddam, M. M.; Baghbanzadeh, M.; Keilbach, A.; Kappe, C. O., *Nanoscale* **2012,** *4* (23), 7435-42.

[125] Segets, D.; Lucas, J. M.; Klupp Taylor, R. N.; Scheele, M.; Zheng, H.; Alivisatos, A. P.; Peukert, W., *ACS Nano* **2012,** *6* (10), 9021-32.

[126] Yu, H.; Li, J.; Loomis, R. A.; Gibbons, P. C.; Wang, L. W.; Buhro, W. E., *J. Am. Chem. Soc.* **2003,** *125* (52), 16168-9.

[127] Jun, Y. W.; Lee, J. H.; Choi, J. S.; Cheon, J., *J. Phys. Chem. B* **2005,** *109* (31), 14795-806.

[128] Pang, Q.; Zhao, L. J.; Cai, Y.; Nguyen, D. P.; Regnault, N.; Wang, N.; Yang, S. H.; Ge, W. K.; Ferreira, R.; Bastard, G.; Wang, J. N., *Chem. Mater.* **2005,** *17* (21), 5263-5267.

[129] Xie, R.; Kolb, U.; Basche, T., *Small* **2006,** *2* (12), 1454-7.

[130] Asokan, S.; Krueger, K. M.; Colvin, V. L.; Wong, M. S., *Small* **2007,** *3* (7), 1164-9.

[131] Fiore, A.; Mastria, R.; Lupo, M. G.; Lanzani, G.; Giannini, C.; Carlino, E.; Morello, G.; De Giorgi, M.; Li, Y.; Cingolani, R.; Manna, L., *J. Am. Chem. Soc.* **2009,** *131* (6), 2274-82.

[132] Liu, L.; Zhuang, Z.; Xie, T.; Wang, Y. G.; Li, J.; Peng, Q.; Li, Y., *J. Am. Chem. Soc.* **2009,** *131* (45), 16423-9.

[133] Deka, S.; Miszta, K.; Dorfs, D.; Genovese, A.; Bertoni, G.; Manna, L., *Nano Lett.* **2010,** *10* (9), 3770-6.

[134] Huang, J.; Kovalenko, M. V.; Talapin, D. V., *J. Am. Chem. Soc.* **2010,** *132* (45), 15866-8.

[135] Lim, S. J.; Kim, W.; Jung, S.; Seo, J.; Shin, S. K., *Chem. Mater.* **2011,** *23* (22), 5029-5036.

[136] Zou, Y.; Li, D.; Yang, D., *Nanoscale Res. Lett.* **2011,** *6* (1), 374.

[137] Ghosh, A.; Paul, S.; Raj, S., *Solid State Commun.* **2013,** *154*, 25-29.

[138] Guo, Y.; Alvarado, S. R.; Barclay, J. D.; Vela, J., *ACS Nano* **2013,** *7* (4), 3616-26.

[139] Lim, J.; Bae, W. K.; Park, K. U.; zur Borg, L.; Zentel, R.; Lee, S.; Char, K., *Chem. Mater.* **2013,** *25* (8), 1443-1449.

[140] Manthiram, K.; Beberwyck, B. J.; Talapin, D. V.; Alivisatos, A. P., *J. Vis. Exp.* **2013,** (82), e50731.

[141] Mirhosseini Moghaddam, M.; Baghbanzadeh, M.; Sadeghpour, A.; Glatter, O.; Kappe, C. O., *Chemistry* **2013,** *19* (35), 11629-36.

[142] Rice, K. P.; Saunders, A. E.; Stoykovich, M. P., *J. Am. Chem. Soc.* **2013,** *135* (17), 6669-76.

[143] Vela, J., *J. Phys. Chem. Lett.* **2013,** *4* (4), 653-68.

[144] Vaneski, A.; Schneider, J.; Susha, A. S.; Rogach, A. L., *APL Mater.* **2014,** *2* (1), 012104.

[145] Hellebusch, D. J.; Manthiram, K.; Beberwyck, B. J.; Alivisatos, A. P., *J. Phys. Chem. Lett.* **2015,** *6* (4), 605-11.

[146] Kodanek, T.; Banbela, H. M.; Naskar, S.; Adel, P.; Bigall, N. C.; Dorfs, D., *Nanoscale* **2015,** *7* (45), 19300-9.

[147] Singh, S.; Liu, P.; Singh, A.; Coughlan, C.; Wang, J. J.; Lusi, M.; Ryan, K. M., *Chem. Mater.* **2015,** *27* (13), 4742-4748.

[148] Wang, X. X.; Liu, M. C.; Zhou, Z. H.; Guo, L. J., *J. Phys. Chem. C* **2015,** *119* (35), 20555-20560.

[149] Wang, Y.; Zhou, Y.; Zhang, Y.; Buhro, W. E., *Inorg. Chem.* **2015,** *54* (3), 1165-77.

[150] Xie, R. G.; Zhou, M., *Chem. Mater.* **2015,** *27* (8), 3055-3064.

[151] Kim, H. B.; Jang, D. J., *Nanoscale* **2016,** *8* (1), 403-10.

[152] Wu, Z.; Yang, S.; Wu, W., *Nanoscale* **2016,** *8* (3), 1237-59.

[153] Mokari, T.; Rothenberg, E.; Popov, I.; Costi, R.; Banin, U., *Science* **2004,** *304* (5678), 1787-90.

[154] Mokari, T.; Sztrum, C. G.; Salant, A.; Rabani, E.; Banin, U., *Nat. Mater.* **2005,** *4* (11), 855-863.

[155] Talapin, D. V.; Yu, H.; Shevchenko, E. V.; Lobo, A.; Murray, C. B., *J. Phys. Chem. C* **2007,** *111* (38), 14049-14054.

[156] Kwon, K. W.; Lee, B. H.; Shim, M., *Chem. Mater.* **2006,** *18* (26), 6357-6363.

[157] Habas, S. E.; Yang, P.; Mokari, T., *J. Am. Chem. Soc.* **2008,** *130* (11), 3294-5.

[158] Menagen, G.; Macdonald, J. E.; Shemesh, Y.; Popov, I.; Banin, U., *J. Am. Chem. Soc.* **2009,** *131* (47), 17406-11.

[159] Alemseghed, M. G.; Ruberu, T. P. A.; Vela, J., *Chem. Mater.* **2011,** *23* (15), 3571-3579.

[160] Ma, Y.; Dai, Y.; Wei, W.; Liu, X.; Huang, B., *J. Solid State Chem.* **2011,** *184* (4), 747-752.

[161] van Huis, M. A.; Figuerola, A.; Fang, C.; Beche, A.; Zandbergen, H. W.; Manna, L., *Nano Lett.* **2011,** *11* (11), 4555-61.

[162] Wu, K.; Rodriguez-Cordoba, W. E.; Yang, Y.; Lian, T., *Nano Lett.* **2013,** *13* (11), 5255-63.

[163] Xu, W.; Niu, J.; Wang, H.; Shen, H.; Li, L. S., *ACS Appl. Mater. Interfaces* **2013,** *5* (15), 7537-43.

[164] Kadirov, M. K.; Litvinov, A. I.; Nizameev, I. R.; Zakharova, L. Y., *J. Phys. Chem. C* **2014,** *118* (34), 19785-19794.

[165] Caddeo, C.; Cazia, V.; Bagolini, L.; Lusk, M. T.; Mattoni, A., *J. Phys. Chem. C* **2015,** *119* (39), 22663-22668.

[166] Park, J.; Park, S.; Selvaraj, R.; Kim, Y., *Rsc Adv.* **2015,** *5* (65), 52737-52742.

[167] Xiong, S. M.; Isaacs, E. B.; Li, Y., *J. Phys. Chem. C* **2015,** *119* (9), 4834-4842.

[168] Saunders, A. E.; Popov, I.; Banin, U., *J. Phys. Chem. B* **2006,** *110* (50), 25421-9.

[169] Casavola, M.; Falqui, A.; Garcia, M. A.; Garcia-Hernandez, M.; Giannini, C.; Cingolani, R.; Cozzoli, P. D., *Nano Lett.* **2009,** *9* (1), 366-76.

[170] Bang, J. U.; Lee, S. J.; Jang, J. S.; Choi, W.; Song, H., *J. Phys. Chem. Lett.* **2012,** *3* (24), 3781-5.

[171] Khon, E.; Lambright, K.; Khnayzer, R. S.; Moroz, P.; Perera, D.; Butaeva, E.; Lambright, S.; Castellano, F. N.; Zamkov, M., *Nano Lett.* **2013,** *13* (5), 2016-23.

[172] Wu, K.; Chen, Z.; Lv, H.; Zhu, H.; Hill, C. L.; Lian, T., *J. Am. Chem. Soc.* **2014,** *136* (21), 7708-16.

[173] Nakibli, Y.; Kalisman, P.; Amirav, L., *J. Phys. Chem. Lett.* **2015,** *6* (12), 2265-8.

[174] Dukovic, G.; Merkle, M. G.; Nelson, J. H.; Hughes, S. M.; Alivisatos, A. P., *Adv. Mater.* **2008,** *20* (22), 4306-4311.

[175] Elmalem, E.; Saunders, A. E.; Costi, R.; Salant, A.; Banin, U., *Adv.Mater.* **2008,** *20* (22), 4312-4317.

[176] Berr, M.; Vaneski, A.; Susha, A. S.; Rodriguez-Fernandez, J.; Doblinger, M.; Jackel, F.; Rogach, A. L.; Feldmann, J., *Appl. Phys. Lett.* **2010,** *97* (9), 093108.

[177] Berr, M. J.; Schweinberger, F. F.; Doblinger, M.; Sanwald, K. E.; Wolff, C.; Breimeier, J.; Crampton, A. S.; Ridge, C. J.; Tschurl, M.; Heiz, U.; Jackel, F.; Feldmann, J., *Nano Lett.* **2012,** *12* (11), 5903-6.

[178] Schweinberger, F. F.; Berr, M. J.; Doblinger, M.; Wolff, C.; Sanwald, K. E.; Crampton, A. S.; Ridge, C. J.; Jackel, F.; Feldmann, J.; Tschurl, M.; Heiz, U., *J. Am. Chem. Soc.* **2013,** *135* (36), 13262-5.

[179] Feng, J.; Liu, J. X.; Wei, G. J.; Zhang, J.; Wang, S. T.; Wang, Z. J.; An, C. H., *Rsc Adv.* **2014,** *4* (69), 36665-36670.

[180] Keng, P. Y.; Bull, M. M.; Shim, I. B.; Nebesny, K. G.; Armstrong, N. R.; Sung, Y.; Char, K.; Pyun, J., *Chem. Mater.* **2011,** *23* (5), 1120-1129.

[181] Hill, L. J.; Bull, M. M.; Sung, Y.; Simmonds, A. G.; Dirlam, P. T.; Richey, N. E.; DeRosa, S. E.; Shim, I. B.; Guin, D.; Costanzo, P. J.; Pinna, N.; Willinger, M. G.; Vogel, W.; Char, K.; Pyun, J., *ACS Nano* **2012,** *6* (10), 8632-45.

[182] Hill, L. J.; Richey, N. E.; Sung, Y.; Dirlam, P. T.; Griebel, J. J.; Lavoie-Higgins, E.; Shim, I. B.; Pinna, N.; Willinger, M. G.; Vogel, W.; Benkoski, J. J.; Char, K.; Pyun, J., *ACS Nano* **2014,** *8* (4), 3272-84.

[183] Hill, L. J.; Richey, N. E.; Sung, Y.; Dirlam, P. T.; Griebel, J. J.; Shim, I. B.; Pinna, N.; Willinger, M. G.; Vogel, W.; Char, K.; Pyun, J., *CrystEngComm* **2014,** *16* (40), 9461-9468.

[184] Pavlopoulos, N. G.; Dubose, J. T.; Pinna, N.; Willinger, M. G.; Char, K.; Pyun, J., *Angew. Chem. Int. Ed.* **2016,** *55* (5), 1787-91.

[185] Liu, C.; Qiu, F.; Peterson, J. J.; Krauss, T. D., *J. Phys. Chem. B* **2015,** *119* (24), 7349-57.

[186] Luo, M. H.; Yao, W. F.; Huang, C. P.; Wu, Q.; Xu, Q. J., *J. Mater. Chem. A* **2015,** *3* (26), 13884-13891.

[187] Meyns, M.; Willing, S.; Lehmann, H.; Klinke, C., *ACS Nano* **2015,** *9* (6), 6077-87.

[188] Sung, Y.; Lim, J.; Koh, J. H.; Hill, L. J.; Min, B. K.; Pyun, J.; Char, K., *CrystEngComm* **2015,** *17* (44), 8423-8427.

[189] Wu, K. F.; Li, Q. Y.; Du, Y. L.; Chen, Z. Y.; Lian, T. Q., *Chem. Sci.* **2015,**

6 (2), 1049-1054.

[190] Xiao, F. X.; Zeng, Z.; Hsu, S. H.; Hung, S. F.; Chen, H. M.; Liu, B., *ACS Appl. Mater. Interfaces* **2015,** *7* (51), 28105-9.

[191] Zhang, L.; Fu, X.; Meng, S.; Jiang, X.; Wang, J.; Chen, S., *J. Mater. Chem. A* **2015,** *3* (47), 23732-23742.

[192] Zhukovskyi, M.; Tongying, P.; Yashan, H.; Wang, Y. X.; Kuno, M., *Acs Catal.* **2015,** *5* (11), 6615-6623.

[193] Aspnes, D. E.; Heller, A., *J. Phys. Chem.* **1983,** *87* (24), 4919-4929.

[194] Chen, H. Y.; Sun, Z. J.; Ye, S.; Lu, D. P.; Du, P. W., *J. Mater. Chem. A* **2015,** *3* (30), 15729-15737.

[195] Leatherdale, C. A.; Woo, W. K.; Mikulec, F. V.; Bawendi, M. G., *J. Phys. Chem. B* **2002,** *106* (31), 7619-7622.

[196] Pietryga, J. M.; Schaller, R. D.; Werder, D.; Stewart, M. H.; Klimov, V. I.; Hollingsworth, J. A., *J. Am. Chem. Soc.* **2004,** *126* (38), 11752-3.

[197] Muller, J.; Lupton, J. M.; Lagoudakis, P. G.; Schindler, F.; Koeppe, R.; Rogach, A. L.; Feldmann, J.; Talapin, D. V.; Weller, H., *Nano Lett.* **2005,** *5* (10), 2044-9.

[198] Protasenko, V.; Bacinello, D.; Kuno, M., *J. Phys. Chem. B* **2006,** *110* (50), 25322-31.

[199] Choi, C. L.; Koski, K. J.; Sivasankar, S.; Alivisatos, A. P., *Nano Lett.* **2009,** *9* (10), 3544-9.

[200] Sitt, A.; Della Sala, F.; Menagen, G.; Banin, U., *Nano Lett.* **2009,** *9* (10), 3470-6.

[201] Bao, N.; Shen, L.; Takata, T.; Domen, K., *Chem. Mater.* **2008,** *20* (1), 110-117.

[202] Yu, J.; Yu, Y.; Cheng, B., *RSC Adv.* **2012,** *2* (31), 11829.

[203] Zhou, H. L.; Qu, Y. Q.; Zeid, T.; Duan, X. F., *Energy Environ. Sci.* **2012,** *5* (5), 6732-6743.

[204] Aslan, E.; Birinci, O.; Aljabour, A.; Ozel, F.; Akin, I.; Hatay Patir, I.; Kus, M.; Ersoz, M., *ChemPhysChem* **2014,** *15* (13), 2668-71.

[205] Jen-La Plante, I.; Teitelboim, A.; Pinkas, I.; Oron, D.; Mokari, T., *J. Phys. Chem. Lett.* **2014,** *5* (3), 590-6.

[206] Reichert, M. D.; Lin, C.-C.; Vela, J., *Chem. Mater.* **2014,** *26* (13), 3900-3908.

[207] Wu, K.; Rodriguez-Cordoba, W.; Lian, T., *J. Phys. Chem. B* **2014,** *118* (49), 14062-9.

[208] Borys, N. J.; Walter, M. J.; Huang, J.; Talapin, D. V.; Lupton, J. M., *Science* **2010,** *330* (6009), 1371-4.

[209] Govan, J. E.; Jan, E.; Querejeta, A.; Kotov, N. A.; Gun'ko, Y. K., *Chem. Commun.* **2010,** *46* (33), 6072-4.

[210] Lee, D. C.; Robel, I.; Pietryga, J. M.; Klimov, V. I., *J. Am. Chem. Soc.* **2010,** *132* (29), 9960-2.

[211] Lutich, A. A.; Mauser, C.; Da Como, E.; Huang, J.; Vaneski, A.; Talapin, D. V.; Rogach, A. L.; Feldmann, J., *Nano Lett.* **2010,** *10* (11), 4646-50.

[212] Hannah, D. C.; Dunn, N. J.; Ithurria, S.; Talapin, D. V.; Chen, L. X.; Pelton, M.; Schatz, G. C.; Schaller, R. D., *Phys. Rev. Lett.* **2011,** *107* (17), 177403.

[213] Nghia, N. X.; Hai, L. B.; Luyen, N. T.; Nga, P. T.; Nguyen, T. T. L.; Phan, T. L., *J. Phys. Chem. C* **2012,** *116* (48), 25517-25524.

[214] Lenngren, N.; Garting, T.; Zheng, K.; Abdellah, M.; Lascoux, N.; Ma, F.; Yartsev, A.; Zidek, K.; Pullerits, T., *J. Phys. Chem. Lett.* **2013,** *4* (19), 3330-6.

[215] Raja, S. N.; Olson, A. C.; Thorkelsson, K.; Luong, A. J.; Hsueh, L.; Chang, G.; Gludovatz, B.; Lin, L.; Xu, T.; Ritchie, R. O.; Alivisatos, A. P., *Nano Lett.* **2013,** *13* (8), 3915-22.

[216] Yao, Y.; Kuroda, T.; Dirin, D. N.; Irkhina, A. A.; Vasiliev, R. B.; Sakoda, K., *Opt. Mater. Express* **2013,** *3* (7), 977.

[217] Bridewell, V. L.; Alam, R.; Karwacki, C. J.; Kamat, P. V., *Chem. Mater.* **2015,** *27* (14), 5064-5071.

[218] Xiong, J. H.; Wu, W. M.; Liu, Y. H.; Shen, L. J.; Wu, L., *J. Nanopart. Res.* **2015,** *17* (1), 1-10.

[219] Zhuang, T. T.; Liu, Y.; Sun, M.; Jiang, S. L.; Zhang, M. W.; Wang, X. C.; Zhang, Q.; Jiang, J.; Yu, S. H., *Angew. Chem. Int. Ed.* **2015,** *54* (39),

11495-500.

[220] Kim, W. D.; Kim, J. H.; Lee, S.; Lee, S.; Woo, J. Y.; Lee, K.; Chae, W. S.; Jeong, S.; Bae, W. K.; McGuire, J. A.; Moon, J. H.; Jeong, M. S.; Lee, D. C., *Chem. Mater.* **2016,** *28* (3), 962-968.

[221] Nyk, M.; Szeremeta, J.; Wawrzynczyk, D.; Samoc, M., *J. Phys. Chem. C* **2014,** *118* (31), 17914-17921.

[222] Tarafder, K.; Surendranath, Y.; Olshansky, J. H.; Alivisatos, A. P.; Wang, L. W., *J. Am. Chem. Soc.* **2014,** *136* (13), 5121-31.

[223] Wong, J. I.; Mishra, N.; Xing, G.; Li, M.; Chakrabortty, S.; Sum, T. C.; Shi, Y.; Chan, Y.; Yang, H. Y., *ACS Nano* **2014,** *8* (3), 2873-9.

[224] Wu, W. Y.; Li, M.; Lian, J.; Wu, X.; Yeow, E. K.; Jhon, M. H.; Chan, Y., *ACS Nano* **2014,** *8* (9), 9349-57.

[225] Razgoniaeva, N.; Lambright, S.; Sharma, N.; Acharya, A.; Khon, E.; Moroz, P.; Razgoniaev, A.; Ostrowski, A.; Zamkov, M., *J. Phys. Chem. C* **2015,** *119* (27), 15562-15571.

초 록

금속-반도체 헤테로구조 나노입자는 단일 나노입자 안에서 금속 및 반도체와 같은 다양한 기능의 재료들이 복합적인 효율을 발현하는 특성으로 각광받고 있다. 기본적인 합성법, 광전자적 특성의 분석 및 여러 응용분야에 관련된 연구가 활발히 진행되고 있다. 특히, 빛에너지를 흡수하여 전기에너지를 형성하는 반도체 나노입자의 역할과, 생성된 전자와 전공을 효율적으로 응용할 수 있는 금속 나노입자의 도입에 따라 광촉매, 광전자소자 및 자기조립과 같은 응용분야에 널리 적용되고 있다.

이러한 다양한 조성 및 형태를 지니는 콜로이드 형태의 금속-반도체 헤테로구조 나노입자가 발전하게 된 계기는, 콜로이드 형태의 반도체 나노입자에 대한 활발한 연구 덕분이라고 할 수 있겠다. 3차원 양자국한 현상에 의해 특수한 광전자적 특성을 지니는 콜로이드 반도체 나노입자인 양자점의 발견으로, 다양한 조성 및 형태를 지니는 반도체 나노입자의 합성법 및 특수한 광전자적 특성에 대한 연구가 활발히 진행 되었다. 반도체 나노입자의 형태 조절을 위해서는 크게 세 가지의 접근법이 적용된다. 첫째, 비등방

형태의 반도체 나노입자를 성장시키기 위한 시드의 결정구조이다. Wurtzite와 같은 결정구조를 가지는 반도체 나노입자는 1차원적인 나노막대와 같은 반도체 나노입자가 형성된다. Zincblende와 같은 결정구조를 가지는 반도체 나노입자는 3차원적인 사지성형 테트라포드와 같은 형태가 성장하게 된다. 둘째, 반도체 나노입자의 특정 결정면에 다양한 결합에너지를 가지는 유기리간드의 적절한 선택이다. 포스폰산 계열의 리간드는 특히 반도체 나노입자의 형태조절에 많이 사용된다. 그 이유는, 특정 결정면의 성장을 강하게 억제하기 때문이다. 일반적으로 널리 사용되는 올레산과 같은 리간드와 더불어 할로겐계열의 리간드를 첨가하게 되면, 포스폰산 계열의 리간드를 사용하지 않고 반도체 나노입자의 형태를 조절할 수 있게 된다. 셋째, 반도체 나노입자의 합성 메커니즘이다. 일반적으로 고온에서 전구체들을 단시간에 주입하여 순식간에 핵생성과 성장을 거치는 열역학적인 거동에서는 반응온도가 큰 영향을 미치게 된다. 하지만, 동역학적인 성장 구간에서는 반응에 참여하는 전구체의 농도에 따라 반도체 나노입자의 형태가 조절된다. 이와 같은 전략적 접근을 토대로, 형태가 조절된 카드뮴계열의 반도체 나노막대 및 테트라포드가 성공적으로 제조되었다.

앞서 설명된 전략적 접근을 토대로 합성되어진 반도체 나노입자는 각각 다른 표면화학적 거동을 보이게 된다. 포스폰산이 도입된 반도체 나노막대는 리간드의 밀도가 대체적으로 낮으며 금속 나노입자가 성장할 수 있는 높은 확률 및 에너지를 지니는 반도체 나노막대의 말단에 금속 나노입자가 성장하게 된다. 2차 금속 나노입자의 성장은 1차적으로 성장된 금속 나노입자에서만 선택적으로 일어나며, 자성 나노입자가 도입되게 되면 특이한 자기조립 현상을 보이게 된다. 또한, 동역학적인 성장구간에서 합성된 CdSe 테트라포드 형태의 나노입자는 표면에 존재하는 할로겐 계열의 리간드의 역할로 반도체 나노입자의 전반적으로 금속 나노입자가 성장하게 된다. 반응시간에 따른 관찰 결과, 우선 금속 나노입자가 자체적으로 성장하게 되고, 반도체 나노입자 안에서도 말단 부분에서 먼저 성장하며 반응시간이 지나면 전체적으로 금속 나노입자가 성장하게 된다. 이와 같이 반도체 나노입자의 합성 및 표면의 제어를 통해 다양한 조성 및 형태의 금속-반도체 헤테로구조 나노입자를 제조할 수 있게 된다.

금속-반도체 헤테로구조 나노입자의 다양한 응용분야 중에서도, 특히 광촉매 분야로의 응용이 가장 각광받고 있다. 반도체 나노입

자가 빛을 흡수하여 전기에너지를 형성하게 되고, 적절한 에너지 준위를 가지는 금속 나노입자가 생성된 전자를 이용하여 최종적으로 물을 분해하여 수소와 같은 신재생 에너지원을 생성, 연료전지에 사용할 수 있게 된다. 앞서 언급된 바와 같이, 금속 및 반도체 나노입자는 그 조성 및 형태에 따라 특이한 광전자적 특성을 보이므로, 최종적으로 고효율 광촉매를 설계하고 합성하기 위해서 각각의 영역이 최종 효율에 미치는 영향에 대한 체계적인 기초 연구가 필수적이라고 할 수 있겠다.

이에, 다양한 전략적 접근법을 통해 형태가 조절된 반도체 나노입자를 합성하고, 표면의 제어를 통해 다양한 조성 및 형태의 금속-반도체 헤테로구조 나노입자를 제조하는 합성기술을 바탕으로, 각각의 금속 및 반도체의 형태가 최종 광촉매 수소발생 효율에 미치는 영향에 대한 연구를 수행하였다. 우선, CdSe 테트라포드 나노입자에 백금 나노입자를 도입하며, 백금 전구체의 양 조절을 통해 백금 나노입자의 크기에 따른 Pt-CdSe 테트라포드 나노입자의 광촉매 효율에 대한 연구가 진행되었다. 그 결과, 백금 나노입자가 ~1.5 nm 정도로 매우 작은 크기로 도입되었을 때, 보다 높은 광촉매 효율을 보이는 것을 확인하였다. 이는, 백금 나노입자의

크기에 따라 백금 나노입자의 LUMO가 변하게 되는데, 이때 반도체 나노입자의 Conduction Band 및 수소 환원 전위 사이에 에너지준위가 위치하게 되어 높은 광촉매 효율을 보이는 것으로 생각된다. 또한, 지속적 전구체 주입법 (CPI, Continuous Precursor Injection Approach) 를 통하여 CdSe 테트라포드 반도체 나노입자의 형태를 미세하게 조절하게 되면, CdSe 테트라포드 반도체 나노입자의 팔 길이를 선택적으로 조절할 수 있게 된다. 백금 나노입자를 도입 시, 백금 나노입자의 밀도는 변하지 않고 균일한 크기의 백금 나노입자가 각각 팔길이가 다른 CdSe 테트라포드 나노입자에 도입되는 것을 확인할 수 있었으며, 팔길이가 짧은 광촉매가 보다 높은 효율을 보이는 것을 확인할 수 있었다. 이는, 광촉매 수소발생 실험에 사용되는 정량의 광촉매에서, 비록 정량에 도입되는 각각의 원소들의 양은 일정하나, 전체적으로 가벼운 무게의 팔길이가 짧은 광촉매가 많이 도입되게 된다. 일반적으로 반도체 나노입자에서 생성된 전공과 전자는 테트라포드 형태의 중앙에 밀집하려는 경향을 보이는데, 따라서 다수의 반도체 나노입자 개수의 광촉매가 소수의 광촉매보다 전자와 전공이 보다 효율적으로 분리될 수 있는 확률을 가지는 것이라고 볼 수 있겠다.

이상의 연구 결과는 금속-반도체 헤테로구조 나노입자의 각각 부분이 광촉매 효율에 미치는 영향을 토대로, 차세대 고효율 광촉매를 설계하고 합성하는 데 종합적인 접근이 필요함을 시사한다. 각각의 요소에 대한 심도깊은 연구결과들을 토대로, 인류사회의 에너지 문제를 해결할 수 있는 실마리를 제공할 수 있길 기대한다.

주요어: 반도체 나노입자, 금속-반도체 헤테로구조 나노입자, 나노막대, 테트라포드, 광촉매, 수소

학 번: 2010-22815